

INDIAN INSTITUTE OF TECHNOLOGY, KANPUR

MASTER'S THESIS

A study for Seismic Isolation under long period waves of Near-Fault earthquakes

Author:

Shubham TRIVEDI

Supervisor:

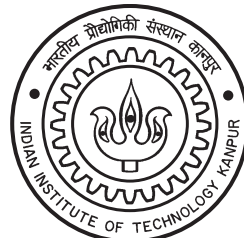
Dr. Sekhar K. CHAKRABARTI

*A thesis submitted in fulfilment of the requirements
for the degree of Master of Technology*

in the

Department of Civil Engineering

May 2015



Certificate

It is certified that the work contained in the thesis titled *A study for Seismic Isolation under long period waves of Near-Fault earthquakes*, by *Shubham Trivedi*, has been carried out under my supervision and that this work has not been submitted elsewhere for a degree.



Dr. Sekhar K. CHAKRABARTI

(Supervisor)

June 2013



“As far as successful design for earthquakes is concerned, I think we have hit the top with base isolation.”

Eric Elsesser

INDIAN INSTITUTE OF TECHNOLOGY, KANPUR

Abstract

Dr. Sekhar K. Chakrabarti

Department of Civil Engineering

Master of Technology

A study for Seismic Isolation under long period waves of Near-Fault earthquakes

by Shubham TRIVEDI

Friction Pendulum Systems have been the favorable technique for Seismic Isolation of buildings in recent years. In spite of many advantageous characteristics of the friction pendulum over elastomeric isolators some issues still exist with its performance as an earthquake proof seismic isolation device. Long period waves of the near-fault earthquake ground motions have been identified in the past researches as one of the major concern for seismic isolation systems. In this study, various existing isolation techniques for near-fault earthquakes are critically discussed. In conclusion to this detailed review, a new design is proposed that offers a more practically feasible solution to achieve seismic isolation in near-fault and far-field earthquake zones. A detailed description of the design of the isolator is presented and an analytical model of the problem is developed for a multi-storey shear-type building frame. The differential equations of motion hence formulated are solved using Newmark's Beta method with constant average acceleration. The system response against various near-fault and far-field earthquake ground motions (obtained from PEER Ground Motion Database) is computed and compared with the response of fixed base structural system and conventional Friction Pendulum isolated building. The results obtained illustrate the reduction in response facilitated by the proposed isolator as compared to a fixed base system. And in comparison to a conventionally isolated structure, the proposed isolator does show lower base displacement although other response quantities show only minor or no reduction under some ground motions.

Acknowledgements

I would like to express my sincere thanks and gratitude to Professor SK Chakrabarti, my thesis supervisor, for his consistent motivation for pursuing excellence in my study, enthusiastic encouragement and useful insight into this research work. His support was fundamental in the success of my research, from inception to conclusion.

I would also like to thank the PK Kelkar Library technical staff arranging the required journal papers that were not originally available within the institute repository.

Finally, I wish to thank my respectful parents for the constant support and motivation that they provided me throughout my study.

Shubham TRIVEDI

Contents

Abstract	iii
Acknowledgements	iv
List of Figures	vii
List of Tables	xiii
1 Introduction	1
1.1 A brief about Seismic Isolation	1
1.2 Impact of Near-Fault Earthquakes	2
1.3 Scope of the Thesis	4
1.4 Organization of the Thesis	4
2 Seismic Isolation Systems for Near-Fault Earthquakes	6
2.1 Existing approaches to Seismic Isolation	6
2.1.1 Elastomeric Isolators	6
2.1.2 Sliding-type Isolators	7
2.2 Proposition of a new advanced isolator design	10
2.2.1 Variable Friction Isolator with concentric strips	11
3 Friction Pendulum System with variable friction profile	12
3.1 Design of the Isolator	12
3.1.1 Material Specifications	13
3.2 Analytical Modeling	14
3.2.1 Building Model	14
3.2.2 Isolator Model	17
4 Solution Strategy	21
4.1 Solution Strategy	21
4.1.1 Newmark- β Procedure	21
4.1.2 Application to the given system	22
4.1.2.1 Sticking Phase	22
4.1.2.2 Sliding Phase	23
4.1.2.3 Transition between phases	24

4.2 Solution steps for Variable Friction isolator and conventional FPS with constant friction	25
5 Computer Implementation	26
5.1 Step-by-step MATLAB algorithm	26
5.1.1 For the proposed isolator	26
5.1.2 For the conventional FPS	27
6 Results and Discussions	29
6.1 Earthquake Ground motions	29
6.2 System Characteristics	31
6.2.1 Superstructure	31
6.2.2 Seismic Isolator	33
6.3 Response Quantities Considered	35
6.4 Response to Near-Fault and Far-Field Earthquakes	35
6.4.1 Comparison with a Fixed base Structure	35
6.4.2 Comparison with a conventional FPS isolated structure	36
6.4.3 Force-Deformation diagrams of the Isolator	36
7 Summary and Conclusions	44
7.1 Conclusions	44
7.2 Scope of Future Work	45
A Response Plots	46
A.1 Response Comparison with Fixed base model	46
A.2 Base Displacement of the Isolator	64
A.3 Comparison with conventional FPS isolator	74
A.4 Force-Deformation diagrams of the Isolator	101
Bibliography	108

List of Figures

1.1	Comparison of Near-Fault and Far-Field Earthquakes	3
2.1	Comparison of the articulated slider of conventional (right) and variable curvature (left) FPS	10
2.2	Variable friction isolator with concentric strips	11
3.1	Orthographic view of the isolator	13
3.2	A 3-Dimensional view of a section of the isolator	13
3.3	An isometric view of a section through the isolator	14
3.4	N-Storey shear building model	15
3.5	Forces acting on the sliding interface	18
4.1	Friction profile of the considered isolator	25
6.1	Acceleration time history of the near-fault records	30
6.2	Acceleration response spectra of the near-fault earthquake records	31
6.3	Acceleration time history of the far-field records	32
6.4	Acceleration response spectra of the far-field earthquake records	33
A.1	Top storey acceleration (3-storey building) under far-field Hector Mine earthquake	46
A.2	Total Storey Drift (3-storey building) under far-field Hector Mine earthquake	47
A.3	Top storey acceleration (3-storey building) under far-field Imperial Valley earthquake	47
A.4	Total Storey Drift (3-storey building) under far-field Imperial Valley earthquake	48
A.5	Top storey acceleration (3-storey building) under far-field Loma Prieta earthquake	48
A.6	Total Storey Drift (3-storey building) under far-field Loma Prieta earthquake	49
A.7	Top storey acceleration (3-storey building) under far-field Northridge-01 earthquake	49
A.8	Total Storey Drift (3-storey building) under far-field Northridge-01 earthquake	50
A.9	Top storey acceleration (3-storey building) under near-fault Chi-Chi earthquake	50
A.10	Total Storey Drift (3-storey building) under near-fault Chi-Chi earthquake	51

A.11 Top storey acceleration (3-storey building) under near-fault Erzican earthquake	51
A.12 Total Storey Drift (3-storey building) under near-fault Erzican earthquake	52
A.13 Top storey acceleration (3-storey building) under near-fault Kobe earthquake	52
A.14 Total Storey Drift (3-storey building) under near-fault Kobe earthquake	53
A.15 Top storey acceleration (3-storey building) under near-fault Loma Prieta earthquake	53
A.16 Total Storey Drift (3-storey building) under near-fault Loma Prieta earthquake	54
A.17 Top storey acceleration (3-storey building) under near-fault Northridge-01 earthquake	54
A.18 Total Storey Drift (3-storey building) under near-fault Northridge-01 earthquake	55
A.19 Top storey acceleration (5-storey building) under far-field Imperial Valley earthquake	55
A.20 Total Storey Drift (5-storey building) under far-field Imperial Valley earthquake	56
A.21 Top storey acceleration (5-storey building) under far-field Loma Prieta earthquake	56
A.22 Total Storey Drift (5-storey building) under far-field Loma Prieta earthquake	57
A.23 Top storey acceleration (5-storey building) under far-field Northridge-01 earthquake	57
A.24 Total Storey Drift (5-storey building) under far-field Northridge-01 earthquake	58
A.25 Top storey acceleration (5-storey building) under near-fault Chi-Chi earthquake	58
A.26 Total Storey Drift (5-storey building) under near-fault Chi-Chi earthquake	59
A.27 Top storey acceleration (5-storey building) under near-fault Erzican earthquake	59
A.28 Total Storey Drift (5-storey building) under near-fault Erzican earthquake	60
A.29 Top storey acceleration (5-storey building) under near-fault Kobe earthquake	60
A.30 Total Storey Drift (5-storey building) under near-fault Kobe earthquake	61
A.31 Top storey acceleration (5-storey building) under near-fault Loma Prieta earthquake	61
A.32 Total Storey Drift (5-storey building) under near-fault Loma Prieta earthquake	62
A.33 Top storey acceleration (5-storey building) under near-fault Northridge-01 earthquake	62
A.34 Total Storey Drift (5-storey building) under near-fault Northridge-01 earthquake	63
A.35 Isolator Displacement (3-storey building) under far-field Imperial Valley earthquake	64
A.36 Isolator Displacement (3-storey building) under far-field Imperial Valley earthquake	65

A.37 Isolator Displacement (3-storey building) under far-field Loma Prieta earthquake	65
A.38 Isolator Displacement (3-storey building) under far-field Northridge-01 earthquake	66
A.39 Isolator Displacement (3-storey building) under near-fault Chi-Chi earthquake	66
A.40 Isolator Displacement (3-storey building) under near-fault Erzican earthquake	67
A.41 Isolator Displacement (3-storey building) under near-fault Kobe earthquake	67
A.42 Isolator Displacement (3-storey building) under near-fault Loma Prieta earthquake	68
A.43 Isolator Displacement (3-storey building) under near-fault Northridge-01 earthquake	68
A.44 Isolator Displacement (5-storey building) under far-field Imperial Valley earthquake	69
A.45 Isolator Displacement (5-storey building) under far-field Imperial Valley earthquake	69
A.46 Isolator Displacement (5-storey building) under far-field Loma Prieta earthquake	70
A.47 Isolator Displacement (5-storey building) under far-field Northridge-01 earthquake	70
A.48 Isolator Displacement (5-storey building) under near-fault Chi-Chi earthquake	71
A.49 Isolator Displacement (5-storey building) under near-fault Erzican earthquake	71
A.50 Isolator Displacement (5-storey building) under near-fault Kobe earthquake	72
A.51 Isolator Displacement (5-storey building) under near-fault Loma Prieta earthquake	72
A.52 Isolator Displacement (5-storey building) under near-fault Northridge-01 earthquake	73
A.53 Top storey acceleration (3-storey building) under far-field Hector Mine earthquake	74
A.54 Total Storey Drift (3-storey building) under far-field Hector Mine earthquake	75
A.55 Isolator Displacement (3-storey building) under far-field Hector Mine earthquake	75
A.56 Top storey acceleration (3-storey building) under far-field Imperial Valley earthquake	76
A.57 Total Storey Drift (3-storey building) under far-field Imperial Valley earthquake	76
A.58 Isolator Displacement (3-storey building) under far-field Imperial Valley earthquake	77
A.59 Top storey acceleration (3-storey building) under far-field Loma Prieta earthquake	77
A.60 Total Storey Drift (3-storey building) under far-field Loma Prieta earthquake	78

A.61 Isolator Displacement (3-storey building) under far-field Loma Prieta earthquake	78
A.62 Top storey acceleration (3-storey building) under far-field Northridge-01 earthquake	79
A.63 Total Storey Drift (3-storey building) under far-field Northridge-01 earthquake	79
A.64 Isolator Displacement (3-storey building) under far-field Northridge-01 earthquake	80
A.65 Top storey acceleration (3-storey building) under near-fault Chi-Chi earthquake	80
A.66 Total Storey Drift (3-storey building) under near-fault Chi-Chi earthquake	81
A.67 Isolator Displacement (3-storey building) under near-fault Chi-Chi earthquake	81
A.68 Top storey acceleration (3-storey building) under near-fault Erzican earthquake	82
A.69 Total Storey Drift (3-storey building) under near-fault Erzican earthquake	82
A.70 Isolator Displacement (3-storey building) under near-fault Erzican earthquake	83
A.71 Top storey acceleration (3-storey building) under near-fault Kobe earthquake	83
A.72 Total Storey Drift (3-storey building) under near-fault Kobe earthquake	84
A.73 Isolator Displacement (3-storey building) under near-fault Kobe earthquake	84
A.74 Top storey acceleration (3-storey building) under near-fault Loma Prieta earthquake	85
A.75 Total Storey Drift (3-storey building) under near-fault Loma Prieta earthquake	85
A.76 Isolator Displacement (3-storey building) under near-fault Loma Prieta earthquake	86
A.77 Top storey acceleration (3-storey building) under near-fault Northridge-01 earthquake	86
A.78 Total Storey Drift (3-storey building) under near-fault Northridge-01 earthquake	87
A.79 Isolator Displacement (3-storey building) under near-fault Northridge-01 earthquake	87
A.80 Top storey acceleration (5-storey building) under far-field Imperial Valley earthquake	88
A.81 Total Storey Drift (5-storey building) under far-field Imperial Valley earthquake	89
A.82 Isolator Displacement (5-storey building) under far-field Imperial Valley earthquake	89
A.83 Top storey acceleration (5-storey building) under far-field Loma Prieta earthquake	90
A.84 Total Storey Drift (5-storey building) under far-field Loma Prieta earthquake	90
A.85 Isolator Displacement (5-storey building) under far-field Loma Prieta earthquake	91

A.86 Top storey acceleration (5-storey building) under far-field Northridge-01 earthquake	91
A.87 Total Storey Drift (5-storey building) under far-field Northridge-01 earthquake	92
A.88 Isolator Displacement (5-storey building) under far-field Northridge-01 earthquake	92
A.89 Top storey acceleration (5-storey building) under near-fault Chi-Chi earthquake	93
A.90 Total Storey Drift (5-storey building) under near-fault Chi-Chi earthquake	93
A.91 Isolator Displacement (5-storey building) under near-fault Chi-Chi earthquake	94
A.92 Top storey acceleration (5-storey building) under near-fault Erzican earthquake	94
A.93 Total Storey Drift (5-storey building) under near-fault Erzican earthquake	95
A.94 Isolator Displacement (5-storey building) under near-fault Erzican earthquake	95
A.95 Top storey acceleration (5-storey building) under near-fault Kobe earthquake	96
A.96 Total Storey Drift (5-storey building) under near-fault Kobe earthquake	96
A.97 Isolator Displacement (5-storey building) under near-fault Kobe earthquake	97
A.98 Top storey acceleration (5-storey building) under near-fault Loma Prieta earthquake	97
A.99 Total Storey Drift (5-storey building) under near-fault Loma Prieta earthquake	98
A.100 Isolator Displacement (5-storey building) under near-fault Loma Prieta earthquake	98
A.101 Top storey acceleration (5-storey building) under near-fault Northridge-01 earthquake	99
A.102 Total Storey Drift (5-storey building) under near-fault Northridge-01 earthquake	99
A.103 Isolator Displacement (5-storey building) under near-fault Northridge-01 earthquake	100
A.104 Force-Deformation diagram (3-storey building) under far-field Imperial Valley earthquake	101
A.105 Force-Deformation diagram (3-storey building) under far-field Loma Prieta earthquake	102
A.106 Force-Deformation diagram (3-storey building) under far-field Northridge-01 earthquake	102
A.107 Force-Deformation diagram (3-storey building) under near-fault Chi-Chi earthquake	103
A.108 Force-Deformation diagram (3-storey building) under near-fault Erzican earthquake	103
A.109 Force-Deformation diagram (3-storey building) under near-fault Loma Prieta earthquake	104
A.110 Force-Deformation diagram (5-storey building) under far-field Imperial Valley earthquake	104

A.111Force-Deformation diagram (5-storey building) under far-field Loma Prieta earthquake	105
A.112Force-Deformation diagram (5-storey building) under far-field Northridge-01 earthquake	105
A.113Force-Deformation diagram (5-storey building) under near-fault Chi-Chi earthquake	106
A.114Force-Deformation diagram (5-storey building) under near-fault Erzican earthquake	106
A.115Force-Deformation diagram (5-storey building) under near-fault Loma Prieta earthquake	107

List of Tables

6.1	Near-Fault Earthquake Ground Motions	30
6.2	Far-Field Earthquake Ground Motions	31
6.3	Building Properties	34
6.4	3-Storey Building	34
6.5	5-Storey Building	34
6.6	Peak Response Quantities for the 3-storey building	37
6.7	Peak Response Quantities for the 5-storey building	38
6.8	Average Response Quantities under far-field and near-fault earthquakes .	39
6.9	Peak Response Quantities for the 3-storey building	40
6.10	Peak Response Quantities for the 5-storey building	41
6.11	Average Response Quantities under far-field and near-fault earthquakes .	42

*Dedicated to the survivors of the
Great 2011 Tohoku Earthquake*

Chapter 1

Introduction

ARTHQUAKES have been the most destructive natural force throughout human history. Houses have been obliterated, towns have been burned away in fires and cities have been completely disfigured. But as is the case with so many other natural forces, the catastrophe associated with earthquakes can be evaded by following the appropriate building practices. Flexible structures with effective energy dissipation are more resilient against earthquake damage. The increasingly popular practice of Seismic isolation is another approach to building earthquake resistant structures which has shown potential for better performance than the presently prevalent ductile design approach. But the Near-Fault earthquakes have been a major cause for concern with seismically isolated buildings. This thesis consists of a study dealing with some possible improvement in the design of seismic isolators.

1.1 A brief about Seismic Isolation

Seismic Isolation (or Base Isolation) is a technique of building structures with high degree of earthquake resistance by isolating or detaching the structure from the rigid ground support. This detachment provides excellent flexibility in the event of an earthquake, so that the large sways of the building are concentrated only at the base and no additional demands are imposed on other load carrying elements of the structure. The basic philosophy behind this idea is, what is often referred to as, "Period-Shifting." The fundamental period of a building is shifted by seismic isolation to a longer period range,

away from the acceleration amplification frequency band of the earthquake response spectra.

This basic approach has been implemented in various ways over the past hundred years ranging from early attempts with plane low friction surfaces as sliding isolators to ball type roller bearings. A historical sketch of this development is provided by [Kelly \[1986\]](#). Since the recent advancements in the isolation technology, two main types of bearings have emerged as most popular in practical implementation [[Kani, 2008](#)], namely elastomeric and sliding isolator bearings. Elastomeric bearings provide isolation through a low horizontal stiffness layer. These bearings also provide energy dissipation through a lead core or through synthetic rubber components. Sliding isolation bearings isolate the structure by providing a low friction surface for the base to slide on. This friction also contributes to coulomb damping.

A full scale study illustrating the effectiveness of seismic isolation using elastomeric isolators was presented by [Moroni et al. \[1998\]](#) and large number of buildings have been built using this concept in earthquake prone countries [[Naeim and Kelly, 1999a](#), Chapter 1]. New Zealand was one of the first countries to begin with the implementation of seismic isolation in buildings and since then there has been continuous adoption in other countries, particularly Japan [[Kani, 2008; Nakata, 2009](#)]. And over the years, the superior performance of isolated buildings [[Zakoda, 2011](#)] in earthquake events has further reinforced this ideology.

Seismic Isolation is a particularly attractive strategy for earthquake protection of buildings because of the reduced transmitted accelerations in the building through the isolated base. Therefore the non-structural component damage is greatly reduced and this technique is extremely favorable for application in buildings with valuable instruments/equipments [[Myslimaj et al., 2003](#)].

1.2 Impact of Near-Fault Earthquakes

Seismic Isolation does accomplish advanced seismic protection; objectives but this technique still has some shortcomings. Presence of long period pulses in Near-Fault earthquakes have been identified as a major concern in the seismic design of flexible buildings

[Alavi and Krawinkler, 2000; Hall et al., 1995]. Most far-field earthquakes are generally rich in low period range of the spectral acceleration; so building flexible structure provides safety from the damaging effect of such earthquake events. A comparison of the typical response spectrum of near fault and far-field earthquakes is shown in Figure 1.1. But this also means that these structures are not well suited to resist earthquakes with significant long period components. These long period components have also been associated with the soft sub soil conditions [Mendoza and Auvinet, 1988].

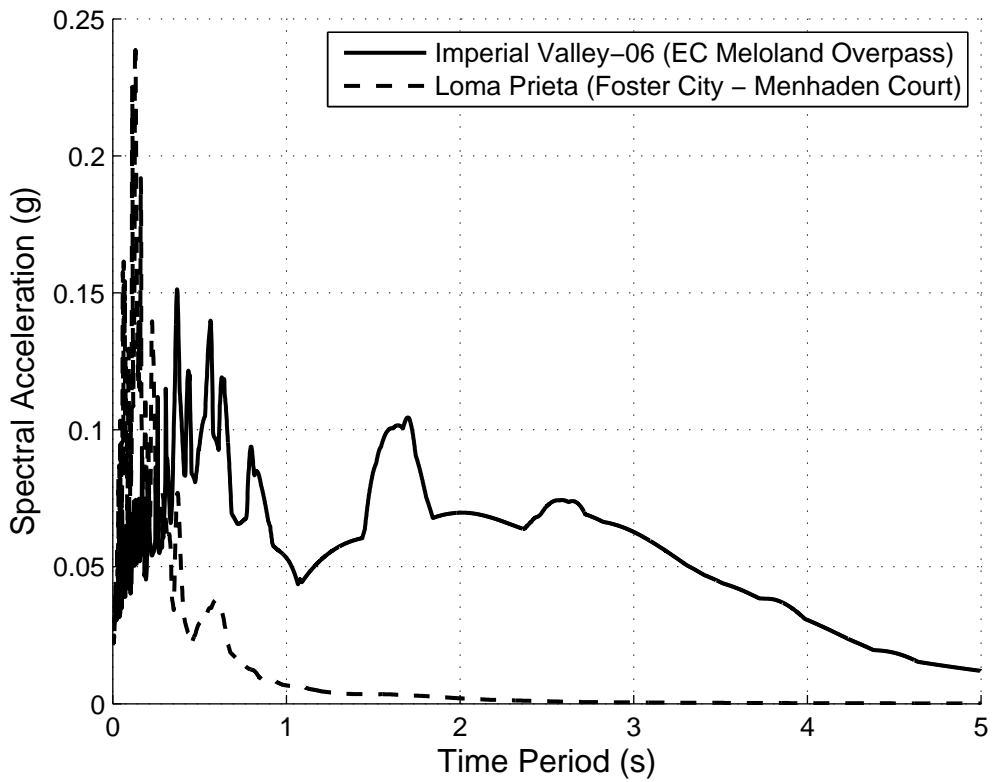


FIGURE 1.1: Comparison of Near-Fault and Far-Field Earthquakes

This susceptibility of flexible structures also applies to the otherwise superior seismic isolation systems as the idea of period shift fails to deliver favorable effects. The fundamental period of the isolated structures, which is away from the dominant period of far field earthquakes, fall dangerously close to the dominant period of near fault earthquakes resulting resonating response of the isolated structure. Because of this reason, the use seismic isolation systems is avoided near active fault zones.

1.3 Scope of the Thesis

With the objective of achieving an effective seismic isolation system for adoption in near-fault earthquake zones, the scope of the present study covers the following:

- Detailed review of the existing/proposed approaches of seismic isolation for near-fault earthquakes.
- Proposition of a new innovative isolation system for better performance in near-fault earthquakes.
- Evaluation of the response of the proposed isolation system based on the comparison of the analysis results of the dynamic response of a multi-storey shear frame type building structure with the proposed isolation system against the results of the dynamic response analysis of the same structure with the conventional isolation system.

1.4 Organization of the Thesis

This thesis has been organized into the following chapters.

Chapter 1 gives a brief introduction of the problem by describing the seismic isolation systems and the conflict with near-fault earthquakes.

Chapter 2 covers a detailed review of various design and isolation approaches for suitable performance in near-fault earthquakes.

Chapter 3 details the design of a new proposed seismic isolation system with formulations of the analytical models for the proposed system.

Chapter 4 develops a solution strategy for the developed model equations for response under selected earthquake ground motions.

Chapter 5 describes the computer implementation of the solution strategy using MATLAB.

Chapter 6 discusses the response results obtained from the analysis and compares the new proposed isolator against the fixed base structure and the conventional Friction Pendulum System (FPS).

Chapter 7 provides a conclusion to the thesis by summarizing the response results and listing the limitations and the scope of future work of the study.

Chapter 2

Seismic Isolation Systems for Near-Fault Earthquakes

SINCE the identification of the issue of long period waves in the performance of seismic isolation systems many studies have attempted to devise new improvements into the seismic isolation technique. This chapter will provide a critical review of such approaches before proposing a new isolation system for near fault earthquakes.

2.1 Existing approaches to Seismic Isolation

Many researchers have studied the effect of near-fault earthquakes on the various types of isolation systems. These approaches can be broadly divided into two categories: elastomeric and sliding-type isolators.

2.1.1 Elastomeric Isolators

The breakthrough in the rubber technology in early 80s was crucial to the success of elastomeric isolators. This allowed the rubber with desirable properties to be used for seismic isolation. *Linear Rubber* bearings (with linear force-deformation behavior,) *High Damping Rubber* bearings (with hardening properties at higher displacements,) *Lead Rubber* bearings (with a lead core to provide hysteretic damping) and other hybrid isolation bearings have been used in the past to provide seismic isolation in buildings[[Naeim and Kelly, 1999b](#), Chapter 3].

Since elastomeric bearings are the most popular in terms of commercial use [Kani, 2008], many researchers have studied their performance under near-fault earthquakes. Shen et al. [2004] investigated the response of lead rubber bearings under near-fault earthquake motions and found the structural response be amplified for the cases where the effective period of the isolated structure is close to the dominant pulse period of the near fault earthquakes. Mazza and Vulcano [2012] emphasized the effect of considering the vertical earthquake component in the response of an isolated buildings resting on deformable high damping rubber bearings. The amplification in the response of the isolated buildings may be countered by using supplemental viscous damping. Providakis [2009] and Jangid [2007] studied the effect of using supplemental dampers in conjunction with elastomeric bearings to improve response under near-fault ground motions. Using additional damping results in isolation being relatively ineffective for moderate far-field earthquakes and higher accelerations and forces being transferred into the structure, although the base displacements are sufficiently controlled.

Use of costly additional viscous dampers and compromised seismic performance in moderate earthquakes thus render the use of popular elastomeric isolators in near-fault earthquake prone region to be highly uneconomical and unsuitable.

2.1.2 Sliding-type Isolators

Sliding isolators are based on the simple concept of providing protection from earthquakes by completely detaching the building from ground by means of friction bearings. Most practical implementations of sliding isolation systems, called Friction Pendulum Systems (FPS,) use a curved surface in order to provide a restoring force. Mokha et al. [1991] experimentally evaluated performance of FPS and established it to be effective in protecting the building during strong earthquake shaking. Friction Pendulum Systems are more durable, temperature-insensitive and torsion-resistant as compared to the elastomeric bearings. Its high strength and stability also make it versatile for applications in varied structural systems [Wang, 2002]. The presence of static friction also provides sufficiently high initial stiffness to resist wind loads as well as provides energy dissipation in the form of coulomb damping.

The capability to support large displacements without any instability issues makes the pendulum bearings the preferred choice of isolation for near-fault earthquakes over elastomeric bearings. Various approaches for seismic isolation using friction pendulum system in near fault earthquakes have been attempted. [Zayas and Low \[2000\]](#) covered the use of large FPS for isolation in few engineering projects in near fault zones. Near-fault earthquakes impose unusually high drift and force demands for conventional ductile design. Use of FPS bearings with large periods (5 seconds) in such cases is possible to ensure desired levels of safety. And the large displacement demands at the isolator level can be met by having a large size of the pendulum bearing as has been done in *San Francisco Airport International Terminal, Benicia-Martinez Bridge and Hayward City Hall* [[Zayas and Low, 2000](#)].

Provision of supplemental damping with FPS isolators is another possible solution in near fault earthquake zones. [Providakis \[2009\]](#) found that using damping reduced the superstructure accelerations in near-fault motions but it failed to provide similar reductions for far-field motions. [Jangid \[2005b\]](#) researched the response of FPS under near-fault motions to find optimum values of friction coefficient associated with the sliding surface. [Kelly \[1999\]](#) also concluded that the use of damping may not be the best solution to effective seismic isolation under various earthquake hazard levels.

Since conventional Friction Pendulum Systems have a constant radius of curvature, and hence a fixed isolation time period, they are susceptible to long period waves of near-fault ground motions. However if this frequency of oscillation of the friction pendulum can be varied, then the pendulum system may record better performance in long period waves. This approach has been adopted by using variable curvature sliding surfaces in pendulum oscillators. [Pranesh and Sinha \[2000\]](#) proposed a design of pendulum isolator using an elliptical sliding surface to provide the fundamental frequency of the isolator that continuously decreases with increasing isolator displacement resulting in softening of the isolator response. [Tsai et al. \[2003\]](#) investigated the response of variable curvature isolator under near-fault earthquakes and found these devices to be effective in reducing force and acceleration responses in the superstructure but ineffective in controlling isolator base displacements. [Sharma and Jangid \[2012\]](#) investigated the performance of variable curvature isolators using supplemental damping and found the results to be similar with damping application in constant curvature FPS. [Lu et al. \[2004\]](#) suggested using a sixth-order polynomial function to represent the sliding surface of a pendulum

isolator. This design incorporated the softening and hardening of response with increasing isolator displacement into the pendulum design. [Lu et al. \[2006\]](#) researched using a curvature variation in the form of conical shape to provide varying isolation frequency. A significant amount of research has been invested into studying the behavior of the elliptical sliding isolators including study about torsional response [[Murnal and Sinha, 2004](#); [Soni et al., 2010](#)] and investigations about double pendulum systems [[Panchal et al., 2010](#); [Soni et al., 2011](#)].

The use of multiple sliding surfaces in pendulum systems is another popular modification to the conventional isolator design. [Constantinou \[2004\]](#) and [Fenz and Constantinou \[2006\]](#) presented the design and operational principles of a pendulum isolator sliding on two sliding concave surfaces. The flexibility in design facilitated by the possibility of using different materials on different sliding surfaces of different radii of curvature is considered to be the major advantage of this design. [Malekzadeh and Taghikhany \[2010\]](#) compared the performance of double pendulum with single FPS and found the adaptive properties associated with using dual sliding surfaces to be effective in providing reduced earthquake response during earthquake shaking. [Morgan and Mahin \[2008\]](#) investigated seismic isolation with triple pendulum bearings to obtain seismic protection for a range of seismic hazard. The trilinear force-deformation behavior does provide protection in strong earthquakes but it can be too stiff for moderate, more frequent earthquake motions. The softening and hardening characteristics of triple pendulum bearings can be effective against near-fault earthquakes but no conclusive research has been done this area.

[Panchal and Jangid \[2008\]](#) suggested another approach to provide seismic isolation in near fault zones by using varying friction coefficient for the sliding surface. The study postulates that the use of increased friction with increasing slider displacements may provide an opportunity for the slider to stick during motion, thus shifting the period of vibration away from the dominant period of near fault earthquakes. This isolation strategy resulted in better isolator displacements and base shears while keeping accelerations in the superstructure to be almost same as compared the conventional FPS design.

2.2 Proposition of a new advanced isolator design

The previous section reviewed various approaches for isolation against long period waves of near fault earthquakes. However, these approaches appear to be ineffective due to the following reasons:

Supplemental Damping increases the cost of the isolation system and only provides partial solution by reducing isolator displacements. Higher base shears are observed and the isolation is not as effective for moderate earthquakes.

Large Isolators are often uneconomical and their implementation is not suitable for all types of building projects.

Variable Curvature Isolators do provide shift in the isolation period with increasing isolator displacements but their implementation poses a practical problem. Having a constant curvature in FPS means that the articulated slider and the sliding surface have consistent contact, which facilitates smooth sliding and allows proper transfer of superstructure gravity loads into the foundation. But with variable curvature sliders, this contact is not the same. As shown in Figure 2.1, the articulated slider in a variable pendulum system has only a limited contact with the bottom sliding surface, which may result in dangerous stress concentrations at the sliding surface. This insufficient contact is due to the fact that the sliding surface and the articulated slider have different curvatures (elliptical sliding surface.) The articulated slider of the variable curvature oscillator also has a high propensity to roll instead of slide (as with elliptical ball isolators [Butterworth, 2001; Jangid and Londhe, 1998]) on the sliding surface which may lead to undesirable response of pendulum system.



FIGURE 2.1: Comparison of the articulated slider of conventional (right) and variable curvature (left) FPS

Multiple Sliding Surface Isolators provide adaptive behavior with trilinear force-displacement characteristics, but lack any conclusive study with regards to near-fault earthquake input motions. Besides, these bearings can be very costly to implement, owing to their complicated design.

2.2.1 Variable Friction Isolator with concentric strips

As has been discussed previously there is a need for an isolation system that provides safety in both moderate and strong earthquakes, does not amplify response to long period pulses and is practically implementable in its design. The goal of providing softening and hardening characteristics (as suggested by [Kelly \[1999\]](#)) is accomplished by using concentric strips of materials with different tribological properties, as illustrated by Figure 2.2. The central circular region-1 and the outermost circular strip (i.e. region-3) have the same values (μ_1) of frictional coefficient; whereas, the middle circular strip (i.e. region 2) has the value of frictional coefficient (μ_2) lower than μ_1 . This allows a very practical way to allow for variation of friction (as suggested by [Panchal and Jangid \[2008\]](#)) along the sliding surface of the pendulum. Use of various materials in different zones of the isolator will result in desirable frictional characteristics. Detailed modeling and design of this proposed isolator will be discussed in the next chapter.

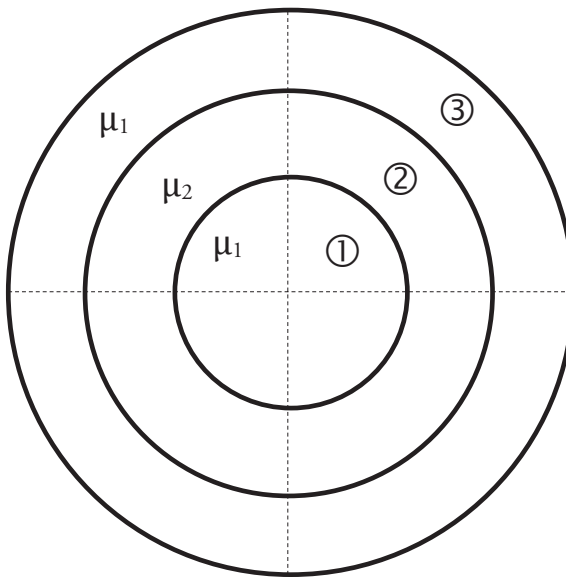


FIGURE 2.2: Variable friction isolator with concentric strips

Chapter 3

Friction Pendulum System with variable friction profile

Friction pendulum with a variable friction profile can provide significantly better performance than the conventional FPS [Panchal and Jangid, 2008]. This chapter will detail the design and other specifications of this newly proposed sliding isolation system followed by analytical modeling for response evaluation.

3.1 Design of the Isolator

Most of the basic physical design of the new proposed pendulum isolator is common with the widely used conventional FPS design [Mokha et al., 1991]. Figures 3.1, 3.2 and 3.3 illustrate the common components of the isolator. The *Concave Sliding Surface* is the spherical bottom surface upon which the pendulum motion of the slider is supposed to take place. The *Articulated Slider* having the same spherical contact surface profile as of the concave sliding surface, is a small sliding piece that facilitates smooth motion between the fixed bottom plate and the superstructure above. The bottom surface of the slider is in continuous contact with the sliding surface as they both have the same curvature while upper surface of the slider is in contact with a housing plate that contains the slider within a segmental spherical depression. This arrangement between the upper housing plate and the slider is made to ensure that the upper housing plate remains horizontal even when the isolator has displaced by some amount, as adjusted by the

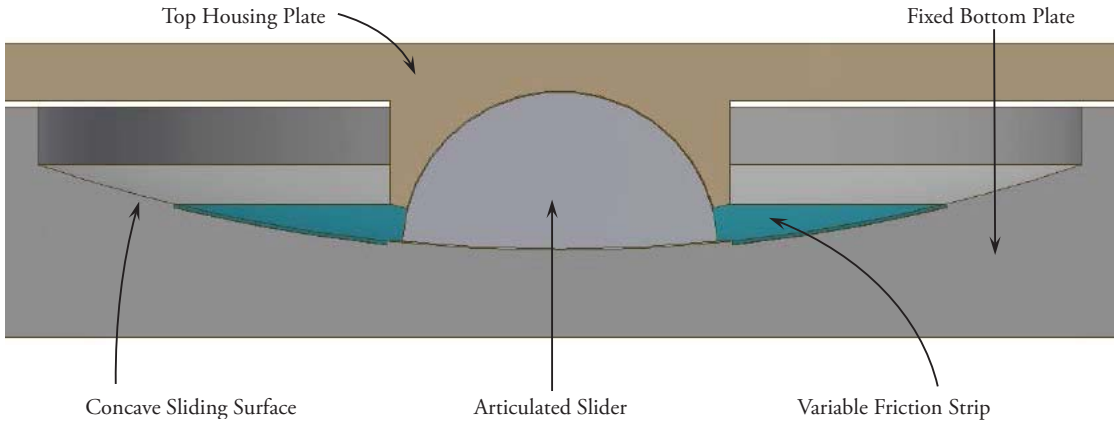


FIGURE 3.1: Orthographic view of the isolator

rotations of the articulated slider. The *Variable Friction Strip* is a concentric ring of a sliding surface having different roughness than that of the adjacent concentric friction strip.

3.1.1 Material Specifications

The isolator bearings are generally made of steel to support the huge gravity loads from the superstructure while all the sliding interfaces are coated or polished appropriately to provide smooth sliding. The sliding concave surface is made of stainless steel and the concentric middle strip used to provide a different frictional surface is made of a low friction material (many commercial alternatives including OILES Techmet and Maurer MSM [Beutler et al., 2011] are available; but this thesis will confine the discussion to the popularly available Teflon or PTFE.) The articulated slider has the lower sliding surface made of PTFE and the upper part that rotates inside the spherical cavity of the

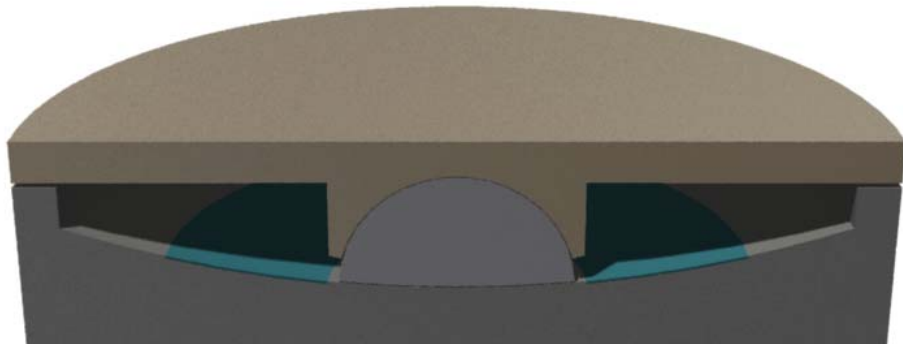


FIGURE 3.2: A 3-Dimensional view of a section of the isolator

housing plate is provided with low friction material which is same as the material inside the spherical cavity of the housing plate.

The PTFE bearing and steel sliding surface have friction coefficient in the range of 0.05 to 0.15 while PTFE on PTFE has friction coefficient of 0.04 [Elert, 1998; Taylor and Stanton, 2010]. This means that the use of PTFE in the concentric friction strip provides a region of low friction as desired for the softening of the response.

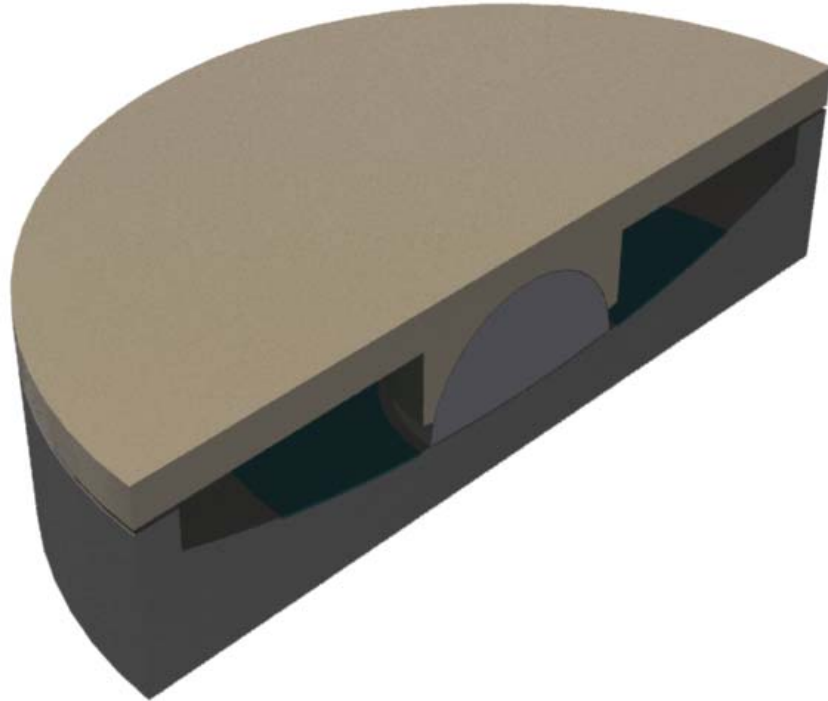


FIGURE 3.3: An isometric view of a section through the isolator

3.2 Analytical Modeling

The response of the proposed isolator bearing will be evaluated subjected to recorded earthquake ground motions from near-fault and far-field regions for comparison of performance of the new system against the conventional isolators.

3.2.1 Building Model

The building model represents the model of the superstructure or the building above the isolator level. The model used for this study is illustrated by Figure 3.4. The various important features of this structural model are discussed in the following:

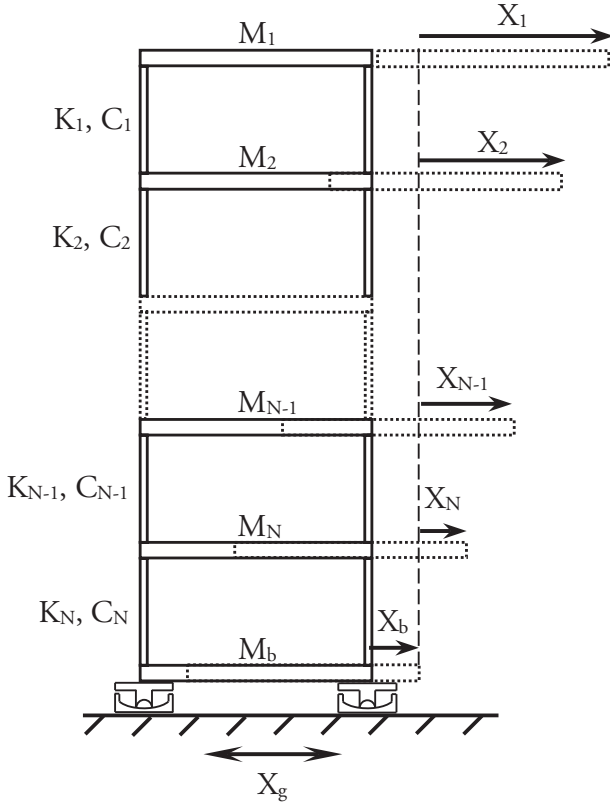


FIGURE 3.4: N-Storey shear building model

Multi-Storey: The building is considered to be consisting of multiple stories to appropriately model the flexibility of the structure. The modeling is illustrated for a general N-storey building.

Elastic Columns: The building columns are modeled as linear elastic. This assumption is made based on the premise that the seismic isolation reduces the forces in the superstructure to such low values that they remain in elastic range during earthquake excitation and do not enter the non-linear elastic range [Jangid, 2005a]. Besides, many studies in seismic isolation have also used a rigid superstructure model assuming that all displacements are concentrated at the isolator level and the superstructure movements are negligible [Barghian and Shahabi, 2007; Kulkarni and Jangid, 2002].

Shear Building: The building frame considered is shear building type, implying that the floor diaphragms are perfectly rigid and have only unidirectional displacements. One degree-of-freedom is considered for each floor.

Structural Damping: Mass and Stiffness proportional Rayleigh Damping is considered and the damping coefficients are determined based on assumed values of damping for the first two modes of vibration of the superstructure.

The governing equations for the considered shear building model can be obtained for response in unidirectional earthquake excitations by Newton's method as:

$$[M] \{ \ddot{X} \} + [C] \{ \dot{X} \} + [K] \{ X \} = -[M] \{ I \} (\ddot{X}_b + \ddot{X}_g) \quad (3.1)$$

where $[M]$ is the mass matrix, size $N \times N$, of the shear building given by,

$$[M] = \begin{bmatrix} M_1 & 0 & \dots \\ 0 & M_2 & \dots \\ \vdots & \vdots & \ddots & \vdots & \vdots \\ & & \dots & M_{N-1} & 0 \\ & & \dots & 0 & M_N \end{bmatrix} \quad (3.2)$$

$[K]$ is the stiffness matrix, size $N \times N$, given by,

$$[K] = \begin{bmatrix} K_1 & -K_1 & \dots \\ -K_1 & K_1 + K_2 & \dots \\ \vdots & \vdots & \ddots & \vdots & \vdots \\ & & \dots & K_{N-2} + K_{N-1} & -K_{N-1} \\ & & \dots & -K_{N-1} & K_{N-1} + K_N \end{bmatrix} \quad (3.3)$$

$\{X\}$, $\{\dot{X}\}$ and $\{\ddot{X}\}$ are the displacement, velocity and acceleration vectors respectively, each of size $N \times 1$, which are determined with reference to the isolator displacement, X_b . $\{I\}$ is the influence vector of size $N \times 1$ and carries the values of unity for the current problem. \ddot{X}_b and \ddot{X}_g are the base and ground accelerations respectively.

$[C]$ is the damping matrix of size $N \times N$ which is proportional to the mass and stiffness matrices and is given by:

$$[C] = a [M] + b [K] \quad (3.4)$$

where a and b are the proportionality constants and can be obtained by using assumed damping for the first two modes [Wilson, 2004], as given below:

$$\begin{bmatrix} \zeta_1 \\ \zeta_2 \end{bmatrix} = \frac{1}{2} \begin{bmatrix} \frac{1}{\omega_1} & \omega_1 \\ \frac{1}{\omega_2} & \omega_2 \end{bmatrix} \begin{bmatrix} a \\ b \end{bmatrix} \quad (3.5)$$

where ω_1 and ω_2 are the modal frequencies of the first two modes obtained from the modal analysis; ζ_1 and ζ_2 are the assumed damping ratios for first two modes.

3.2.2 Isolator Model

The previous section defined the model for the superstructure and this section will continue with the modeling of the behavior at the isolator level. Some important assumptions regarding this model are as following:

Rigid Steel Surfaces: All the steel sliding interfaces are assumed as rigid. No material deformation takes place either in the articulated slider or the sliding interface.

Overturning: The sliding surfaces of the isolator are assumed to be always in contact and no overturning is assumed to take place.

Vertical Acceleration: Mazza and Vulcano [2008, 2009] studied the effects of considering vertical earthquake acceleration component in the response analysis of isolation systems and concluded that the consideration does not have any significant effect on the response of isolation system. Therefore, this study will not consider the vertical acceleration effects.

Friction Coefficient: The friction coefficient of an interface is a function of relative sliding velocity between the interfaces, the contact pressure and the temperature [Nadein et al., 2007]. Constantinou et al. [2007] found that the variation of friction with temperature and pressure for the PTFE bearing to be insignificant. The friction coefficient does vary with sliding velocity [Dolce et al., 2005] but this variation can be neglected for the study of seismic isolation (as has been done by [Fakhouri and Igarashi, 2012; Lu and Yang, 1997; Mostaghel and Khodaverdian, 1987; Su et al., 1989; Yang et al., 1990].) The friction coefficient only slightly reduces with sliding velocity, and hence consideration of its maximum value is considered to be

safe for the purposes of estimating isolator displacements and other related parameters. [Fan et al. \[1990\]](#) also found that the use of sliding velocity dependent friction has only negligible effects on the response of the isolation system. Hence this variation has not been considered in this study.

Small Isolator displacements: The displacements at the isolator level have been assumed to be small enough so that the angular displacement of the articulated slider from the central starting location can be approximated by small angle approximation. This is particularly true due to the large radius of curvature of the sliding surface upon which the isolator slides.

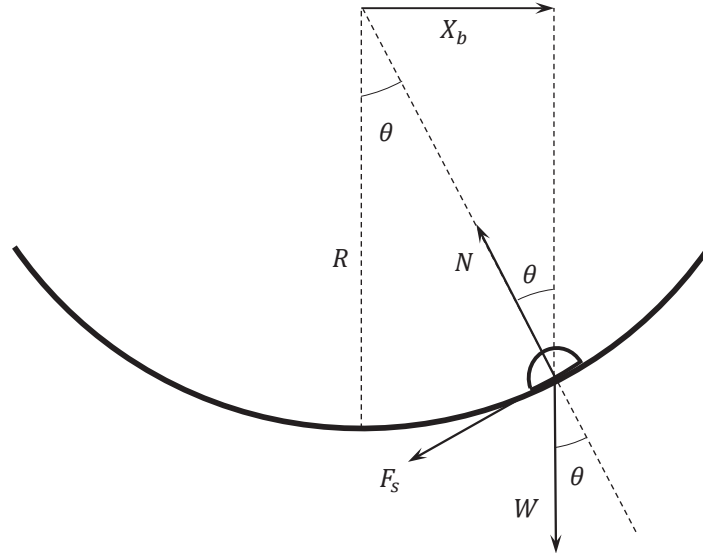


FIGURE 3.5: Forces acting on the sliding interface

The governing equation for the base level where the isolator is located can also be determined based on Newton's Laws. The motion of the pendulum isolator can be considered in stages: the *Sticking Phase*, where the ground motion has not reached strong enough levels to overcome the limiting static frictional force at the base of the isolator; and the *Sliding Phase*, where the articulated slider and the concave sliding surface exhibit relative motion. The approach taken here follows the basic physical operational principle of pendulum motion as described by [Al-Hussaini et al. \[1994\]](#).

The equation for the sliding phase is given as:

$$M_b \ddot{X}_b + F_{restoring} - K_N X_N - C_N \dot{X}_N = -M_b \ddot{X}_g \quad (3.6)$$

where M_b is the base mass, X_b is the displacement of the base and $F_{restoring}$ is the restoring force provided by the friction and the curved geometry of the sliding surface. The $F_{restoring}$ can be determined from the force diagram illustrated by the Figure 3.5.

$$F_{restoring} = F_s \cos \theta + W \tan \theta \quad (3.7)$$

where θ is the angular displacement of the articulated slider, F_s is the dynamic friction force at the sliding interface and W is the total gravity force of the building on the isolators. Since the isolator displacements are small in comparison to the large radius of curvature of the sliding surface, the trigonometric terms can be approximated as follows,

$$F_{restoring} = F_s + W \frac{X_b}{R} \quad (3.8)$$

where R is the radius of curvature of the sliding surface. The dynamic friction force F_s is constant in magnitude during sliding, and can be determined based on the coulomb friction principle with its direction being opposite to the direction of sliding.

$$F_s = sgn(\dot{X}_b) \mu W \quad (3.9)$$

During the sticking phase, the base mass moves with the ground and the internal friction force mobilized at the sliding interface can be given as:

$$F_s = -M_b \ddot{X}_g + K_N X_N + C_N \dot{X}_N \quad (3.10)$$

which is subject to the limiting maximum value of,

$$F_{s_{limit}} = \mu W \quad (3.11)$$

During the sticking phase, the displacement remains static while acceleration and velocity are zero.

$$X_b = constant; \quad \dot{X}_b = 0; \quad \ddot{X}_b = 0; \quad (3.12)$$

The equations 3.1 and 3.6 define the behavior of the system during sliding phase and equations 3.1 and 3.12 determine the system while in sticking phase. The system starts in sticking at the beginning of the time history and transits to the sliding phase when the frictional force at the base (determined by equation 3.10) exceeds the limiting value (determined by equation 3.11.)

Chapter 4

Solution Strategy

THE system model defined in the previous chapter will be solved for evaluating the response under selected input ground motions. The general governing equations for a N-storey building model will be solved in general form.

4.1 Solution Strategy

Although the superstructure is modeled as linear elastic, the overall governing equations of the system are essentially nonlinear due to the presence of the friction force. Due to this nonlinearity, the system equations can not be solved by the conventional modal superposition method. Hence the current system of nonlinear differential equations has to be solved numerically using step-by-step integration procedure.

4.1.1 Newmark- β Procedure

Newmark- β integration scheme with *Constant Average Acceleration* is used in this study. Between any two consecutive time steps, the acceleration is assumed to be constant (as average between the two time steps considered) and the other quantities are calculated accordingly. Based on this principle, the acceleration and velocity for the next time step can be given in terms of the quantities determined for the previous step and the displacement for the next time step. The expressions for this, considering displacement(u ,)

velocity(\dot{u}) and acceleration(\ddot{u}) between two time steps n and $n+1$ have been determined by [Hewett \[2010\]](#) and can be given as:

$$\ddot{u}_{n+1} = \frac{4}{(\Delta t)^2} (u_{n+1} - u_n - \Delta t \dot{u}_n) - \ddot{u}_n \quad (4.1a)$$

$$\dot{u}_{n+1} = \dot{u}_n + \frac{2}{\Delta t} (u_{n+1} - u_n - \Delta t \dot{u}_n) \quad (4.1b)$$

These relations are applied to the equilibrium equation at $(n + 1)^{th}$ time step. So the two equilibrium equations at time step n and $n + 1$ can be solved for the displacements at the respective time steps which in turn can be used to determine other accelerations and displacements from the equations [4.1a](#) and [4.1b](#)

4.1.2 Application to the given system

The approach described in the previous section will be used to solve for the equations formulated in section [3.2](#). This section will discuss the solution steps for the *Sticking Phase* and the *Sliding Phase* separately.

4.1.2.1 Sticking Phase

For the sticking phase, the isolator is static and \ddot{X}_b is determined from equation [3.12](#) to be equal to zero. So the governing equation [3.1](#) reduces to,

$$[M] \{ \ddot{X} \} + [C] \{ \dot{X} \} + [K] \{ X \} = - [M] \{ I \} \ddot{X}_g \quad (4.2)$$

which is the general equation for the dynamic response of a multi storey shear frame and can be solved by using linear analysis.

4.1.2.2 Sliding Phase

For the sliding phase, the system consists of $N + 1$ degrees of freedom as represented by equations 3.1 and 3.6. The equations 4.1a and 4.1b are used for $\{X\}$ and X_b .

$$\{\ddot{X}\}_{n+1} = \frac{4}{(\Delta t)^2} (\{X\}_{n+1} - \{X\}_n - \Delta t \{\dot{X}\}_n) - \{\ddot{X}\}_n \quad (4.3a)$$

$$\{\dot{X}\}_{n+1} = \{\dot{X}\}_n + \frac{2}{\Delta t} (\{X\}_{n+1} - \{X\}_n - \Delta t \{\dot{X}\}_n) \quad (4.3b)$$

$$\ddot{X}_{b_{n+1}} = \frac{4}{(\Delta t)^2} (X_{b_{n+1}} - X_{b_n} - \Delta t \dot{X}_{b_n}) - \ddot{X}_{b_n} \quad (4.4a)$$

$$\dot{X}_{b_{n+1}} = \dot{X}_{b_n} + \frac{2}{\Delta t} (X_{b_{n+1}} - X_{b_n} - \Delta t \dot{X}_{b_n}) \quad (4.4b)$$

These are substituted into the governing system equations (i.e. equations 3.1 and 3.6) at $(n + 1)^{th}$ time step and the resulting equations are:

$$[M] \left\{ \ddot{X} \right\}_{n+1} + [C] \left\{ \dot{X} \right\}_{n+1} + [K] \{X\}_{n+1} = -[M] \{I\} \left(\ddot{X}_{b_{n+1}} + \ddot{X}_{g_{n+1}} \right) \quad (4.5a)$$

$$M_b \ddot{X}_{b_{n+1}} + F_s + \frac{W}{R} X_{b_{n+1}} - K_N X_{N_{n+1}} - C_N \dot{X}_{N_{n+1}} = -M_b \ddot{X}_{g_{n+1}} \quad (4.5b)$$

The substitution and subsequent simplification yields a system of equation in terms of $\{X_{n+1}\}$ and $X_{b_{n+1}}$,

$$\left(\frac{4}{(\Delta t)^2} [M] + \frac{2}{\Delta t} [C] + [K] \right) \{X_{n+1}\} + \frac{4}{(\Delta t)^2} [M] \{I\} X_{b_{n+1}} = F_{\{X\}} \quad (4.6a)$$

$$\left(\frac{4M_b}{(\Delta t)^2} + \frac{W}{R} \right) X_{b_{n+1}} - \left(\frac{2C_N}{\Delta t} + K_N \right) X_{N_{n+1}} = F_{X_b} \quad (4.6b)$$

where $F_{\{X\}}$ and F_{X_b} are given as,

$$\begin{aligned} F_{\{X\}} = & -[M] \{I\} \ddot{X}_{g_{n+1}} + [M] \left\{ \frac{4}{(\Delta t)^2} \left(\{X\}_n + \{I\} X_{b_n} + \Delta t \{\dot{X}\}_n + \Delta t \{I\} \dot{X}_{b_n} \right) + \{\ddot{X}\}_n + \{I\} \ddot{X}_{b_n} \right\} \\ & + [C] \left\{ \frac{2}{\Delta t} \{X_n\} + \{\dot{X}\}_n \right\} \end{aligned} \quad (4.7a)$$

$$F_{X_b} = -M_b \ddot{X}_{g_{n+1}} + M_b \left\{ \frac{4}{(\Delta t)^2} \left(X_{b_n} + \Delta t \dot{X}_{b_n} \right) + \ddot{X}_{b_n} \right\} - C_N \left\{ \frac{2}{\Delta t} X_{N_n} + \dot{X}_{N_n} \right\} - F_s \quad (4.7b)$$

Thus the equations 4.6a and 4.6b represent the system of $N + 1$ equations which will be solved for displacement response of the $N + 1$ degrees of freedom of the system at the $(n + 1)^{th}$ time step.

The friction force F_s is the term that causes nonlinearity in the system. It is constant in magnitude but its direction is determined based on the \dot{X}_b values (equation 3.9.)

4.1.2.3 Transition between phases

The transition between the sliding and sticking phases is determined based on the frictional force at the base. In the sticking phase, the friction force is determined based on equation 3.10 for each time step. Once this friction exceeds the limiting value determined by equation 3.11, the system transits to the sliding phase.

During the sliding phase, the friction force value is determined from equation 3.9 and is constant in magnitude but its sign changes with change in the direction of velocity. Therefore at each time step, the friction force value is determined using the sliding direction obtained from previous time step and the direction is reversed in case there is a change of sliding velocity direction. The system transitions from the sliding phase to sticking phase if the sliding velocity of the isolator drops down to zero. Hence, at the end of each time step, the sliding velocity is checked and the system transits to sticking phase from the next step if the value is found to be zero.

4.2 Solution steps for Variable Friction isolator and conventional FPS with constant friction

The general solution approach described above can be applied to both, the conventional constant friction model and the proposed isolator with variable friction. The friction coefficient (μ) is used at each time step in the calculation of the friction force (F_s) in equation 4.7b obtained using equation 3.9. For the conventional FPS, this value of μ is constant for all the displacement values whereas for the variable friction isolator, these values are determined at beginning of each time step based on the isolator displacement values. The friction coefficient variation for the proposed isolator as defined by the concentric friction strips in Section 2.2.1 and used in this study, is illustrated in Figure 4.1.

The conventional FPS is considered with μ of 0.08, whereas for the proposed variable friction isolator, the values are considered as: $\mu_1 = 0.1$, $\mu_2 = 0.05$ for $X_{b1} = 0.04m$ and $X_{b2} = 0.06m$ respectively.

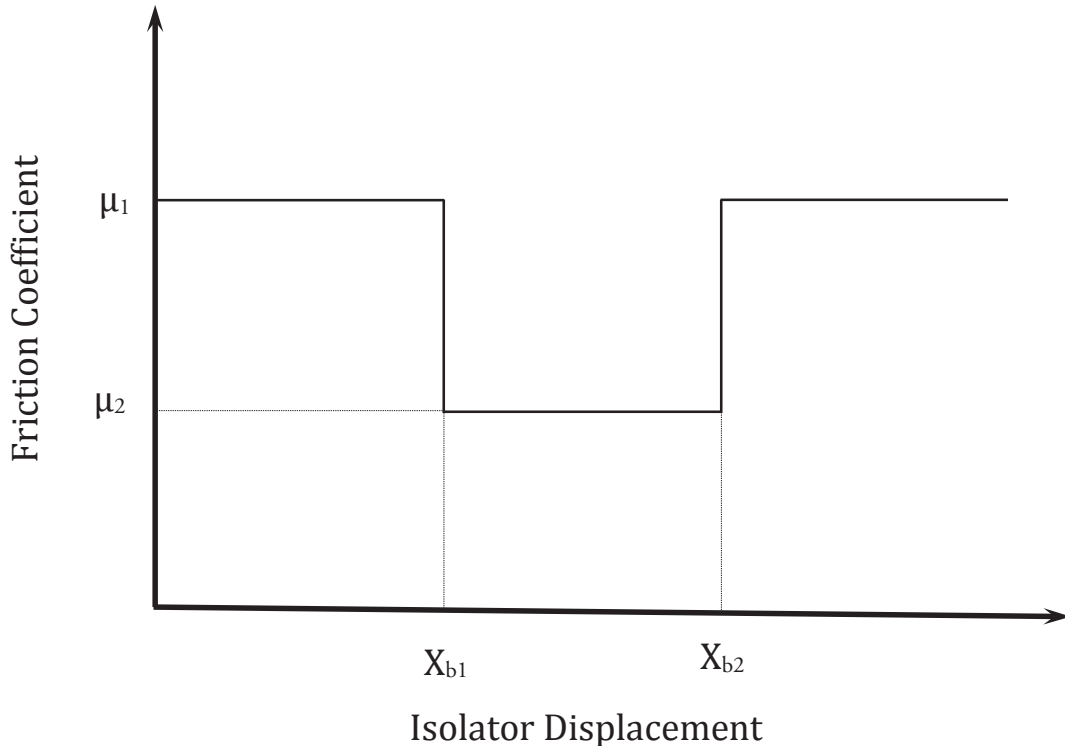


FIGURE 4.1: Friction profile of the considered isolator

Chapter 5

Computer Implementation

THE solution strategy detailed in the previous section is computationally implemented to find the response results using MATLAB © [MATLAB, 2010] numerical computing environment. This chapter will detail the implementation steps.

5.1 Step-by-step MATLAB algorithm

5.1.1 For the proposed isolator

Initial calculations, at the beginning of the analysis:

1. Read the input ground motion data (\ddot{X}_g)
2. Read the building data ($[M]$, $[K]$)
3. Find modal frequencies and mode shapes from the eigenvalue analysis. ($eig(M^{-1}K)$)
4. Find the corresponding a and b values from equation 3.5
5. Determine $[C]$ from equation 3.4
6. Initialize the solution quantities with zero values
7. Start in Sticking Phase

Calculations at each time step, from 0 to the end of the ground motion time-history:

1. In Sticking Phase:
 - (a) X_b , \dot{X}_b and \ddot{X}_b values set from equation 3.12
 - (b) Determine $\{X\}$ from equation 4.6a
 - (c) Determine $\{\dot{X}\}$ and $\{\ddot{X}\}$ from equations 4.3a and 4.3b
 - (d) Determine F_s from equation 3.10 and check against limiting value from equation 3.11
 - i. If limiting value is exceeded, move to Sliding phase
 - ii. If limiting value not exceeded, continue with Sticking phase
2. In Sliding Phase:
 - (a) Find F_s based on the current X_b value from equation 3.9
 - (b) Find $\{X\}$ and X_b from equations 4.6a and 4.6b
 - (c) Determine $\{\dot{X}\}$ and $\{\ddot{X}\}$ from equations 4.3a and 4.3b; \dot{X}_b and \ddot{X}_b from equations 4.4a and 4.4b
 - (d) Check \dot{X}_b value for sliding or non sliding condition in next step
 - i. If value is zero, move to Sticking phase
 - ii. If value is non zero, continue with the Sliding phase

5.1.2 For the conventional FPS

Initial calculations, at the beginning of the analysis:

1. Read the input ground motion data (\ddot{X}_g)
2. Read the building data ($[M]$, $[K]$)
3. Find modal frequencies and mode shapes from the eigenvalue analysis. ($eig(M^{-1}K)$)
4. Find the corresponding a and b values from equation 3.5
5. Determine $[C]$ from equation 3.4
6. Determine F_s from the equation 3.9
7. Initialize the solution quantities with zero values

8. Start in Sticking Phase

Calculations at each time step, from 0 to the end of the ground motion time-history:

1. In Sticking Phase:

- (a) X_b , \dot{X}_b and \ddot{X}_b values set from equation 3.12
- (b) Determine $\{X\}$ from equation 4.6a
- (c) Determine $\{\dot{X}\}$ and $\{\ddot{X}\}$ from equations 4.3a and 4.3b
- (d) Determine F_s from equation 3.10 and check against limiting value from equation 3.11
 - i. If limiting value is exceeded, move to Sliding phase
 - ii. If limiting value not exceeded, continue with Sticking phase

2. In Sliding Phase:

- (a) Find $\{X\}$ and X_b by from equations 4.6a and 4.6b
- (b) Determine $\{\dot{X}\}$ and $\{\ddot{X}\}$ from equations 4.3a and 4.3b; \dot{X}_b and \ddot{X}_b from equations 4.4a and 4.4b
- (c) Check \dot{X}_b value for sliding or non sliding condition in next step
 - i. If value is zero, move to Sticking phase
 - ii. If value is non zero, continue with the Sliding phase

Chapter 6

Results and Discussions

RESPONSE of the proposed system of seismic isolation will be discussed in this chapter. Various near-fault and far-field ground motions will be used as input for the system. And the response results obtained will be discussed and compared with the response results obtained using conventional structures without isolation.

6.1 Earthquake Ground motions

The ground motions used in this study are obtained from the PEER Ground Motion Database [PEER, 2010].

The near-fault ground motions used in this study are listed in Table 6.1. These records were identified with pulse-like characteristics in a study by Baker [2007] and were subsequently incorporated in the PEER database. The original unscaled acceleration time history of the these records is shown in Figure 6.1. The acceleration response spectra of these selected ground motions together with their average spectrum for 5% damping is also given in Figure 6.2.

The far-field ground motions used to evaluate the proposed seismic isolation system are listed in Table 6.2 and their original unscaled acceleration time history is given in Figure 6.3. And their acceleration response spectra along with the average spectrum for 5% damping is given in Figure 6.4.

TABLE 6.1: Near-Fault Earthquake Ground Motions

S. No.	Event	Recording Station	Year	Magnitude	Pulse Period (s)
1	Chi-Chi, Taiwan	CHY006	1999	7.62	2.6
2	Erzican, Turkey	Erzican	1992	6.69	2.7
3	Kobe, Japan	Takatori	1995	6.90	1.6
4	Loma Prieta	Alameda Naval Hanger	1989	6.93	2
5	Northridge-01	Newhall Fire Station	1994	6.69	2.2

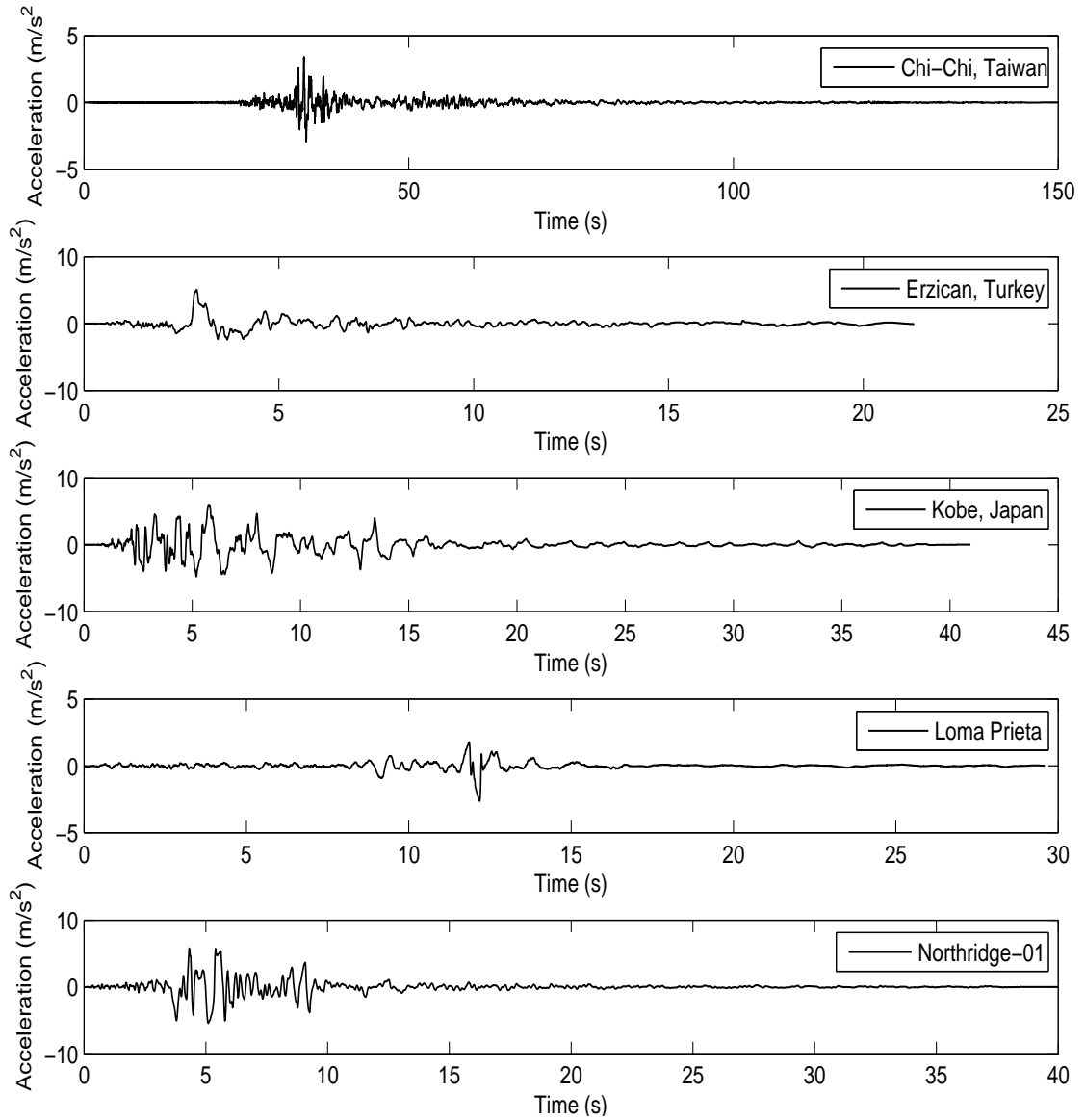


FIGURE 6.1: Acceleration time history of the near-fault records

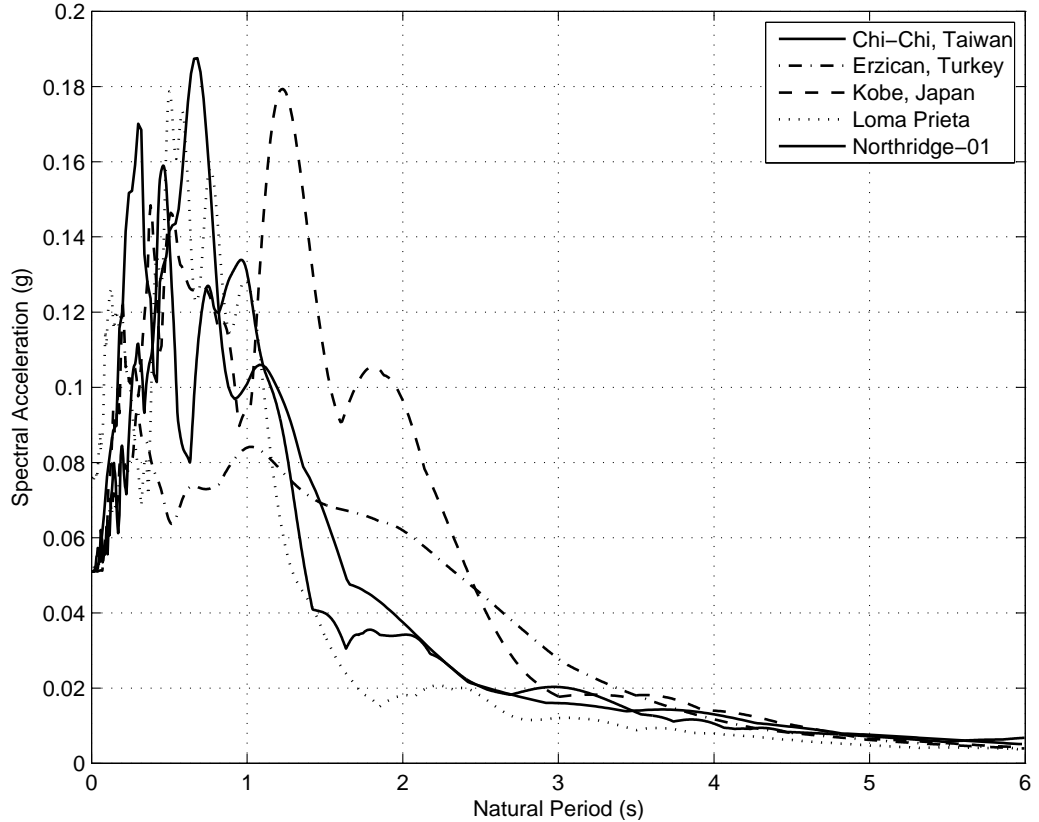


FIGURE 6.2: Acceleration response spectra of the near-fault earthquake records

TABLE 6.2: Far-Field Earthquake Ground Motions

S. No.	Event	Recording Station	Year	Magnitude
1	Hector Mine	Hector	1999	7.13
2	Imperial Valley-06	El Centro Array #1	1979	6.53
3	Loma Prieta	Berkeley LBL	1989	6.93
4	Northridge-01	Canyon Country - W Lost Cany	1994	6.69

6.2 System Characteristics

6.2.1 Superstructure

The general building model developed in Section 3.2 will be used to study the earthquake response of a *three-storey* and a *five-storey* building model. The fundamental properties associated with the models of these superstructures that are used for analysis in this study are detailed in this section.

The superstructure models considered here are out of those adopted by Calió et al. [2003] and Alhan and Srmeli [2011] in their study of seismically isolated buildings. These

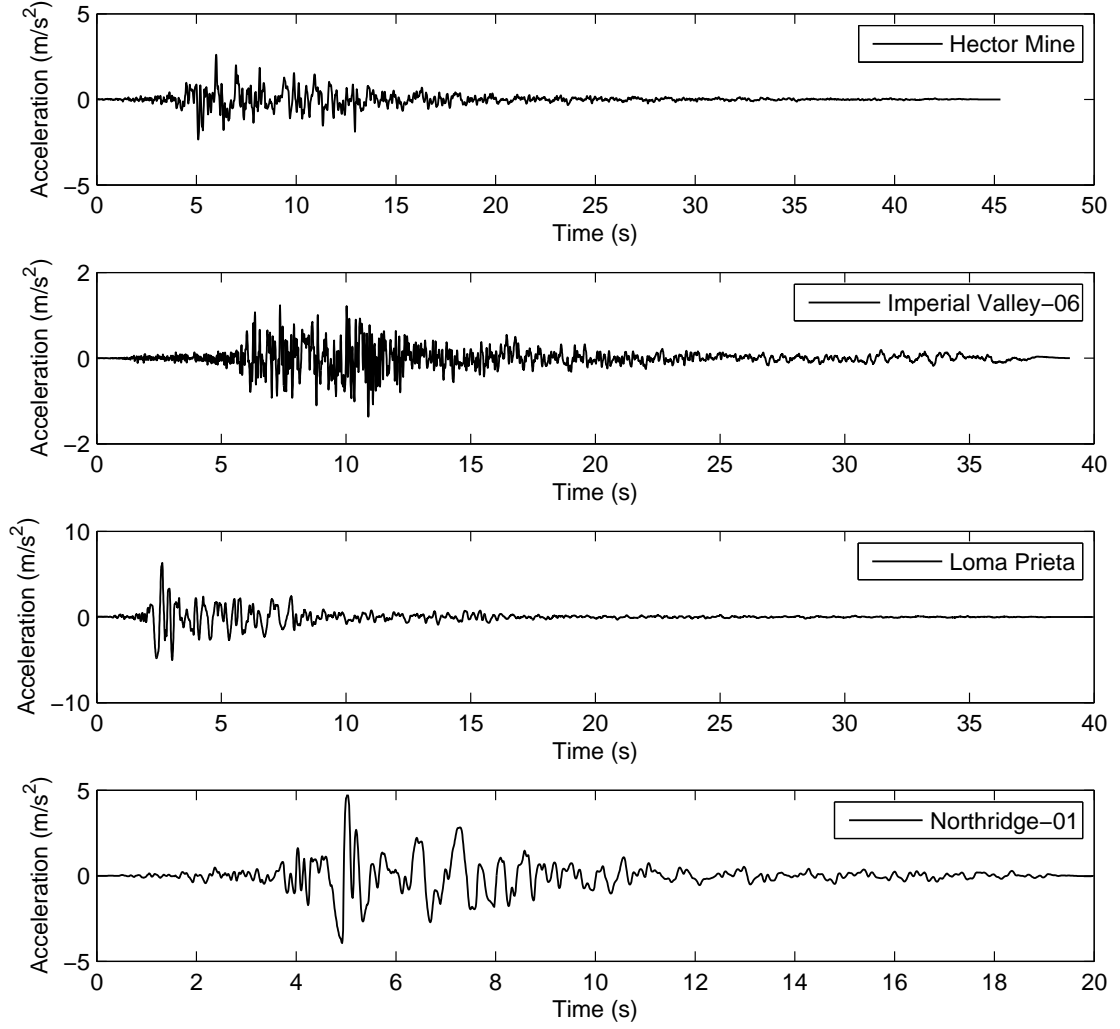


FIGURE 6.3: Acceleration time history of the far-field records

models sufficiently illustrate the application of the isolation system to a flexible superstructure.

The mass and storey stiffness values of the considered models are expressed in Table 6.3. These values are used to find the modal properties of the associated models using eigenvalue analysis as described by the equation 6.1 [Castellani, 1966; Craig, 1981].

$$[M^{-1}K - \omega_i^2 I] \phi_i = 0 \quad (6.1)$$

ω_i^2 is obtained as the eigenvalue and ϕ_i is obtained as the eigenvector of the matrix $M^{-1}K$. The values of the angular frequencies (ω_i) thus obtained are used to determine the Rayleigh damping constants, a and b , from equation 3.5. The damping characteristics of the superstructure are determined based on Rayleigh damping, which is the most

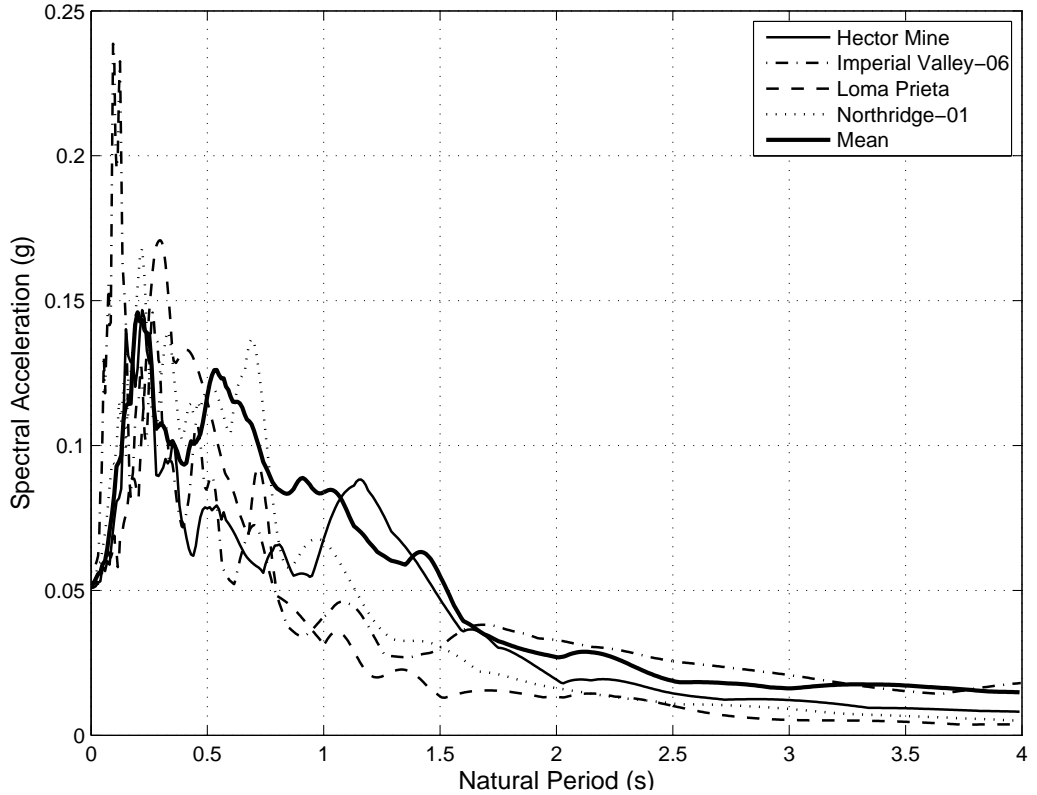


FIGURE 6.4: Acceleration response spectra of the far-field earthquake records

commonly used approach used for viscous damping in building models [Puthanpurayil et al., 2000]. The damping ratios (ζ_1 and ζ_2) for the first two modes are assumed as 5%, which is commonly adopted value for damping in shear frame analysis of buildings [Fakhouri and Igarashi, 2012]. The values of a and b thus obtained are used to determine the damping matrix C of the system (equation 3.4). The damping ratios for the remaining modes can then be determined from the following equation [Luco, 2008]:

$$\zeta_i = \frac{1}{2} \left(\frac{a}{\omega_i} + b\omega_i \right) \quad (6.2)$$

This analysis is thus used to obtain the modal characteristics of the 3-storey and 5-storey frames as listed in Tables 6.4 and 6.5.

6.2.2 Seismic Isolator

The base mass (M_b) in either model is taken to be the same as the mass of the lowest storey of the building. The radius of curvature (R) of the concave sliding surface is an important characteristic from the point of view of seismic isolation as it determines the

TABLE 6.3: Building Properties

Floor	3-Storey		5-Storey	
	Mass(10^3 kg)	Stiffness(MN/m)	Mass(10^3 kg)	Stiffness(MN/m)
1	100	100	100	100
2	150	150	150	150
3	200	200	200	200
4			250	250
5			300	300

TABLE 6.4: 3-Storey Building

Mode	Angular Frequency (rad/s)	Time Period (s)	Damping Ratio
1	13.636	0.460	0.050
2	31.912	0.196	0.050
3	45.960	0.136	0.060

TABLE 6.5: 5-Storey Building

Mode	Angular Frequency (rad/s)	Time Period (s)	Damping Ratio
1	11.060	0.568	0.050
2	25.711	0.244	0.050
3	39.133	0.160	0.063
4	49.814	0.126	0.075
5	57.040	0.110	0.084

fundamental period of the isolation system [Al-Hussaini et al., 1994] as given by the following:

$$T_b = 2\pi \sqrt{\frac{R}{g}} \quad (6.3)$$

For the purpose of this study, R is taken as 2 meters which corresponds to an effective isolation period, T_b , of 2.83 seconds. This sufficiently depicts the common isolation systems that have their fundamental period in the long period range of the near-fault earthquakes [Sharbatdar et al., 2011].

6.3 Response Quantities Considered

The important quantities of the building response that are evaluated in this study can be described as follows:

Base Displacement: The displacement at the base is an important response quantity from the point of view of the design of any seismically isolated building as it is required to determine the isolation gaps for the base floor level. Lower base displacement values ensure that no unusually high gaps are required to be maintained.

Story Drift: The story drifts are an indication of the elastic forces developed in the corresponding columns. High drifts between storeys induce large force demands so the drifts need to be kept to a minimum.

Top Floor Acceleration: The accelerations transmitted to the structure through the isolation system are evident from the top floor acceleration response and are an important indicator of the isolation effect of the seismic isolation system. For an effective seismic isolation, the top floor accelerations should be kept at a minimum.

6.4 Response to Near-Fault and Far-Field Earthquakes

The response of the 3-storey and 5-storey building models described in the previous section will be evaluated in this section under both far-field and near-fault earthquakes. The response is calculated by solving for the formulations developed in Section 3.2 using the solution strategy described by Chapter 4.

The following subsections will describe the response of the isolation system under the considered earthquakes in comparison to the fixed base and conventional isolation model.

6.4.1 Comparison with a Fixed Base Structure

The adoption of an isolation system to a fixed base structure greatly reduces its response in earthquake events. The time history response plots of the isolated system and the fixed base structure under all the considered far-field and near-fault earthquakes are presented

in Appendix A. Based on these figures, the peak response quantities for the 3-storey and 5-storey building models have been enumerated in Tables 6.6 and 6.7 respectively. The average of these quantities for near-fault and far-field earthquake groups are also expressed in Table 6.8.

These results comprehensively illustrate the reduction in response obtained by using seismic isolation in both, 3-storey and 5-storey structural models. The reduction in top storey drifts and top storey accelerations are of the order of 0.3 to 0.5. The reduction values show that the isolation system is effective in reducing response in near-fault earthquakes as well as far-field earthquakes although the base displacements are found to be larger for near-fault cases. The isolation system is more effective for response reduction in 3-storey building model as compared to the 5-storey building model.

6.4.2 Comparison with a conventional FPS isolated structure

The response of the proposed isolation system is also evaluated by comparing with conventional FPS having a constant friction profile. The time history response plots of the proposed isolation system and a system with conventional FPS isolator under all the considered far-field and near-fault earthquakes are presented in Appendix A. Based on these figures, the peak response quantities for the 3-storey and 5-storey building models have been enumerated in Tables 6.9 and 6.10 respectively. The average of these quantities for near-fault and far-field earthquake groups are also expressed in Table 6.11.

The average values of the response quantities show that the proposed isolation system is more effective in application to 3-storey building model than a 5-storey building model. The proposed system performs better than the conventional FPS in terms of the base displacement but it may result in slightly enhanced values for top storey accelerations and storey drifts.

6.4.3 Force-Deformation diagrams of the Isolator

The force-deformation characteristics of the proposed isolation system are also presented in the Appendix section A.4. The force-deformation diagrams sufficiently illustrate the engagement of the friction coefficient drop in the profile of the proposed variable friction isolator. The reduction in force is clearly evident from the figures as the force values

TABLE 6.6: Peak Response Quantities for the 3-storey building

Earthquake	Peak Acceleration (m/s^2)			Peak Storey Drift(Relative to the Base) (m)			Peak Base Displacement (m)
	Fixed Base	Isolated	Reduction	Fixed Base	Isolated	Reduction	
Far Field							
Hector Mine	5.88	3.21	0.545	0.028	0.013	0.475	0.046
Imperial Valley	8.24	3.12	0.379	0.043	0.013	0.302	0.023
Loma Prieta	10.96	3.38	0.308	0.053	0.013	0.250	0.037
Northridge-01	11.06	3.70	0.277	0.049	0.012	0.262	0.035
Near Fault							
Chi-Chi, Taiwan	11.72	3.36	0.286	0.065	0.015	0.233	0.065
Erzican, Turkey	5.87	2.60	0.443	0.029	0.013	0.441	0.129
Kobe, Japan	8.86	3.68	0.415	0.049	0.016	0.326	0.188
Loma Prieta	10.65	3.12	0.292	0.053	0.012	0.241	0.080
Northridge-01	10.62	4.10	0.386	0.055	0.014	0.263	0.088

TABLE 6.7: Peak Response Quantities for the 5-storey building

Earthquake	Peak Acceleration (m/s^2)			Peak Storey Drift(Relative to the Base) (m)			Peak Base Displacement (m)
	Fixed Base	Isolated	Reduction	Fixed Base	Isolated	Reduction	
Far Field							
Hector Mine	9.39	5.38	0.573	0.052	0.024	0.470	0.028
Imperial Valley	6.13	5.19	0.846	0.037	0.025	0.670	0.016
Loma Prieta	11.04	5.40	0.489	0.068	0.028	0.422	0.031
Northridge-01	12.54	4.75	0.378	0.080	0.023	0.288	0.030
Near Fault							
Chi-Chi, Taiwan	8.68	5.28	0.609	0.061	0.032	0.529	0.058
Erzincan, Turkey	6.60	4.75	0.719	0.047	0.027	0.587	0.151
Kobe, Japan	11.33	6.19	0.546	0.090	0.030	0.334	0.208
Loma Prieta	13.83	5.23	0.378	0.113	0.029	0.256	0.103
Northridge-01	14.31	7.54	0.527	0.104	0.024	0.237	0.113

TABLE 6.8: Average Response Quantities under far-field and near-fault earthquakes

	5-Storey Building			3-Storey Building		
	Isolated	Fixed Base	Reduction	Isolated	Fixed Base	Reduction
Far Field						
Peak Acceleration (m/s^2)	5.185	9.781	0.530	3.199	9.037	0.353
Peak Storey Drift (m)	0.025	0.059	0.423	0.013	0.043	0.302
Peak Base Displacement (m)	0.026			0.035		
Near Fault						
Peak Acceleration (m/s^2)	5.804	10.954	0.556	3.376	9.549	0.353
Peak Storey Drift (m)	0.028	0.083	0.389	0.014	0.050	0.301
Peak Base Displacement (m)	0.126			0.110		

TABLE 6.9: Peak Response Quantities for the 3-storey building

Earthquake	Peak Acceleration (m/s^2)			Peak Storey Drift(Relative to the Base) (m)			Peak Base Displacement (m)		
	FPS	Proposed System	Reduction	FPS	Proposed System	Reduction	FPS	Proposed System	Reduction
Far Field									
Hector Mine	4.18	3.21	0.767	0.014	0.013	0.914	0.037	0.046	1.23
Imperial Valley	3.54	3.12	0.883	0.015	0.013	0.869	0.032	0.023	0.72
Loma Prieta	3.73	3.38	0.905	0.014	0.013	0.906	0.043	0.037	0.86
Northridge-01	3.57	3.70	0.860	0.011	0.012	1.163	0.036	0.035	0.97
Near Fault									
Chi-Chi, Taiwan	4.43	3.36	0.757	0.017	0.015	0.861	0.087	0.065	0.75
Erzican, Turkey	3.01	2.60	0.864	0.012	0.013	1.053	0.152	0.129	0.84
Kobe, Japan	3.75	3.68	0.981	0.016	0.016	0.997	0.206	0.188	0.91
Loma Prieta	4.46	3.12	0.698	0.016	0.012	0.760	0.057	0.080	1.38
Northridge-01	4.39	4.10	0.934	0.015	0.014	0.912	0.077	0.088	1.14

TABLE 6.10: Peak Response Quantities for the 5-storey building

Earthquake	Peak Acceleration (m/s^2)			Peak Storey Drift(Relative to the Base) (m)			Peak Base Displacement (m)		
	FPS	Proposed System	Reduction	FPS	Proposed System	Reduction	FPS	Proposed System	Reduction
Far Field									
Hector Mine	4.66	5.38		1.156	0.025		0.964	0.032	
Imperial Valley	4.58	5.19		1.132	0.019		1.295	0.023	
Loma Prieta	5.05	5.40		1.070	0.025		1.119	0.038	
Northridge-01	4.09	4.75		1.160	0.020		1.115	0.036	
Near Fault									
Chi-Chi, Taiwan	4.73	5.28		1.116	0.027		1.190	0.068	
Erzican, Turkey	4.02	4.75		1.183	0.020		1.134	0.164	
Kobe, Japan	5.19	6.19		1.192	0.030		0.999	0.228	
Loma Prieta	4.97	5.23		1.052	0.024		0.029	1.175	
Northridge-01	5.51	7.54		1.368	0.022		0.024	1.113	

TABLE 6.11: Average Response Quantities under far-field and near-fault earthquakes

	5-Storey			3-Storey		
	Proposed System	FPS	Reduction	Proposed System	FPS	Reduction
Far Field						
Peak Acceleration(m/s^2)	5.185	4.597	1.127	3.199	3.75	0.854
Peak Storey Drift (m)	0.025	0.022	1.136	0.013	0.013	0.963
Peak Base Displacement (m)	0.026	0.032	0.812	0.035	0.037	0.945
Near Fault						
Peak Acceleration(m/s^2)	5.804	4.88	1.182	3.376	4.013	0.841
Peak Storey Drift (m)	0.028	0.025	1.120	0.014	0.015	0.933
Peak Base Displacement (m)	0.126	0.128	0.973	0.110	0.116	0.948

drop when the displacement exceeds the point where the friction values drop. The force being transmitted through the isolator is a function of the friction coefficient at the sliding interface, so a drop in force values results directly from the fact that the slider has entered into the low friction zone.

These response features though are not demonstrated by some ground motions where the base displacement is not large enough and their force-deformation diagram is similar to that of a conventional friction pendulum system. The weak ground motions which do not incite the isolator to displace into the low friction zone of the isolator do not exhibit the force drop facilitated by the lower friction values. Hence the variable friction isolator behaves like a conventional isolator for weak ground motions and engages the variations in the friction profile to act as a variable friction isolator for stronger ground motions.

Chapter 7

Summary and Conclusions

THE performance and the related issues of seismic isolation systems under long period waves of near fault earthquakes has been studied. In a conclusion to this detailed review of the existing isolation systems, a new innovative design of seismic isolation was proposed. This proposed design was analytically modeled for a general multi-storey shear building type structure and a solution scheme was developed for time history response under various earthquake ground motions. The response of the proposed system was evaluated under various near-fault and far-field earthquakes (the data for which was available in the public domain through *PEER Ground Motion Database.*) and compared with the responses of fixed base and conventional FPS system. This chapter will give a brief summary of the study based on the results that were obtained in the previous Chapter 5 and also describe the limitations of this study.

7.1 Conclusions

The following conclusions are made regarding the performance of the proposed base isolation system:

- ▷ The proposed isolator system produces response reduction to 0.3 - 0.5 times that of the conventional fixed base system; for both far-field and near-fault earthquakes.
- ▷ The isolator displacements of the proposed system are found to be greater under near-fault earthquakes as compared to that under far-field earthquakes.

- ▷ The proposed isolator is more effective in reducing the response of the less flexible of the two considered building models (i.e. the 3-storey building model) compared to the corresponding fixed base system.
- ▷ The proposed isolation system gives reduced base displacements as compared to those for the conventional FPS isolator while resulting in higher accelerations and storey drifts in some cases of earthquakes.
- ▷ The proposed isolator gives better performance for the less flexible of the two considered building models (i.e. the 3-storey building model) in comparison to the conventional FPS isolator.
- ▷ The hysteresis diagram of the proposed isolator illustrates the reduction in the force being transmitted due to the engagement of the variable friction profile for stronger ground motions.

7.2 Scope of Future Work

The research done in this study can be extended in future to cover the following aspects:

- ▷ The profile of frictional variation adopted can be extended to include more concentric strips of variable friction coefficients to study the possible further improvements in the performance of the structure.
- ▷ The assumption of the point contact between the articulated slider and the concave sliding surface can be extended to include a finite contact area.
- ▷ Other (than shear building model) superstructure models can be studied to take into account the realistic features of the superstructure.
- ▷ Further studies can include possible non-linear behavior of the superstructure.
- ▷ Other possible ground acceleration components can be considered.
- ▷ An experimental verification study can be undertaken to validate and verify the performance of the currently proposed isolation system.

Appendix A

Response Plots

This appendix includes the plots of all the response quantities for all the considered earthquakes that were discussed in Chapter 5.

A.1 Response Comparison with Fixed base model

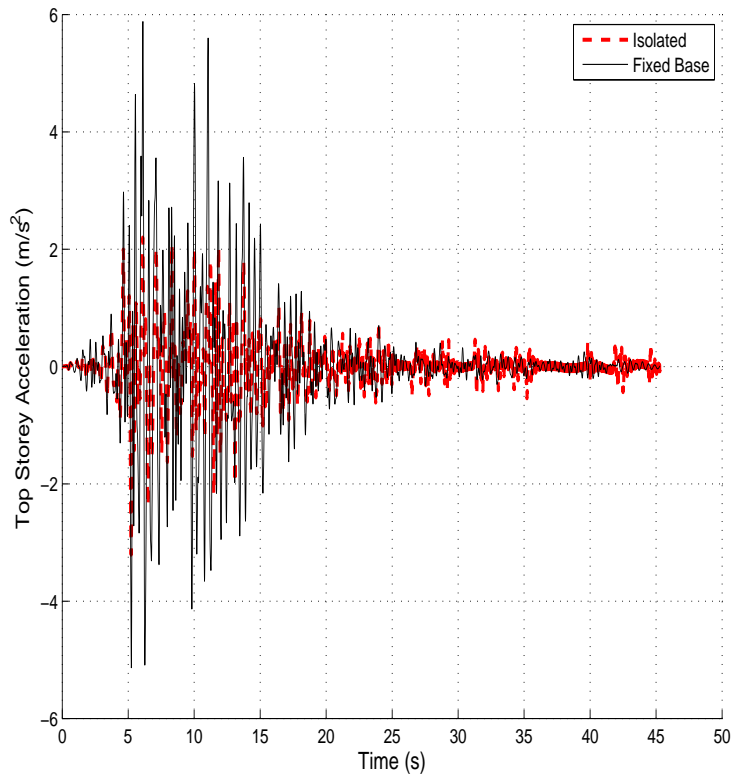


FIGURE A.1: Top storey acceleration (3-storey building) under far-field Hector Mine earthquake

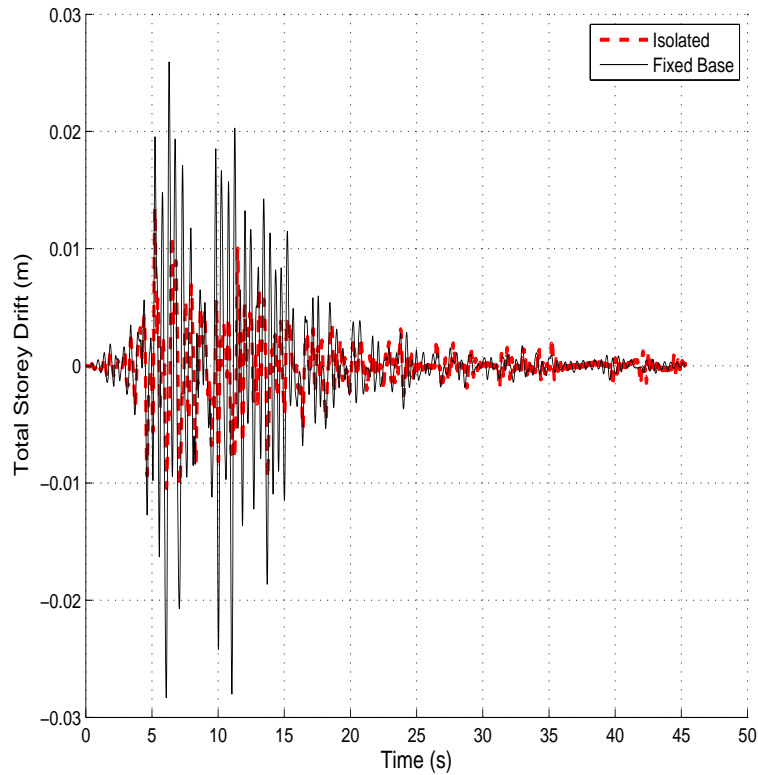


FIGURE A.2: Total Storey Drift (3-storey building) under far-field Hector Mine earthquake

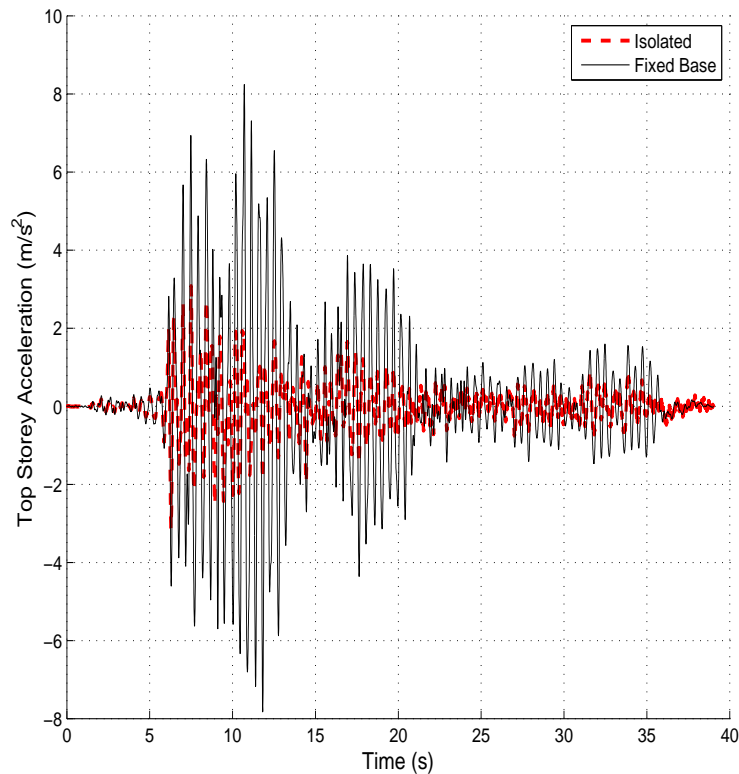


FIGURE A.3: Top storey acceleration (3-storey building) under far-field Imperial Valley earthquake

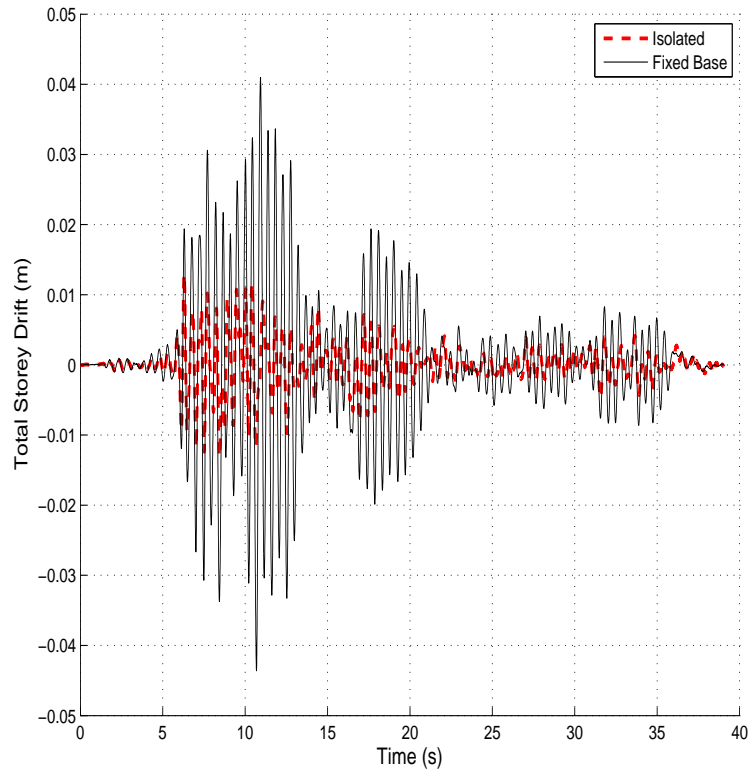


FIGURE A.4: Total Storey Drift (3-storey building) under far-field Imperial Valley earthquake

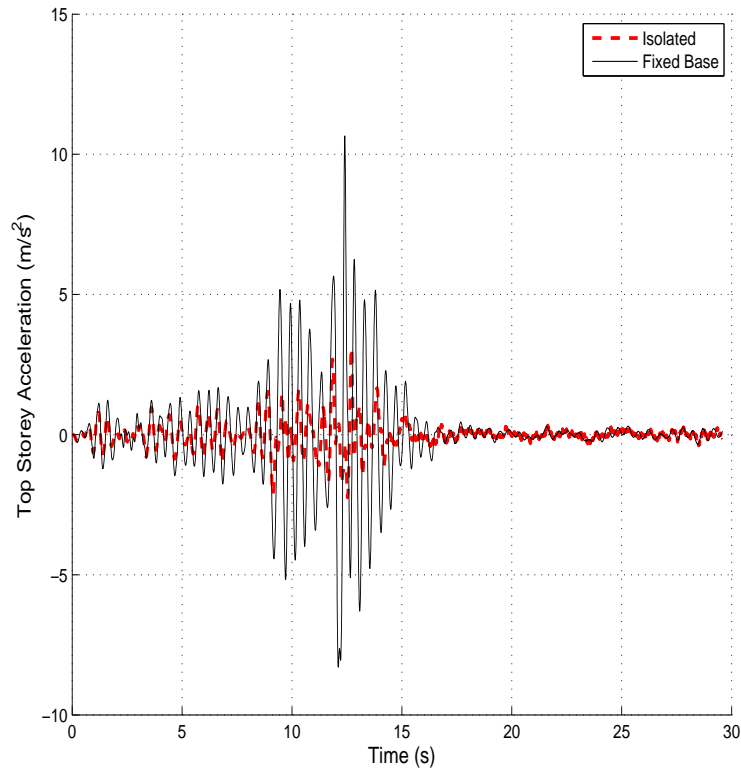


FIGURE A.5: Top storey acceleration (3-storey building) under far-field Loma Prieta earthquake

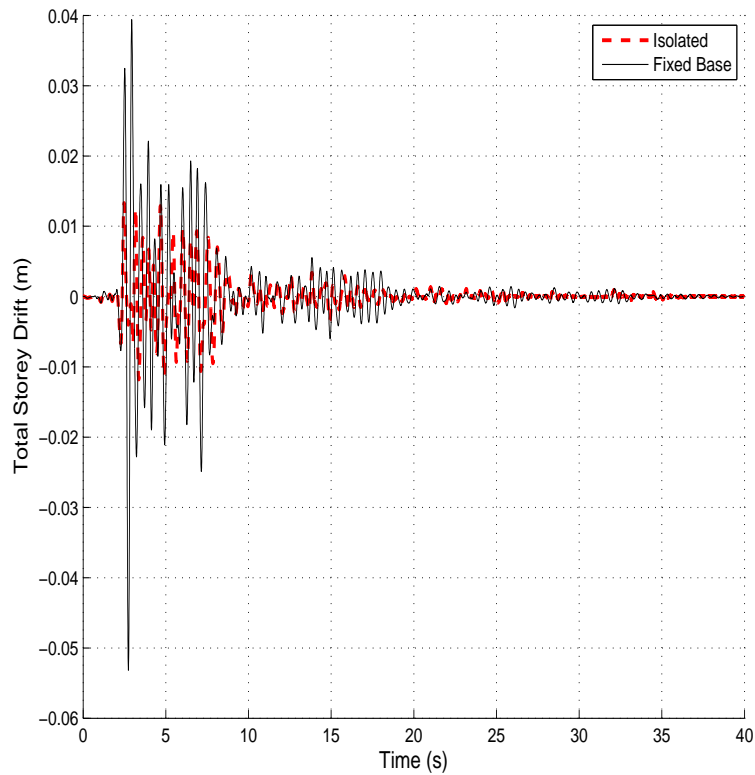


FIGURE A.6: Total Storey Drift (3-storey building) under far-field Loma Prieta earthquake

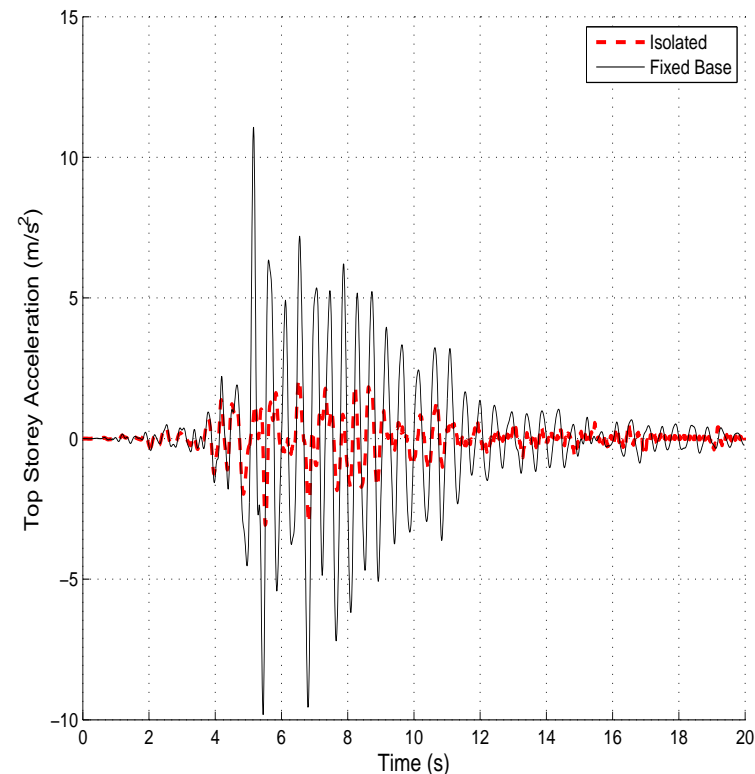


FIGURE A.7: Top storey acceleration (3-storey building) under far-field Northridge-01 earthquake

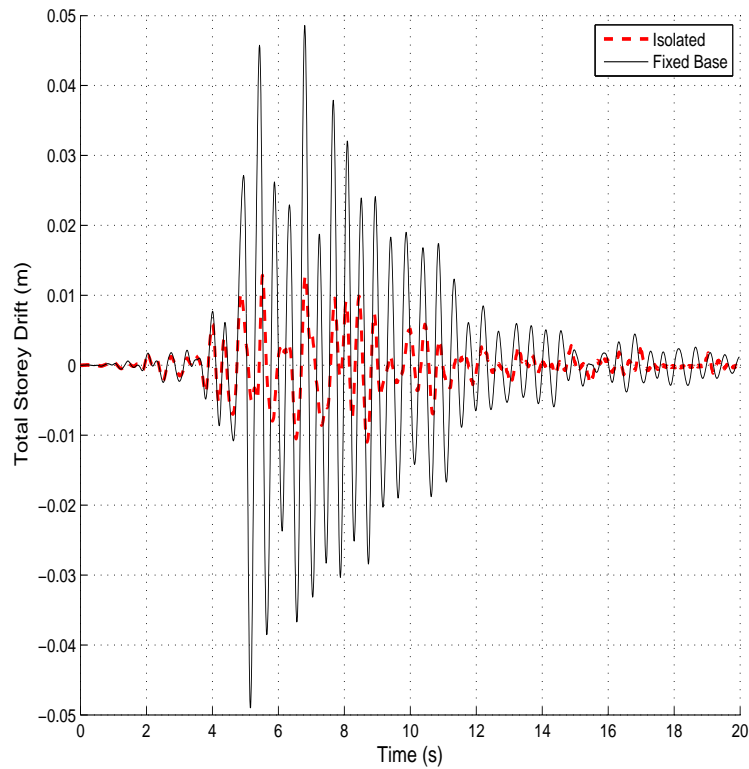


FIGURE A.8: Total Storey Drift (3-storey building) under far-field Northridge-01 earthquake

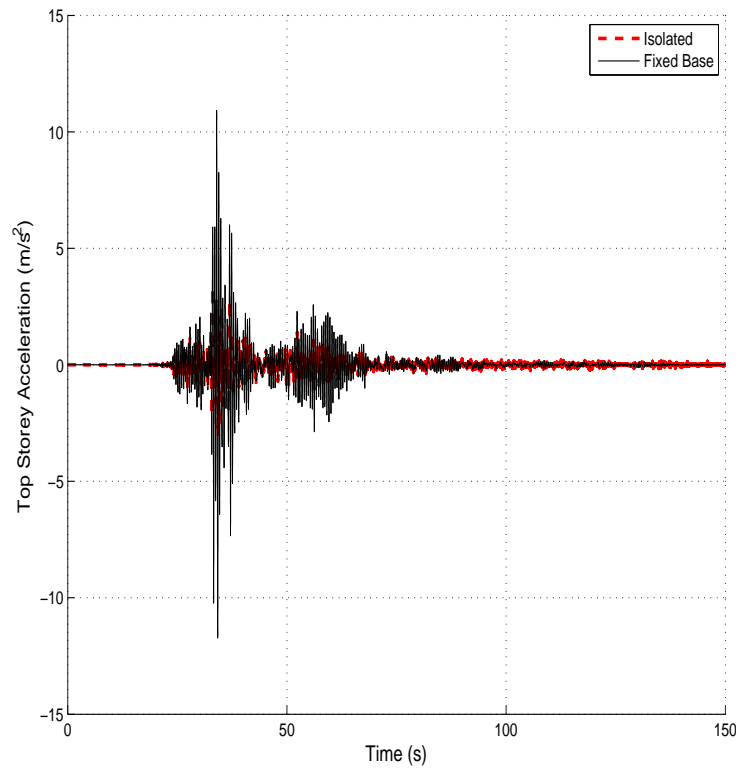


FIGURE A.9: Top storey acceleration (3-storey building) under near-fault Chi-Chi earthquake

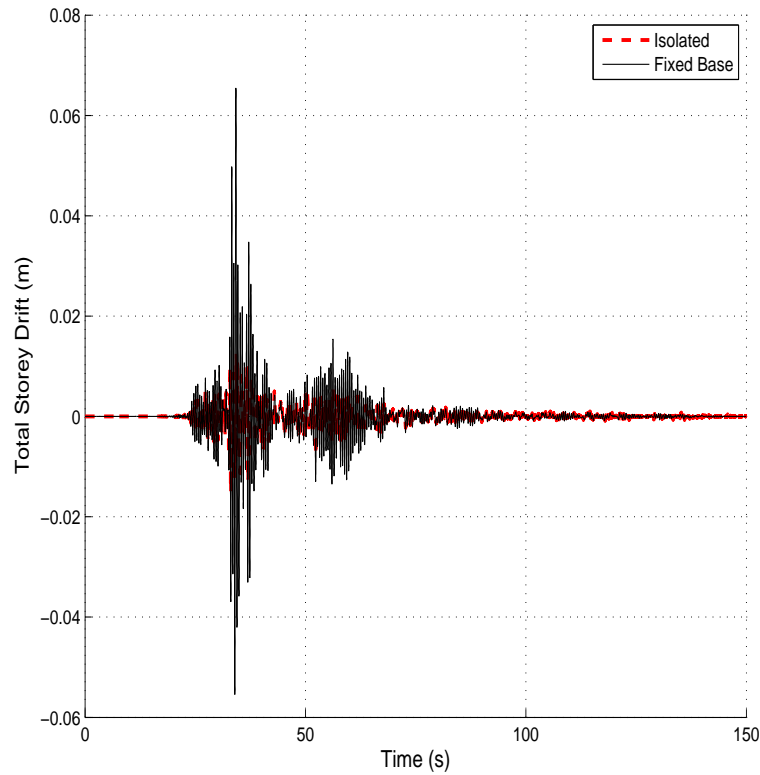


FIGURE A.10: Total Storey Drift (3-storey building) under near-fault Chi-Chi earthquake

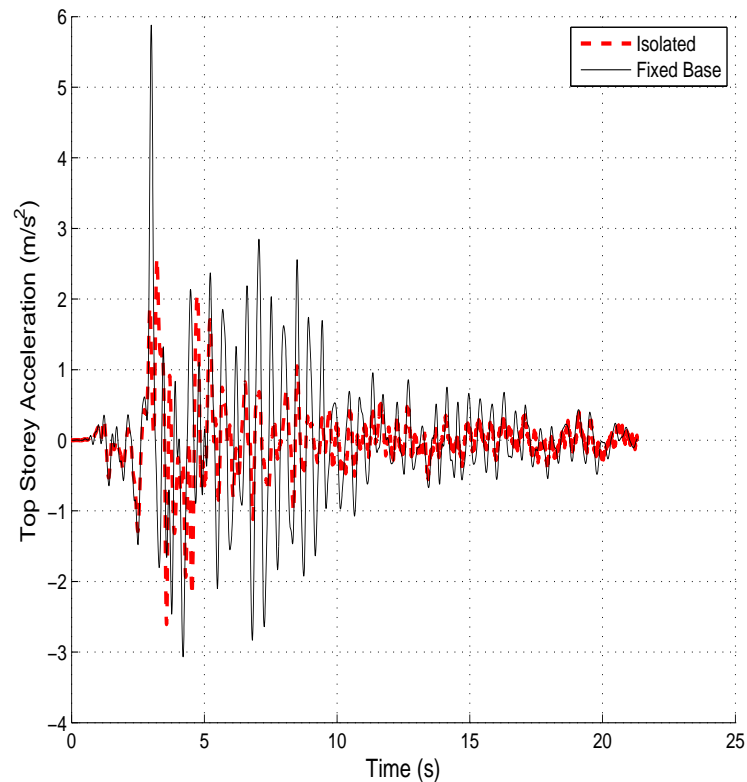


FIGURE A.11: Top storey acceleration (3-storey building) under near-fault Erzican earthquake

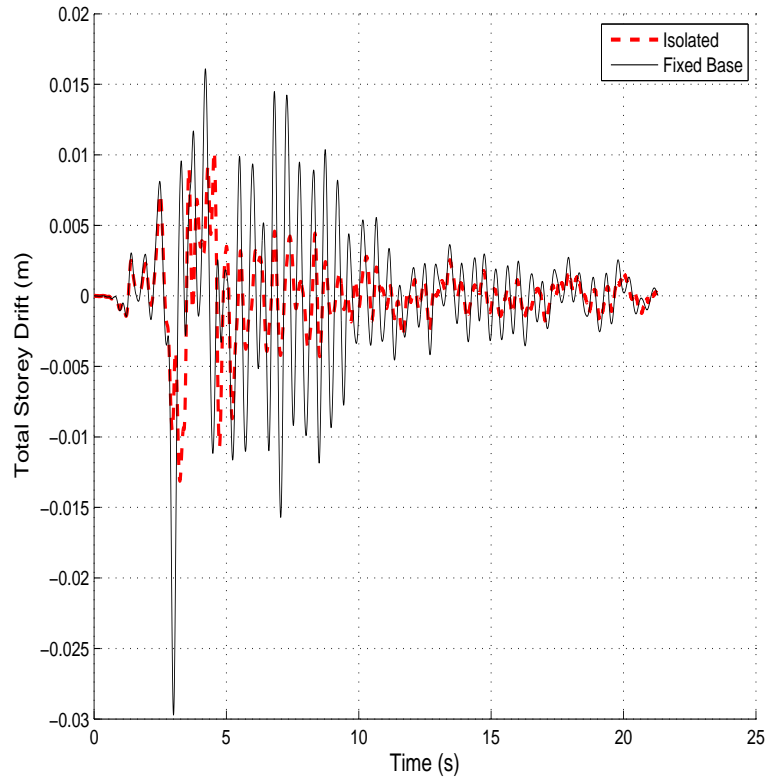


FIGURE A.12: Total Storey Drift (3-storey building) under near-fault Erzican earthquake

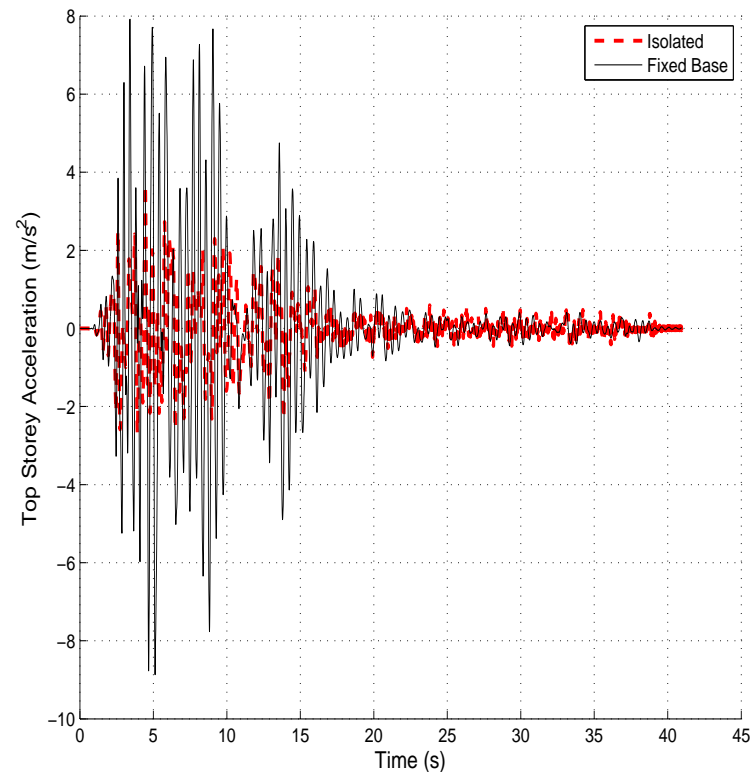


FIGURE A.13: Top storey acceleration (3-storey building) under near-fault Kobe earthquake

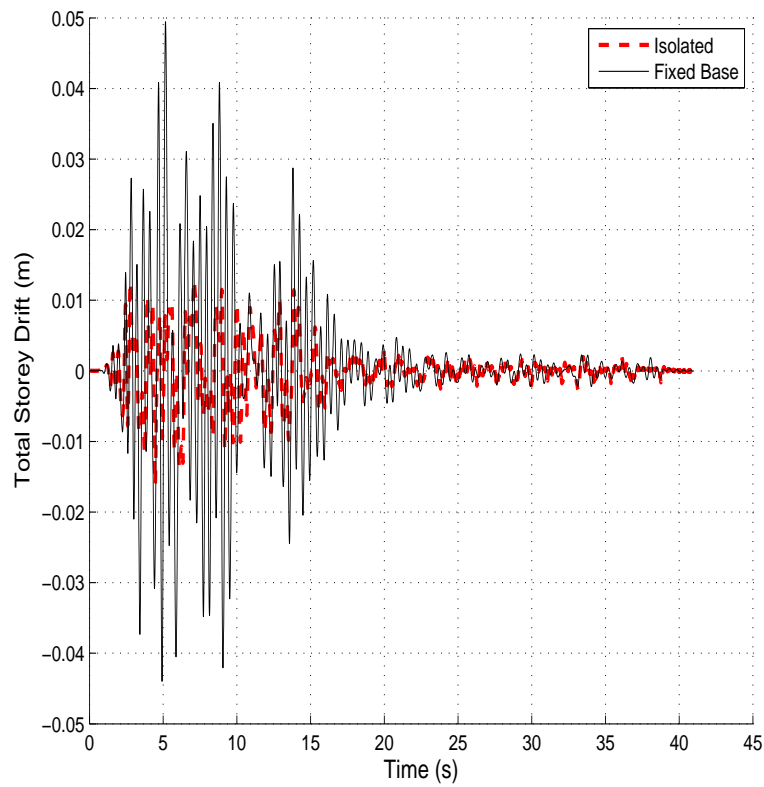


FIGURE A.14: Total Storey Drift (3-storey building) under near-fault Kobe earthquake

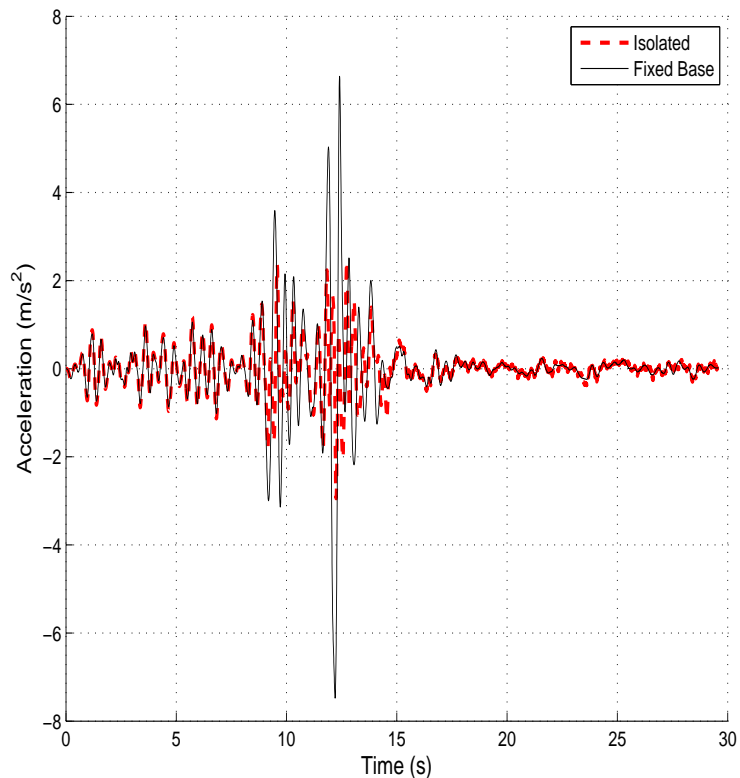


FIGURE A.15: Top storey acceleration (3-storey building) under near-fault Loma Prieta earthquake

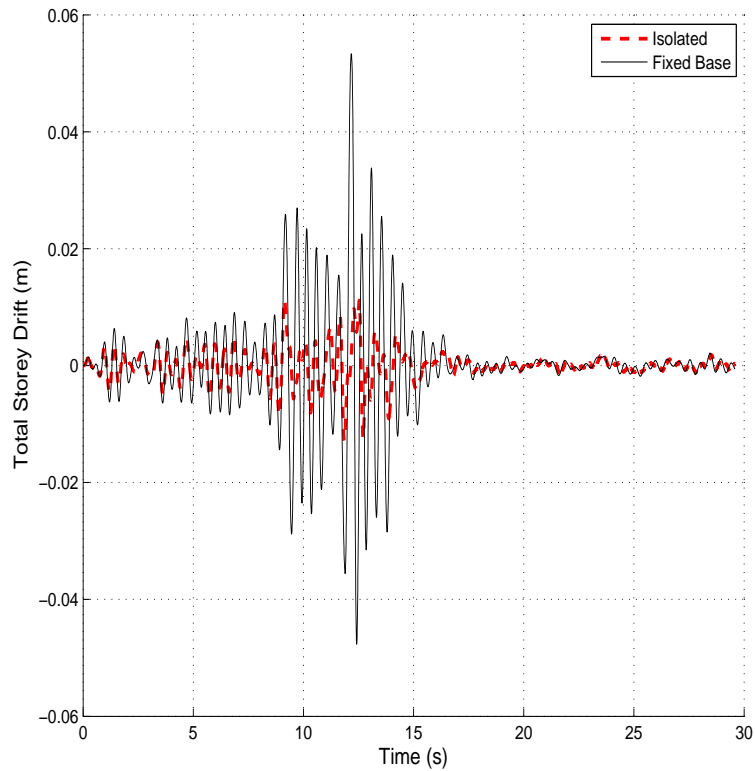


FIGURE A.16: Total Storey Drift (3-storey building) under near-fault Loma Prieta earthquake

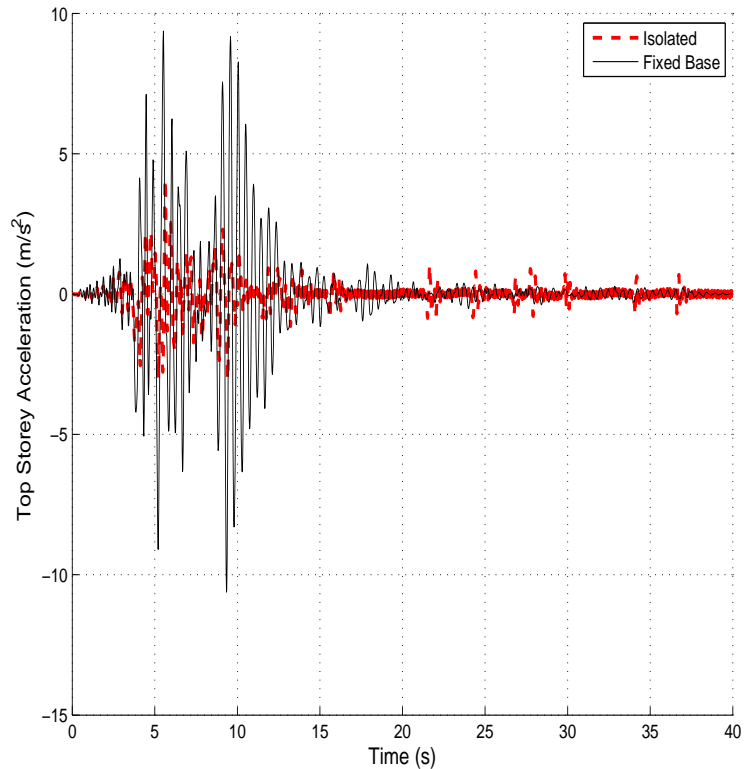


FIGURE A.17: Top storey acceleration (3-storey building) under near-fault Northridge-01 earthquake

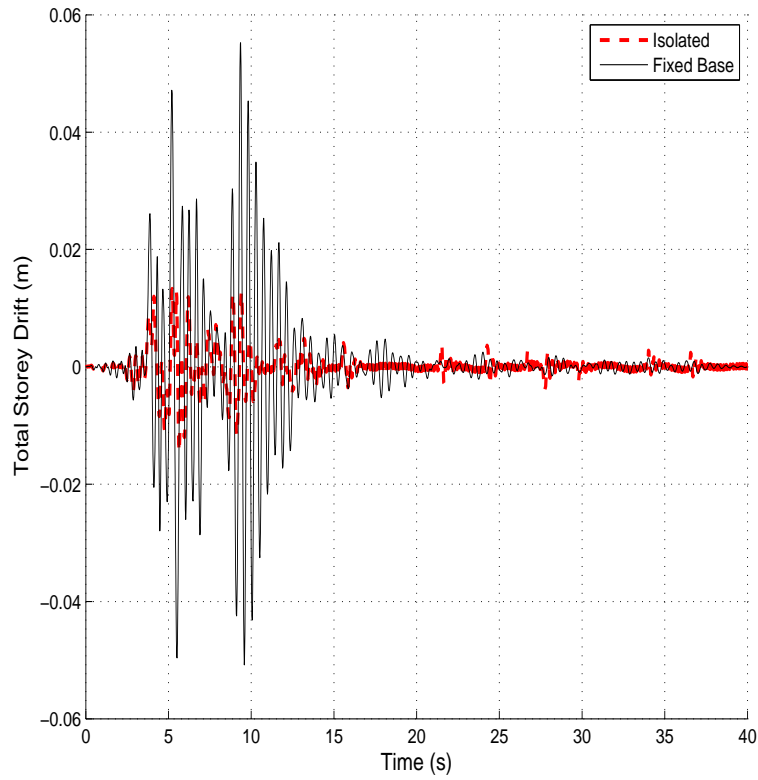


FIGURE A.18: Total Storey Drift (3-storey building) under near-fault Northridge-01 earthquake

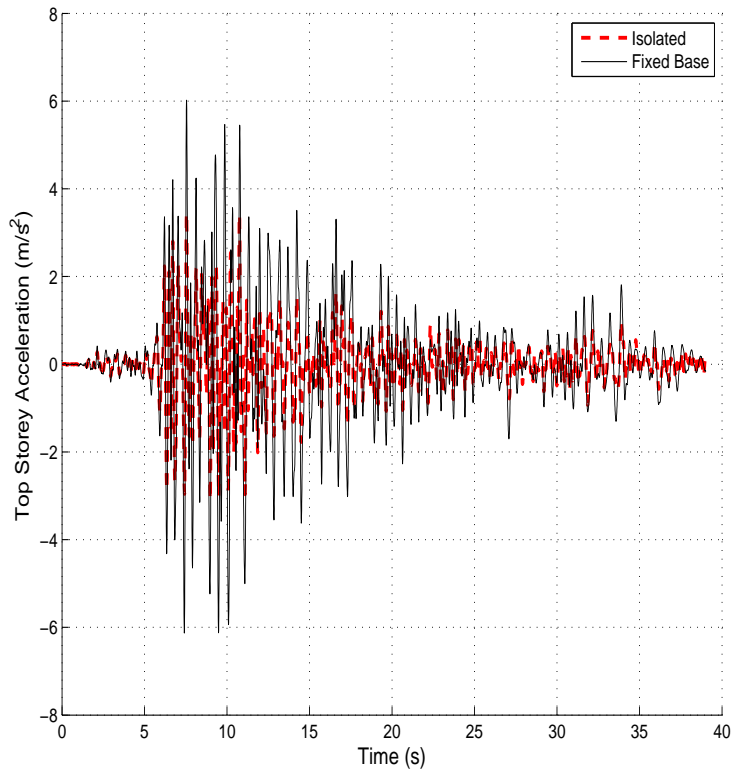


FIGURE A.19: Top storey acceleration (5-storey building) under far-field Imperial Valley earthquake

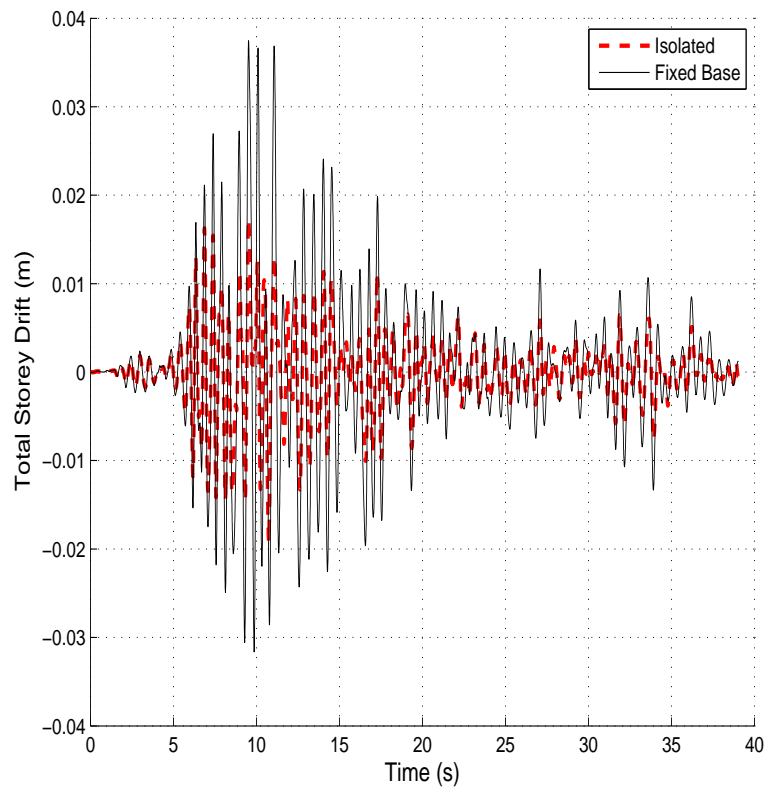


FIGURE A.20: Total Storey Drift (5-storey building) under far-field Imperial Valley earthquake

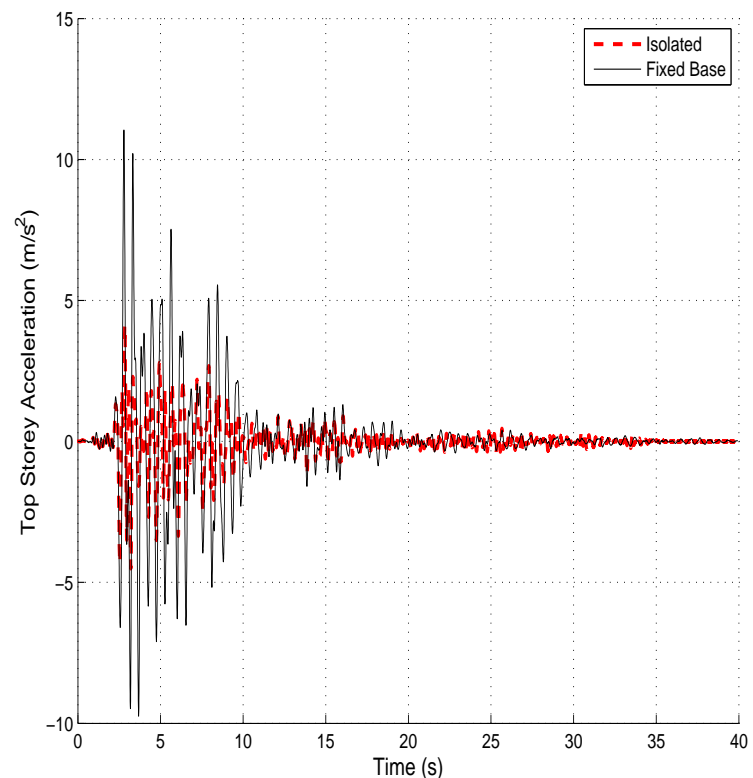


FIGURE A.21: Top storey acceleration (5-storey building) under far-field Loma Prieta earthquake

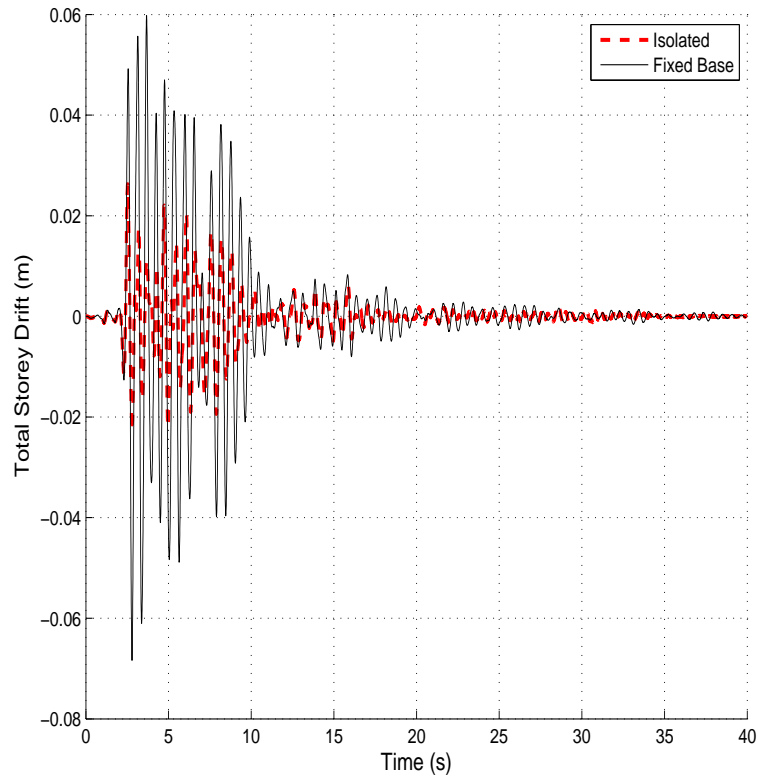


FIGURE A.22: Total Storey Drift (5-storey building) under far-field Loma Prieta earthquake

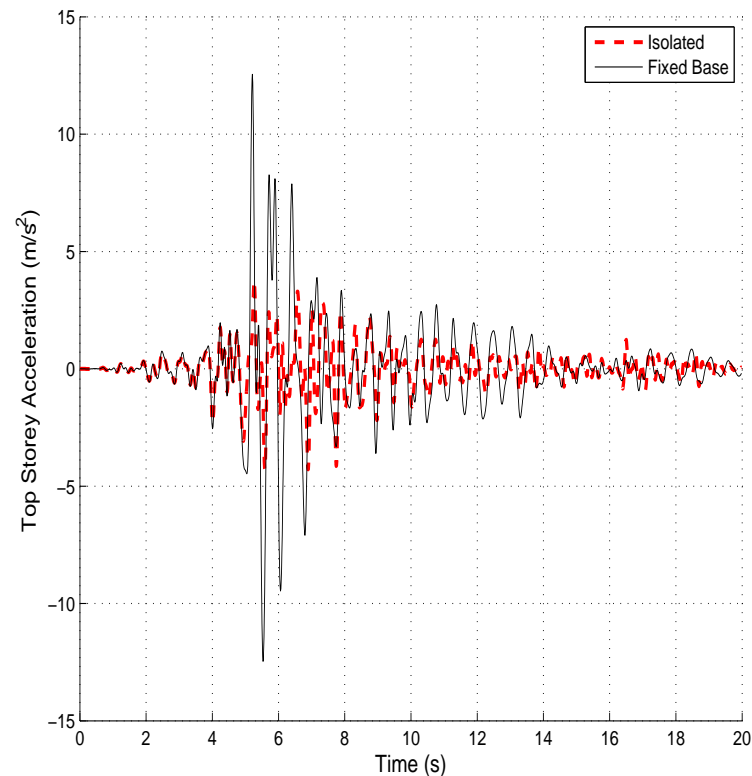


FIGURE A.23: Top storey acceleration (5-storey building) under far-field Northridge-01 earthquake

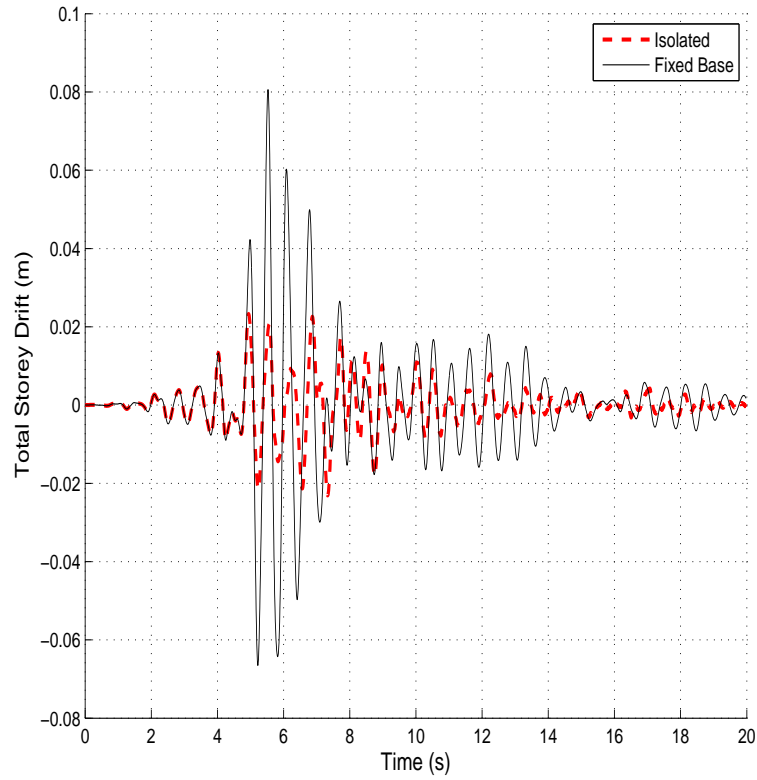


FIGURE A.24: Total Storey Drift (5-storey building) under far-field Northridge-01 earthquake

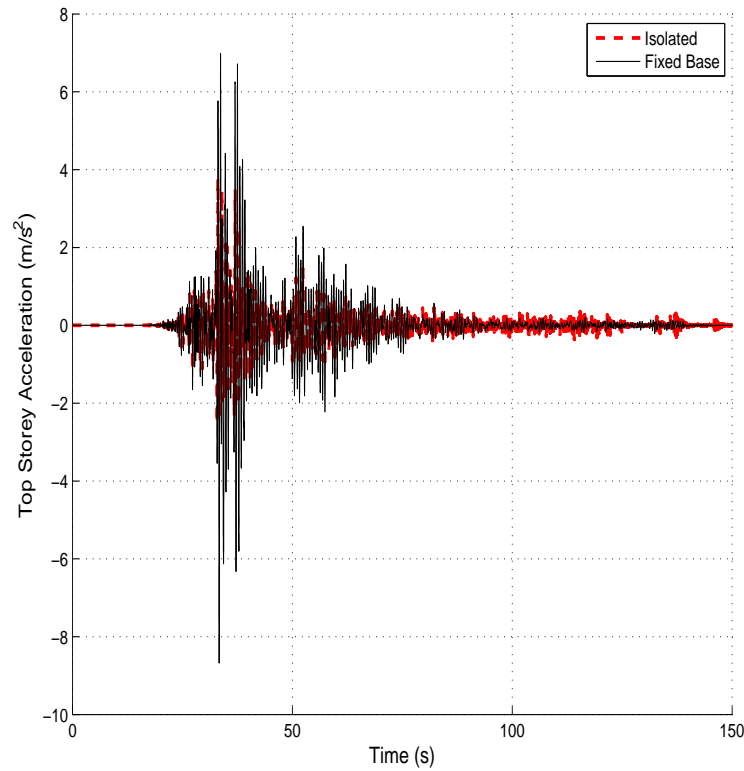


FIGURE A.25: Top storey acceleration (5-storey building) under near-fault Chi-Chi earthquake

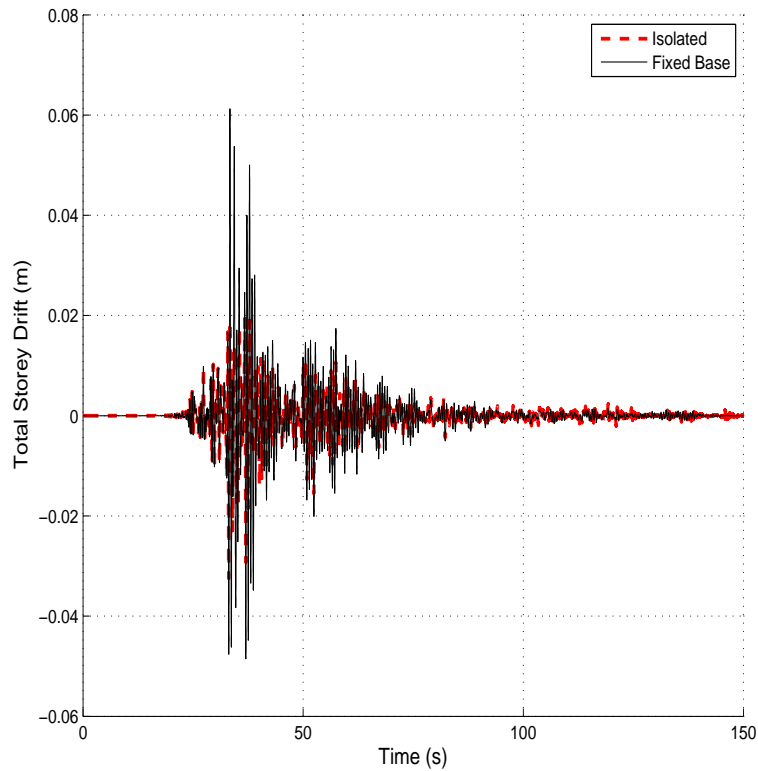


FIGURE A.26: Total Storey Drift (5-storey building) under near-fault Chi-Chi earthquake

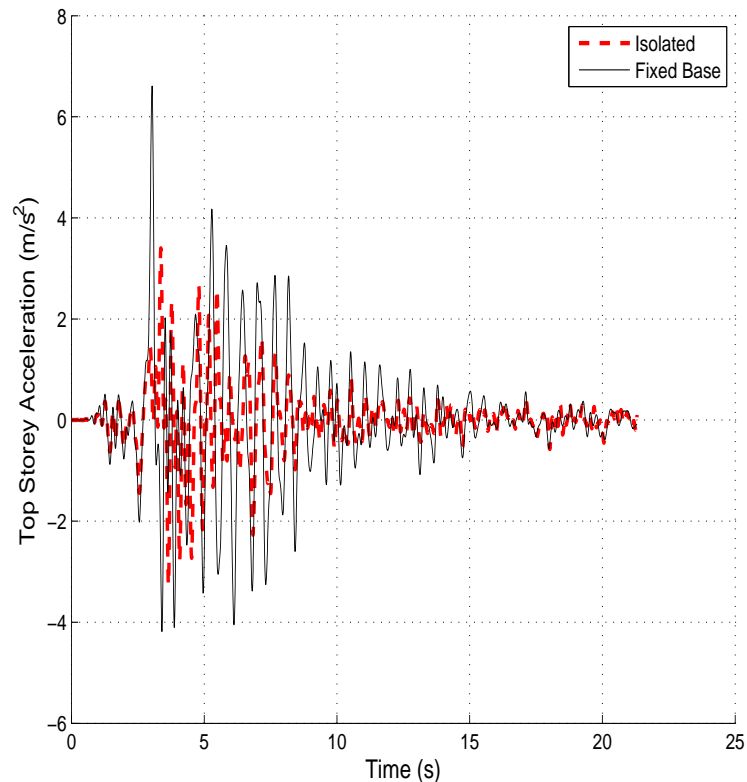


FIGURE A.27: Top storey acceleration (5-storey building) under near-fault Erzican earthquake

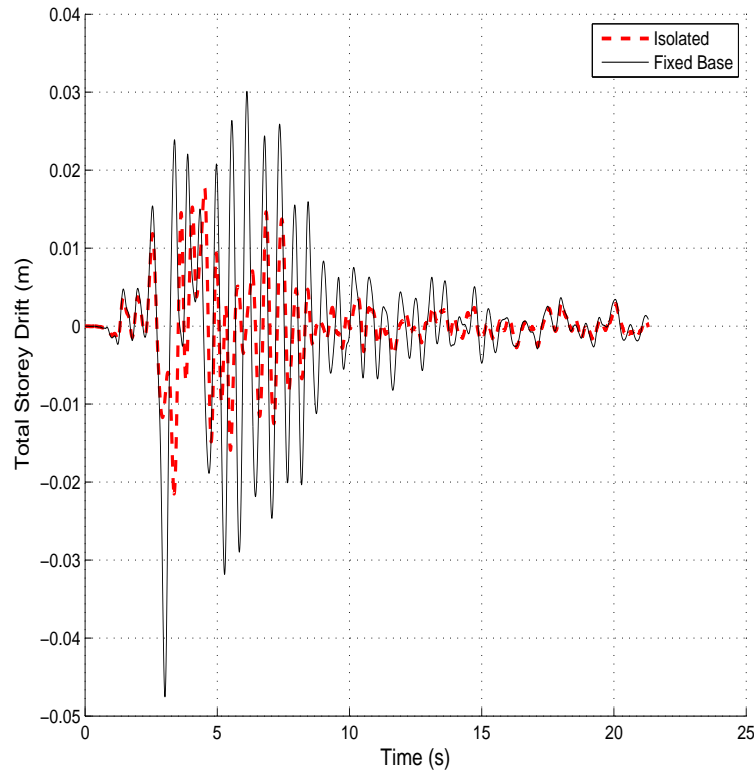


FIGURE A.28: Total Storey Drift (5-storey building) under near-fault Erzican earthquake

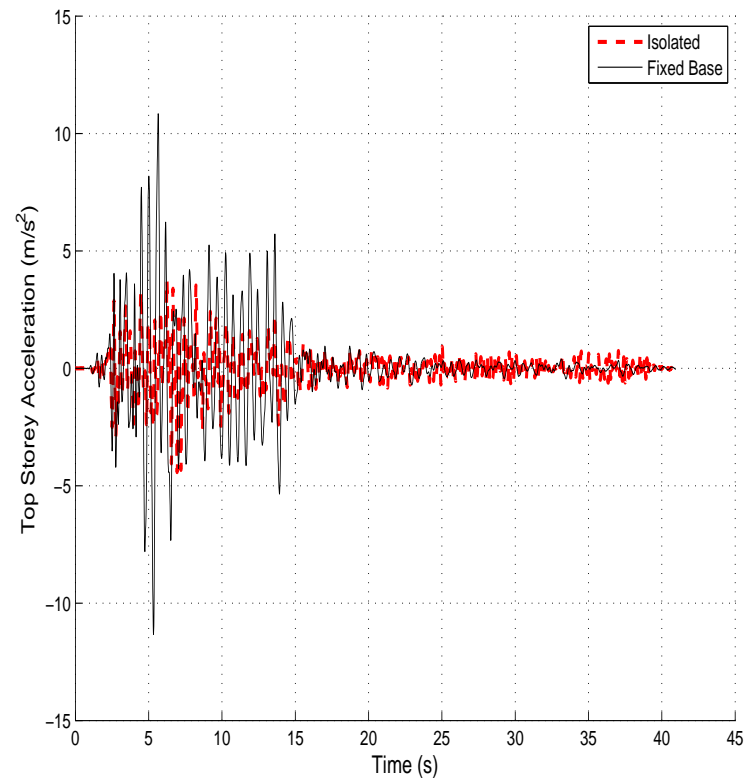


FIGURE A.29: Top storey acceleration (5-storey building) under near-fault Kobe earthquake

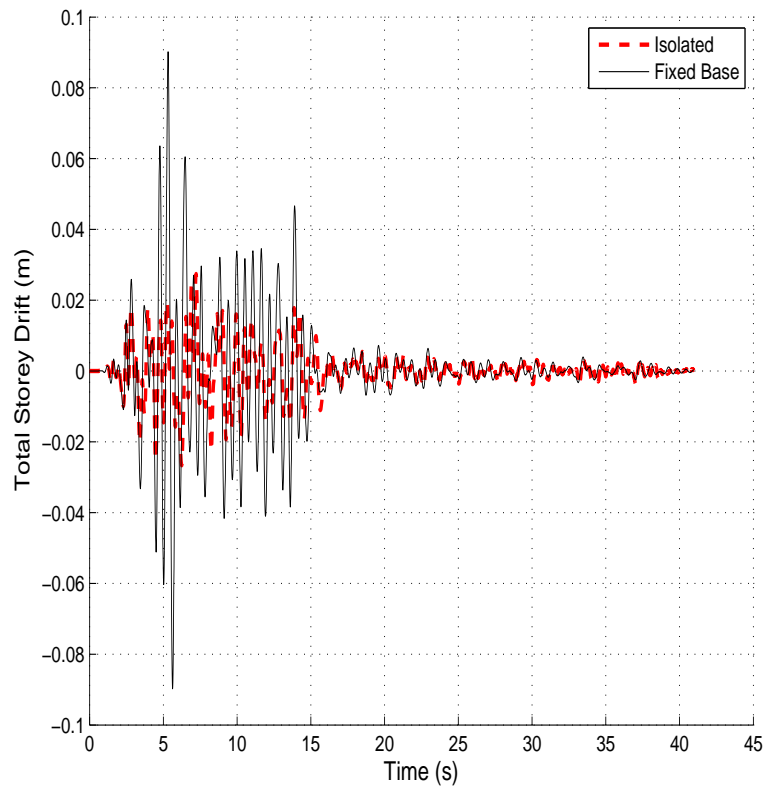


FIGURE A.30: Total Storey Drift (5-storey building) under near-fault Kobe earthquake

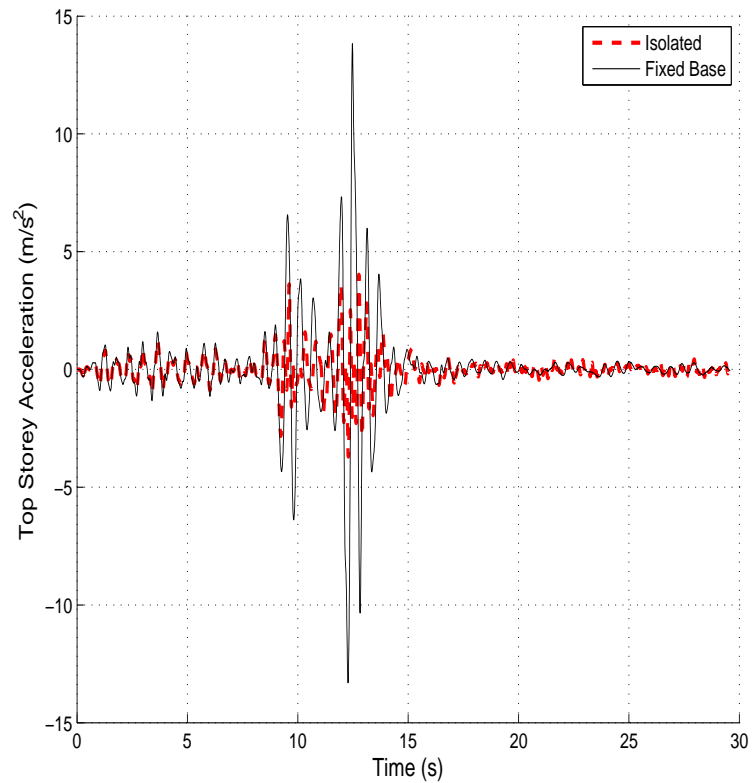


FIGURE A.31: Top storey acceleration (5-storey building) under near-fault Loma Prieta earthquake

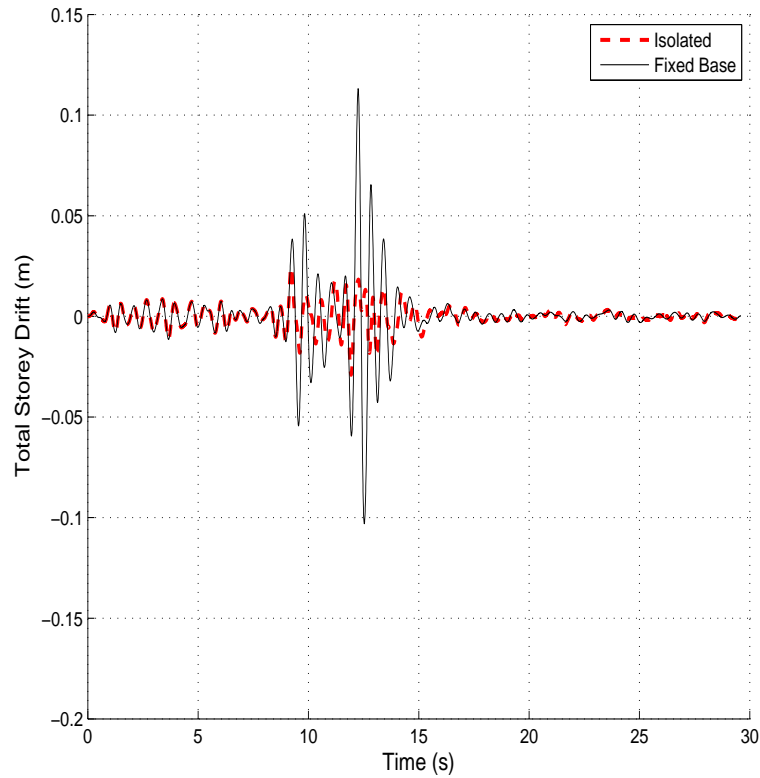


FIGURE A.32: Total Storey Drift (5-storey building) under near-fault Loma Prieta earthquake

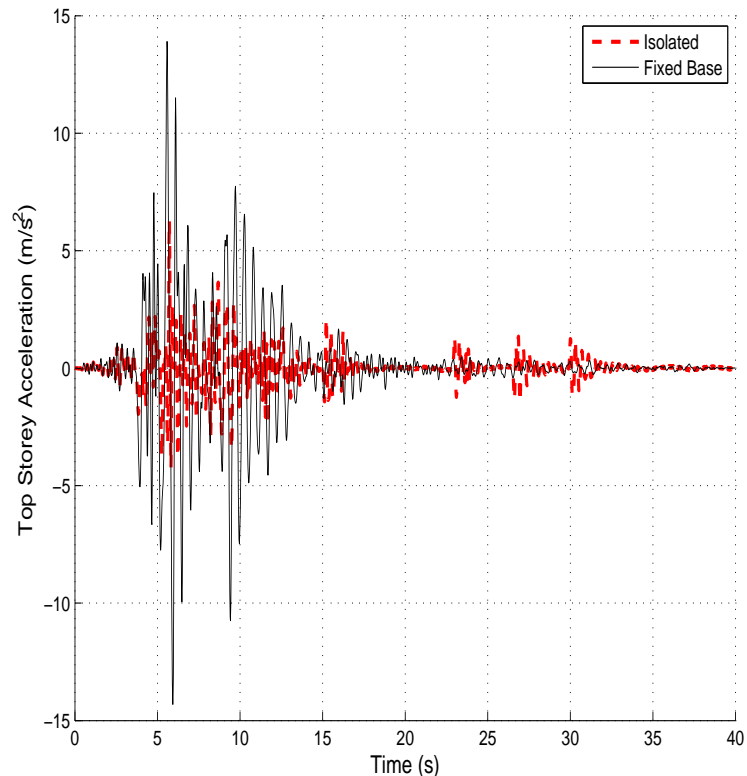


FIGURE A.33: Top storey acceleration (5-storey building) under near-fault Northridge-01 earthquake

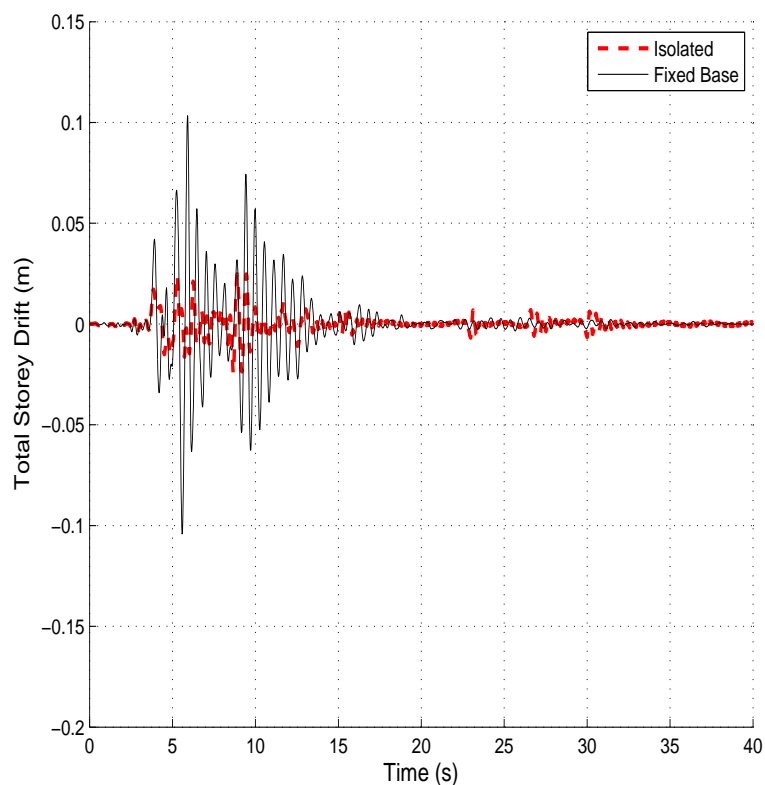


FIGURE A.34: Total Storey Drift (5-storey building) under near-fault Northridge-01 earthquake

A.2 Base Displacement of the Isolator

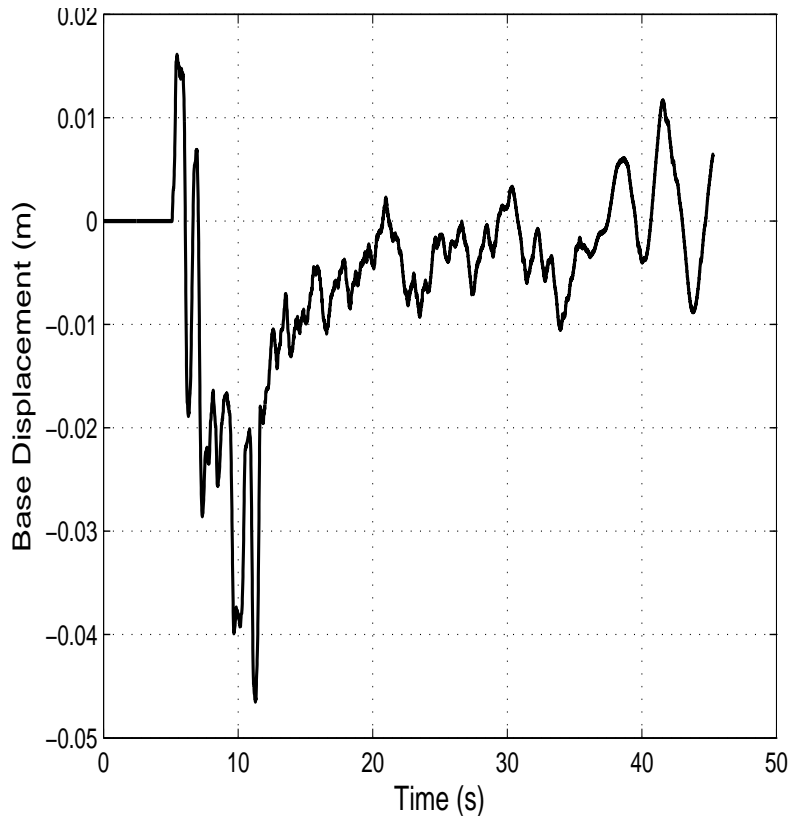


FIGURE A.35: Isolator Displacement (3-storey building) under far-field Imperial Valley earthquake

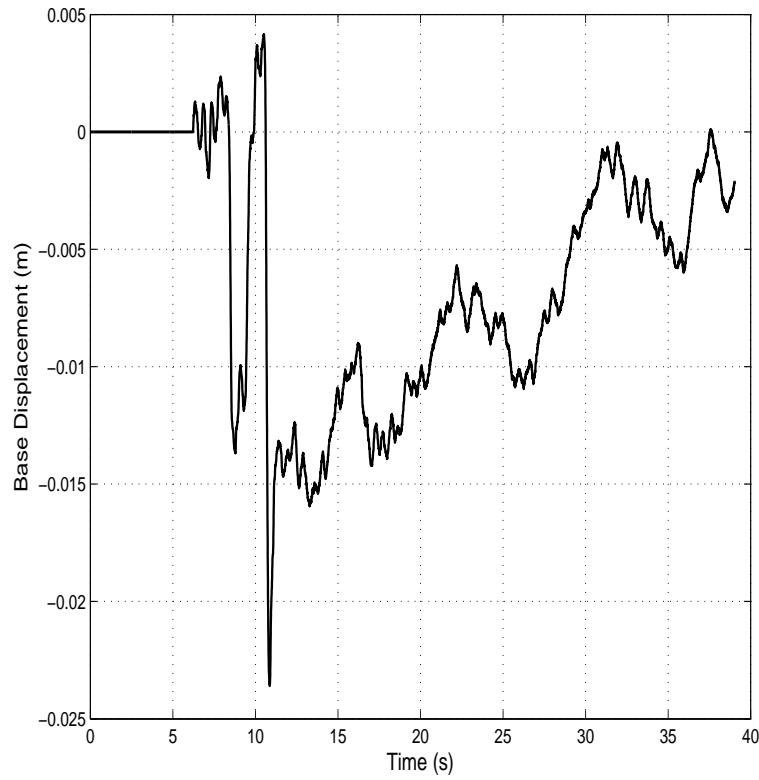


FIGURE A.36: Isolator Displacement (3-storey building) under far-field Imperial Valley earthquake

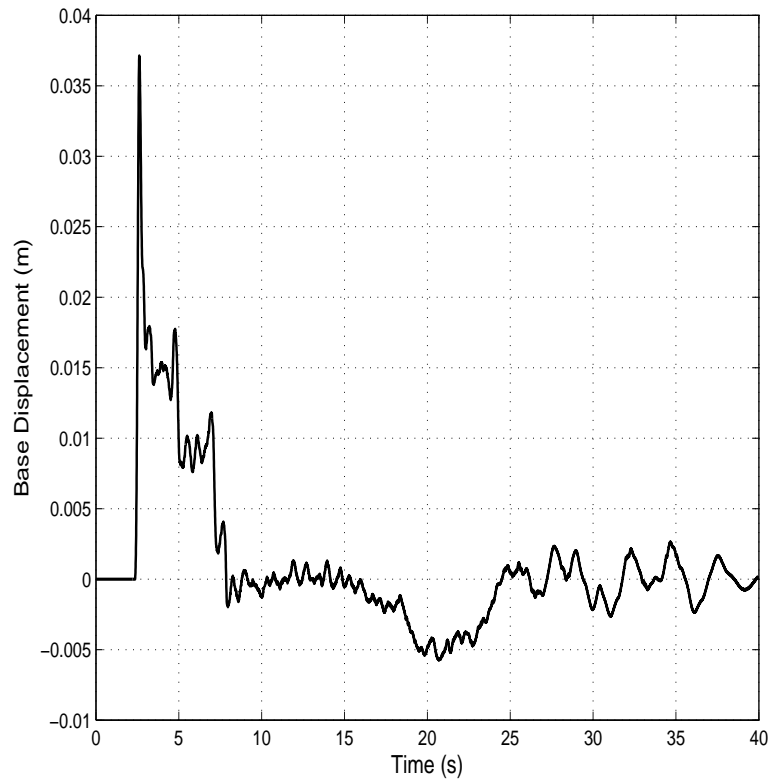


FIGURE A.37: Isolator Displacement (3-storey building) under far-field Loma Prieta earthquake

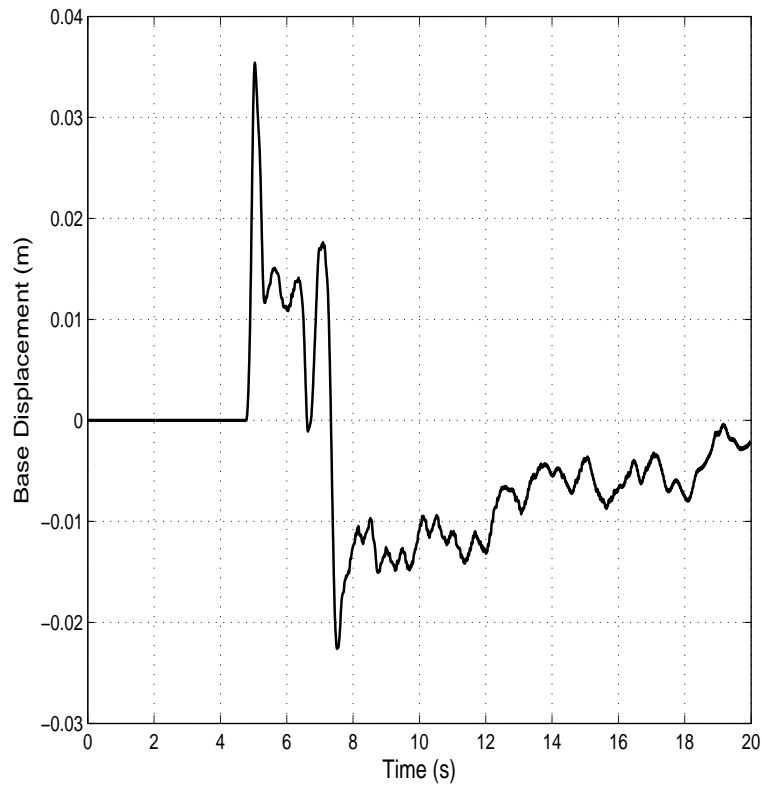


FIGURE A.38: Isolator Displacement (3-storey building) under far-field Northridge-01 earthquake

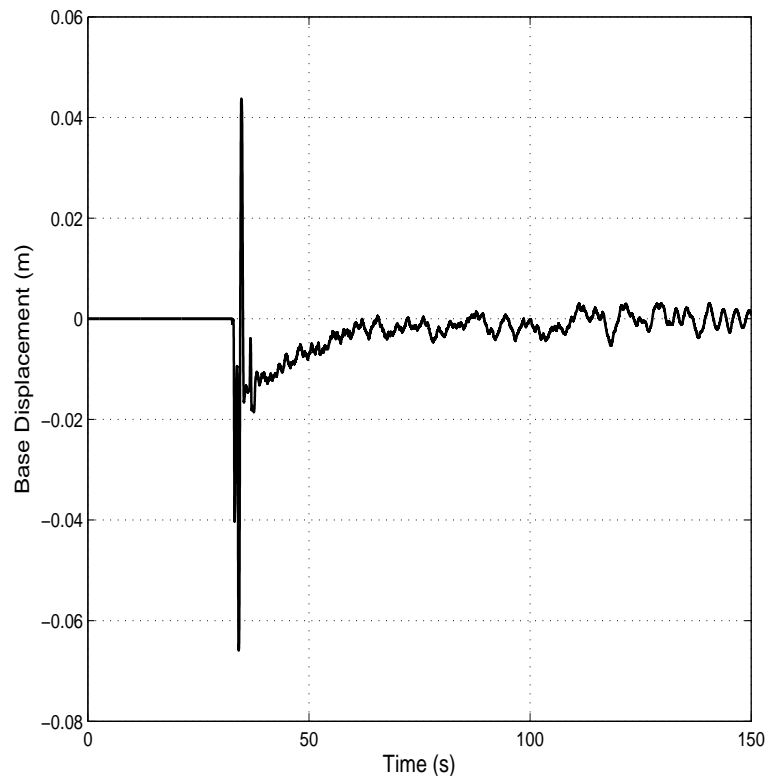


FIGURE A.39: Isolator Displacement (3-storey building) under near-fault Chi-Chi earthquake

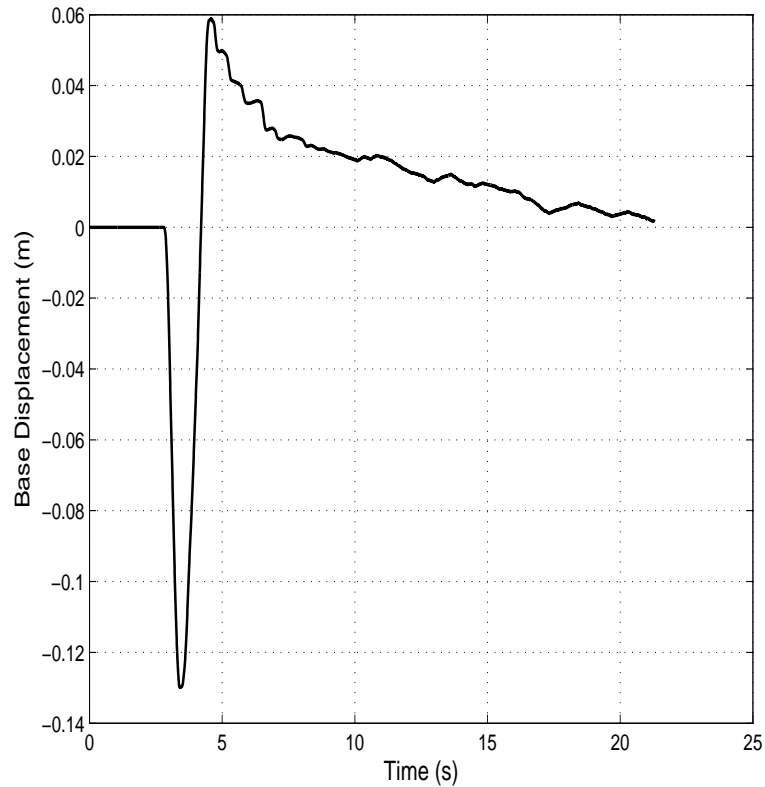


FIGURE A.40: Isolator Displacement (3-storey building) under near-fault Erzican earthquake

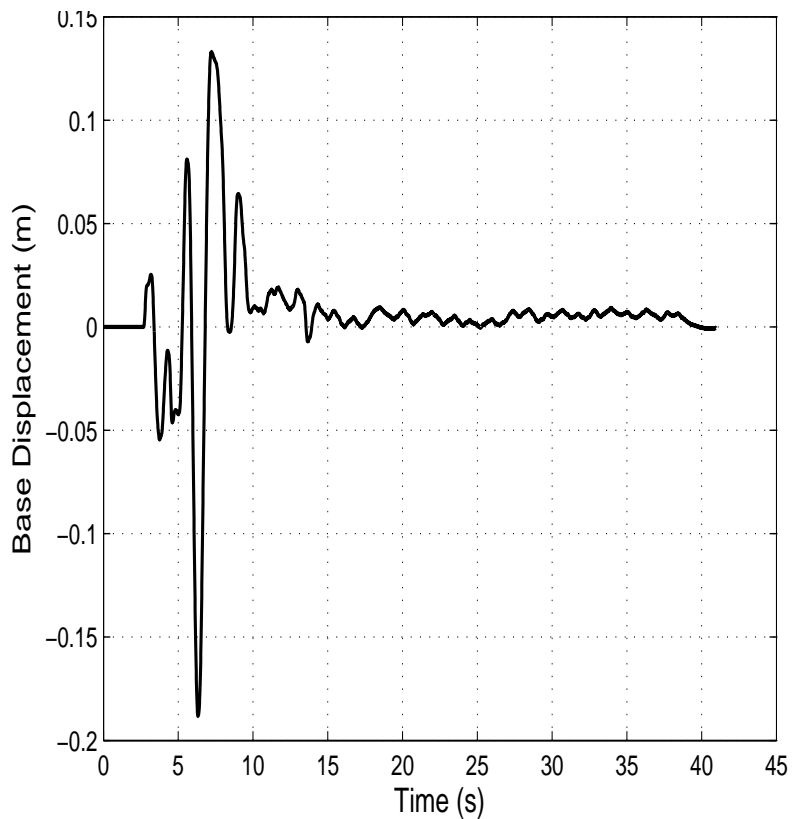


FIGURE A.41: Isolator Displacement (3-storey building) under near-fault Kobe earthquake

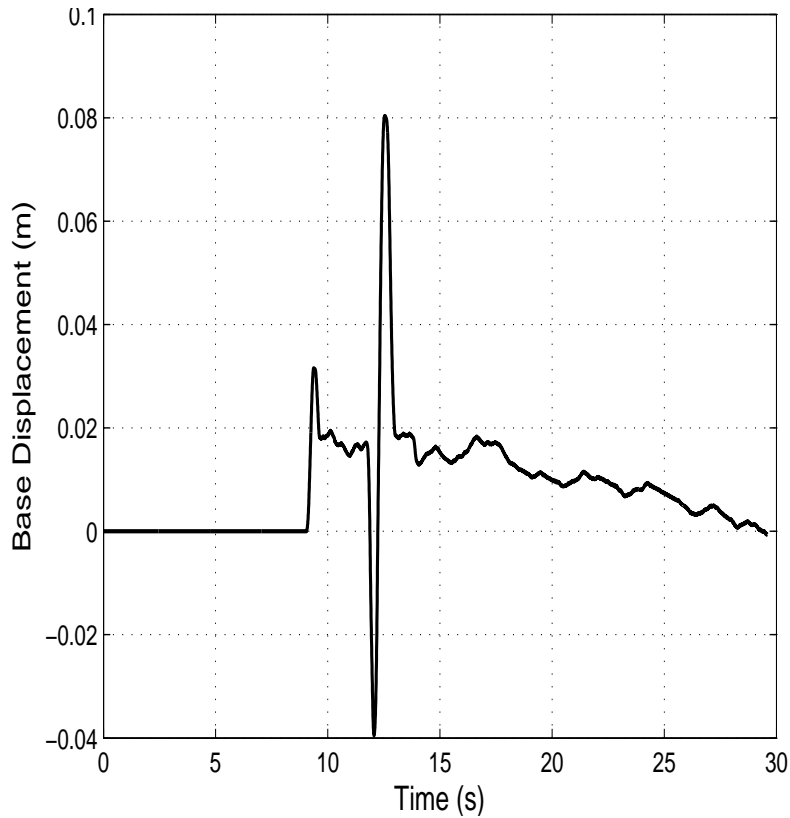


FIGURE A.42: Isolator Displacement (3-storey building) under near-fault Loma Prieta earthquake

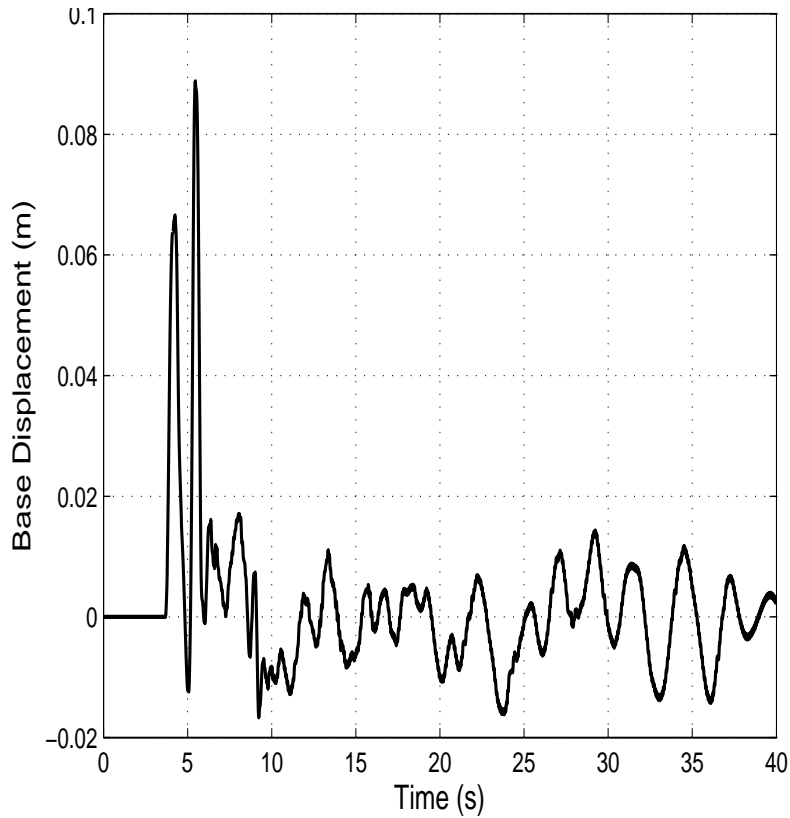


FIGURE A.43: Isolator Displacement (3-storey building) under near-fault Northridge-01 earthquake

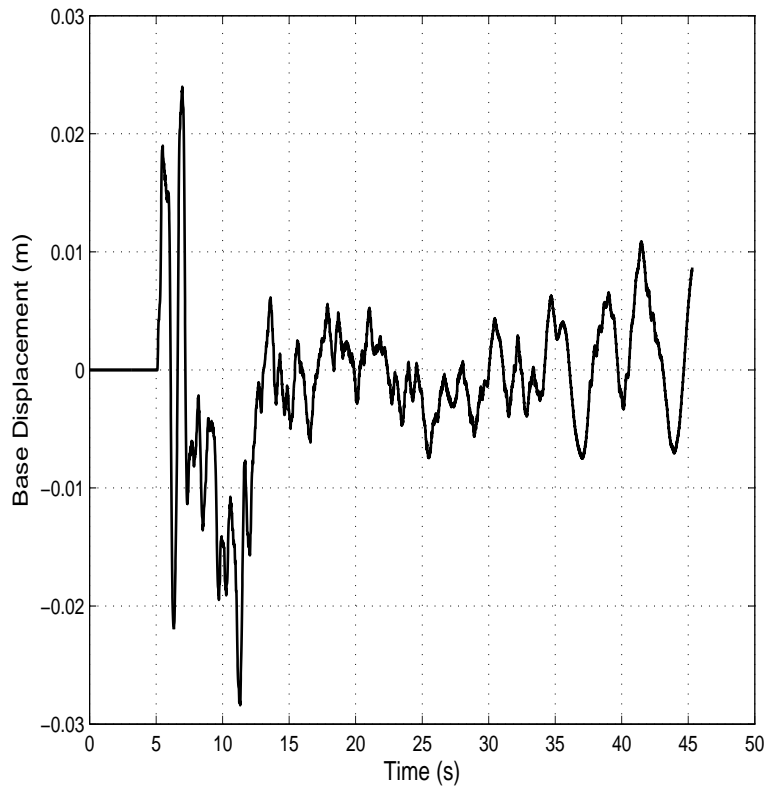


FIGURE A.44: Isolator Displacement (5-storey building) under far-field Imperial Valley earthquake

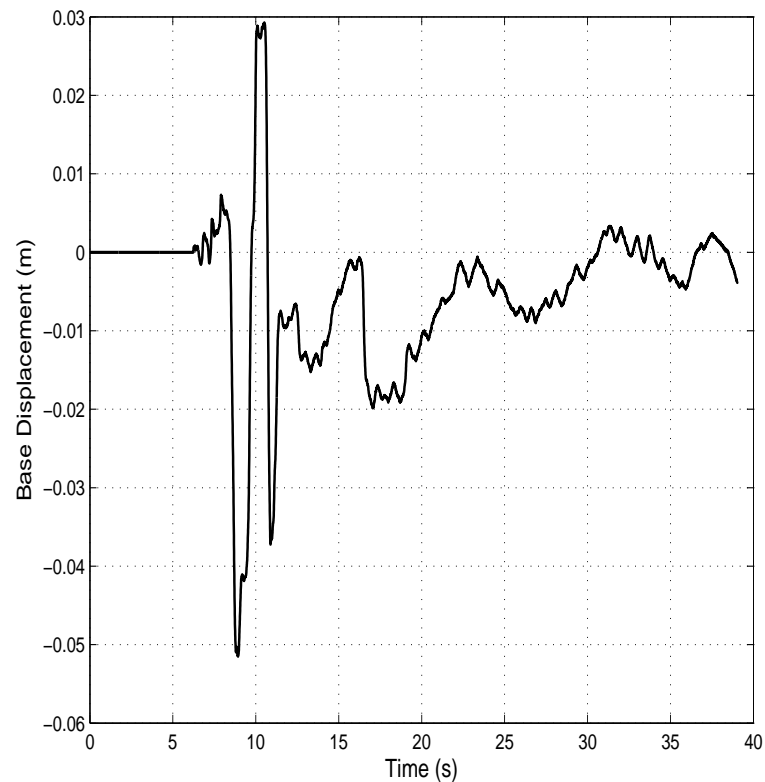


FIGURE A.45: Isolator Displacement (5-storey building) under far-field Imperial Valley earthquake

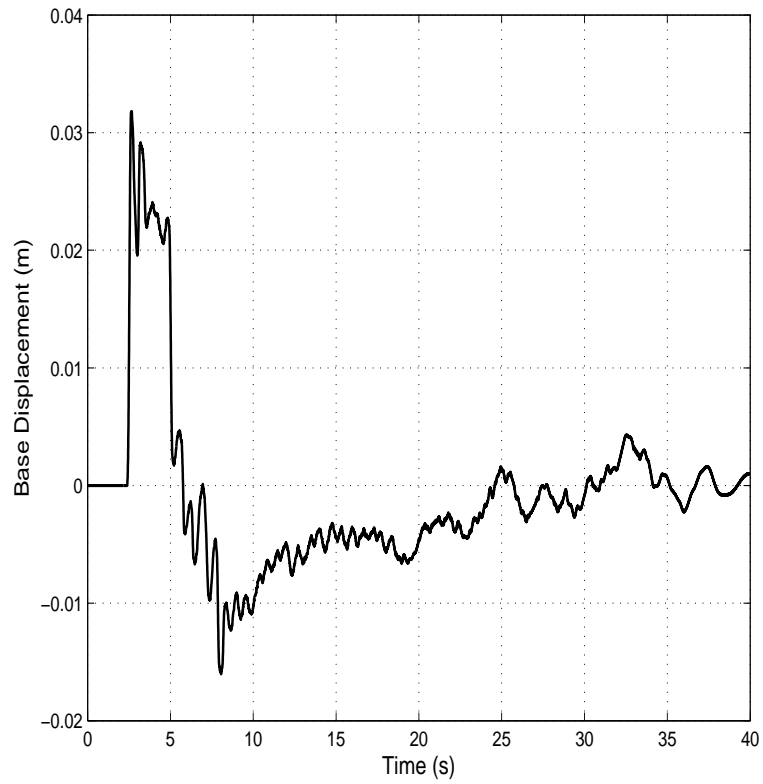


FIGURE A.46: Isolator Displacement (5-storey building) under far-field Loma Prieta earthquake

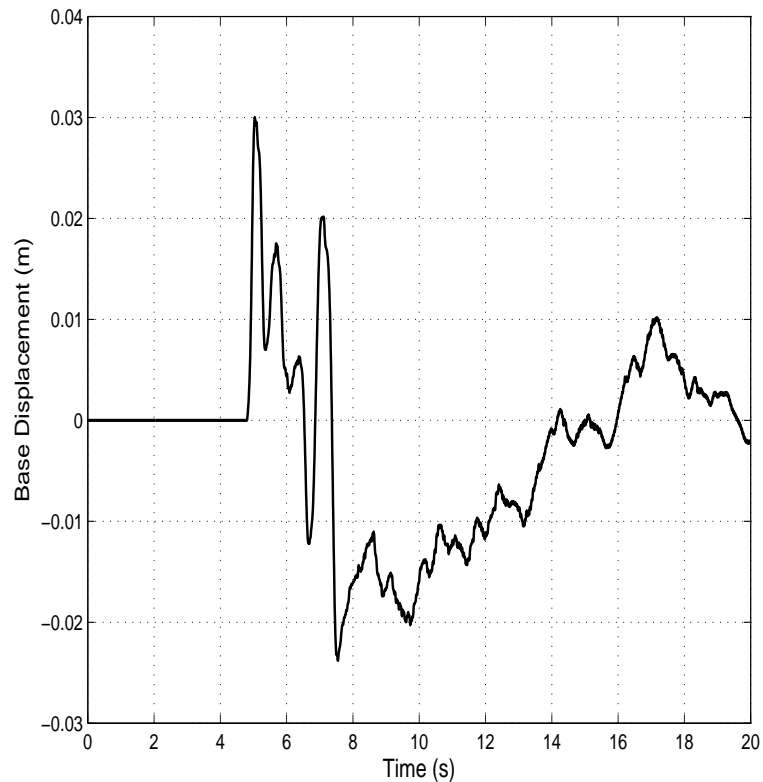


FIGURE A.47: Isolator Displacement (5-storey building) under far-field Northridge-01 earthquake

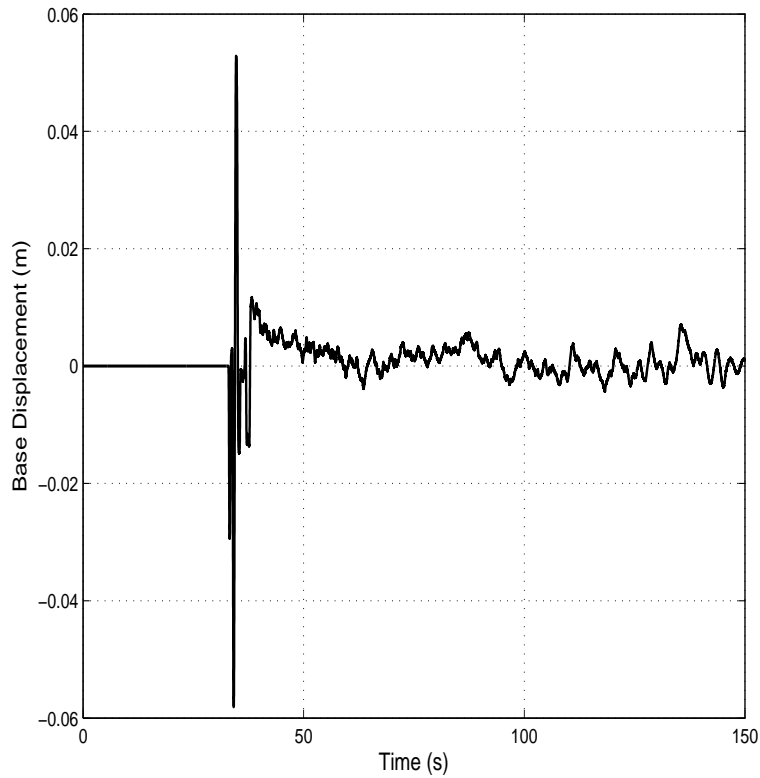


FIGURE A.48: Isolator Displacement (5-storey building) under near-fault Chi-Chi earthquake

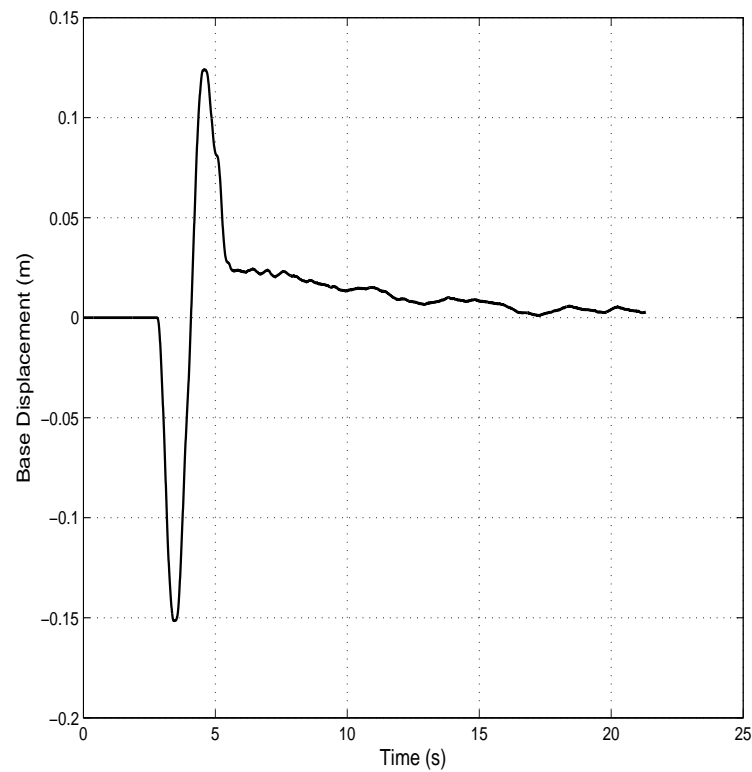


FIGURE A.49: Isolator Displacement (5-storey building) under near-fault Erzican earthquake

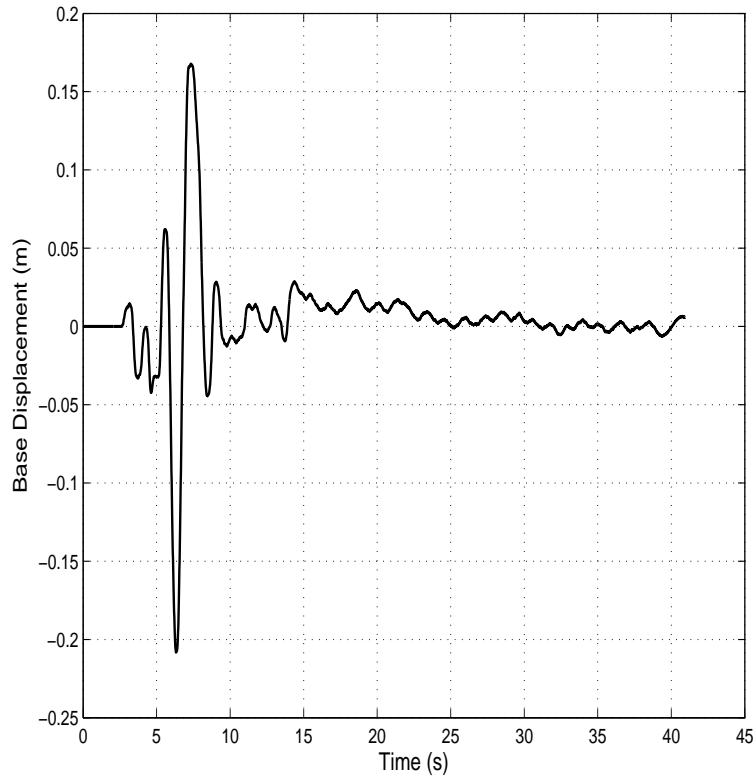


FIGURE A.50: Isolator Displacement (5-storey building) under near-fault Kobe earthquake

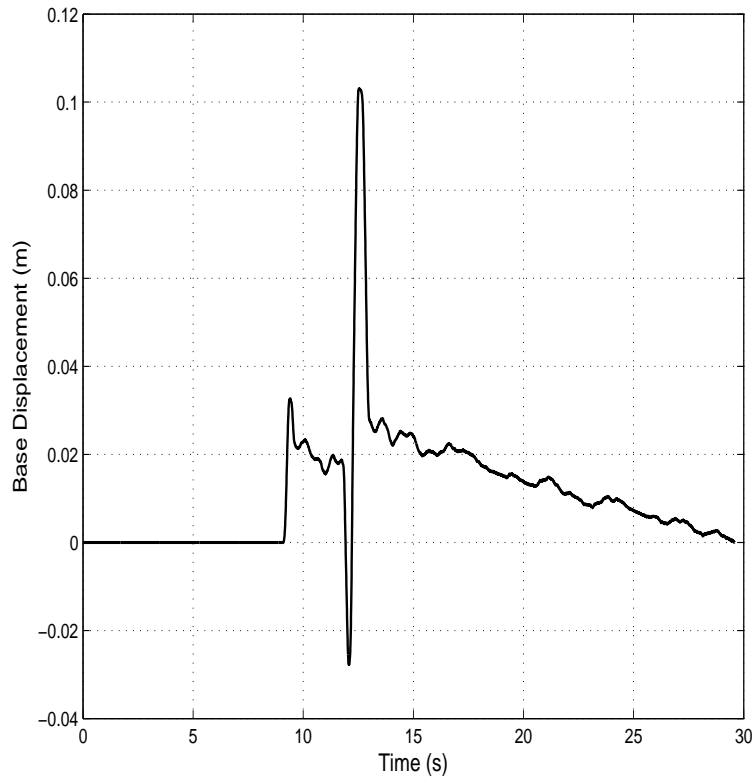


FIGURE A.51: Isolator Displacement (5-storey building) under near-fault Loma Prieta earthquake

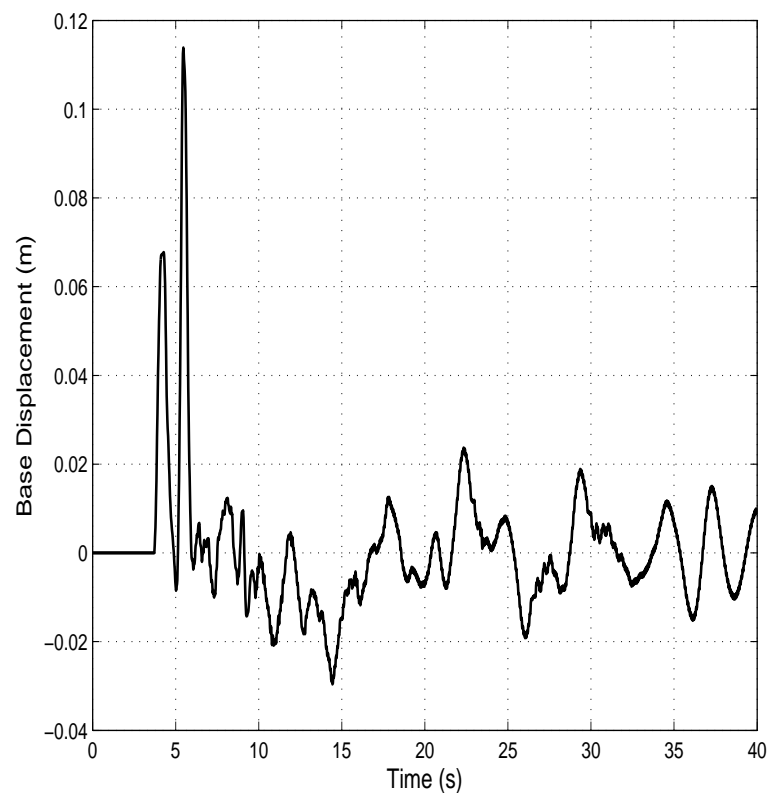


FIGURE A.52: Isolator Displacement (5-storey building) under near-fault Northridge-01 earthquake

A.3 Comparison with conventional FPS isolator

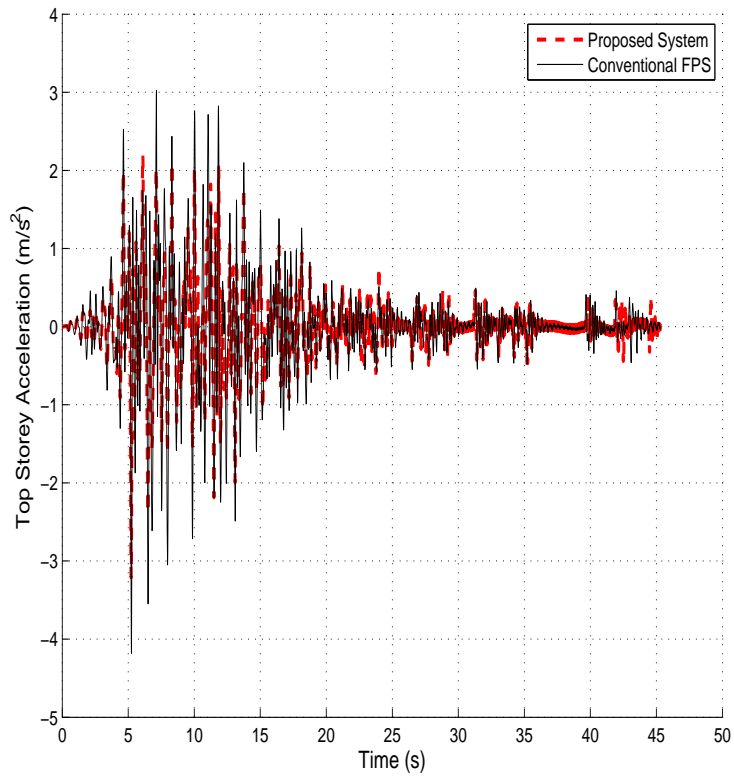


FIGURE A.53: Top storey acceleration (3-storey building) under far-field Hector Mine earthquake

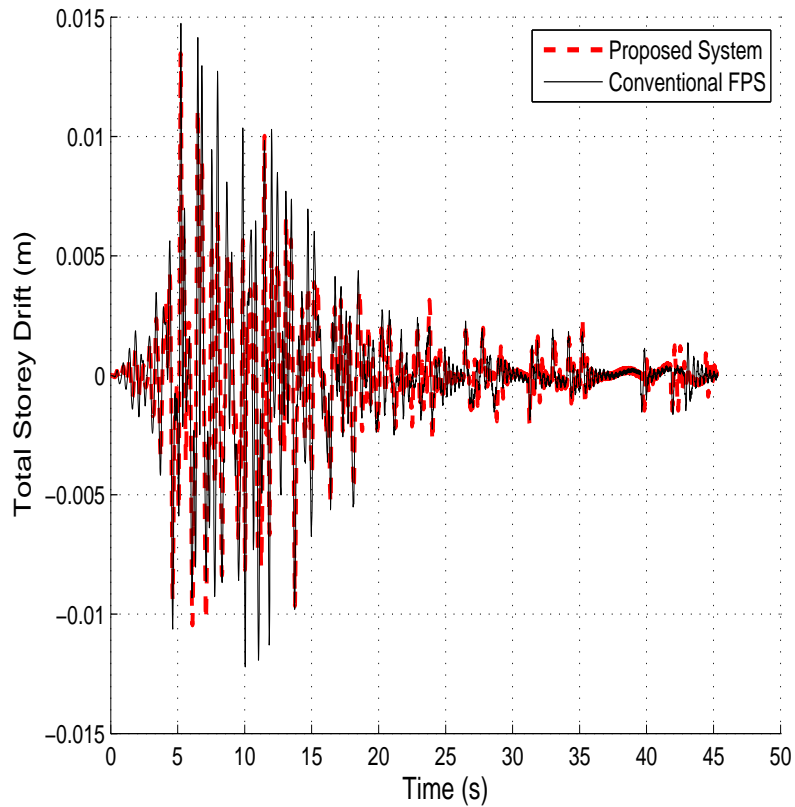


FIGURE A.54: Total Storey Drift (3-storey building) under far-field Hector Mine earthquake

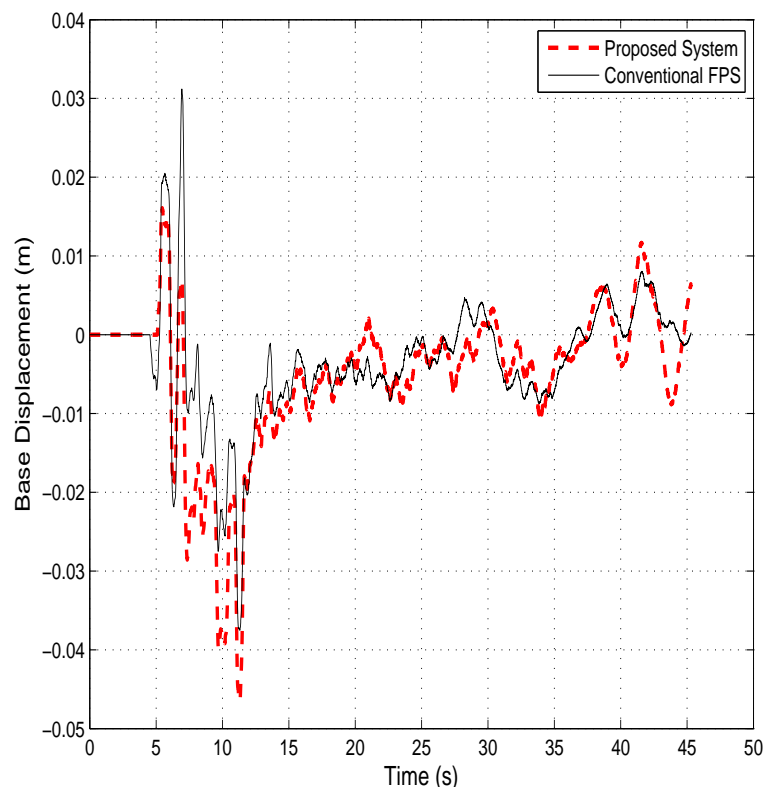


FIGURE A.55: Isolator Displacement (3-storey building) under far-field Hector Mine earthquake

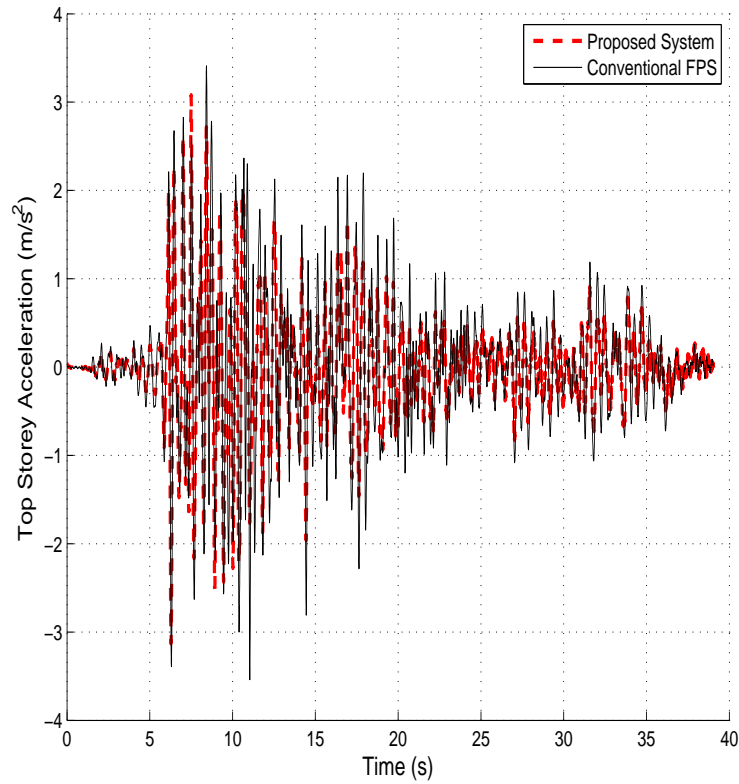


FIGURE A.56: Top storey acceleration (3-storey building) under far-field Imperial Valley earthquake

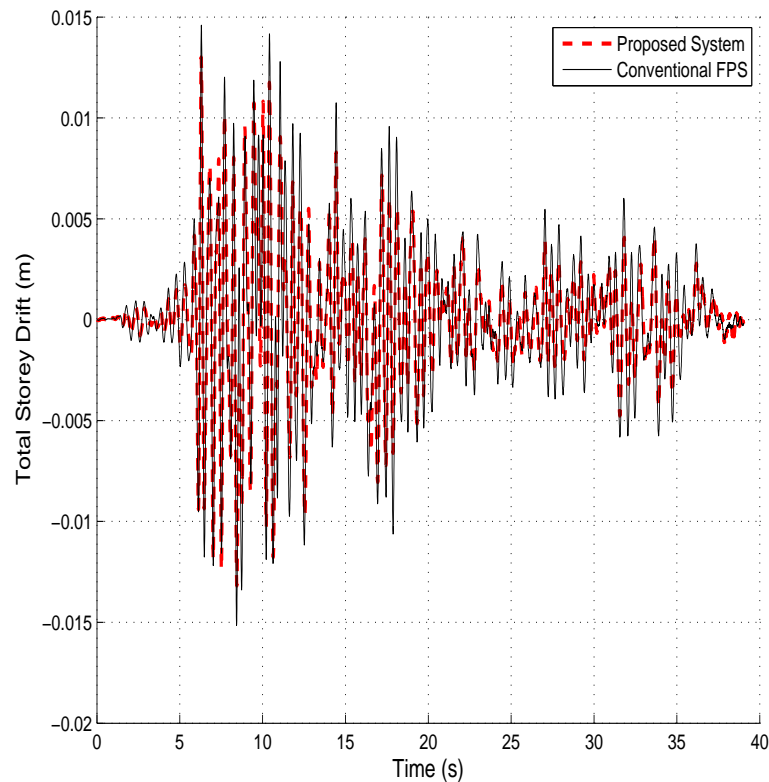


FIGURE A.57: Total Storey Drift (3-storey building) under far-field Imperial Valley earthquake

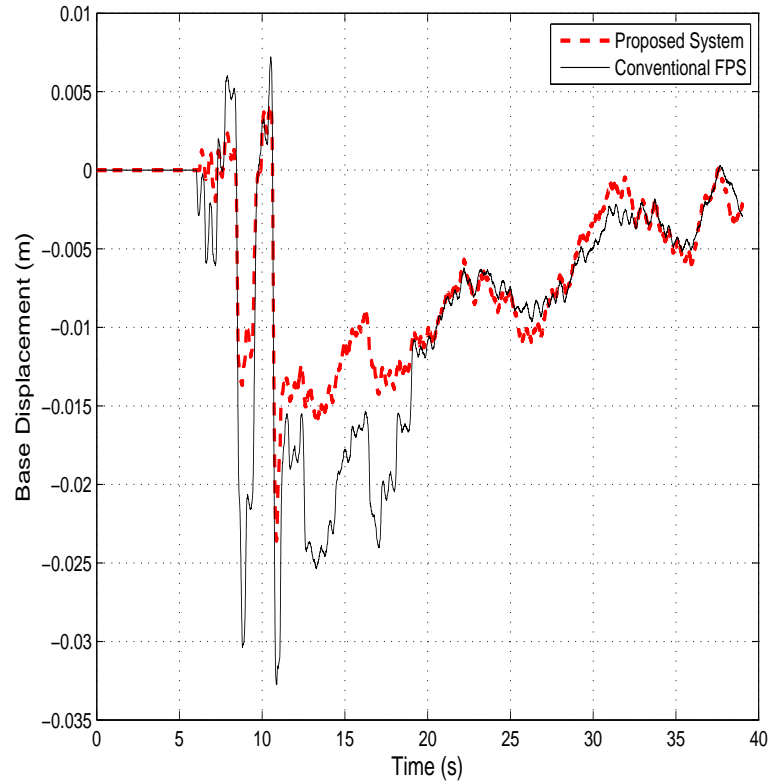


FIGURE A.58: Isolator Displacement (3-storey building) under far-field Imperial Valley earthquake

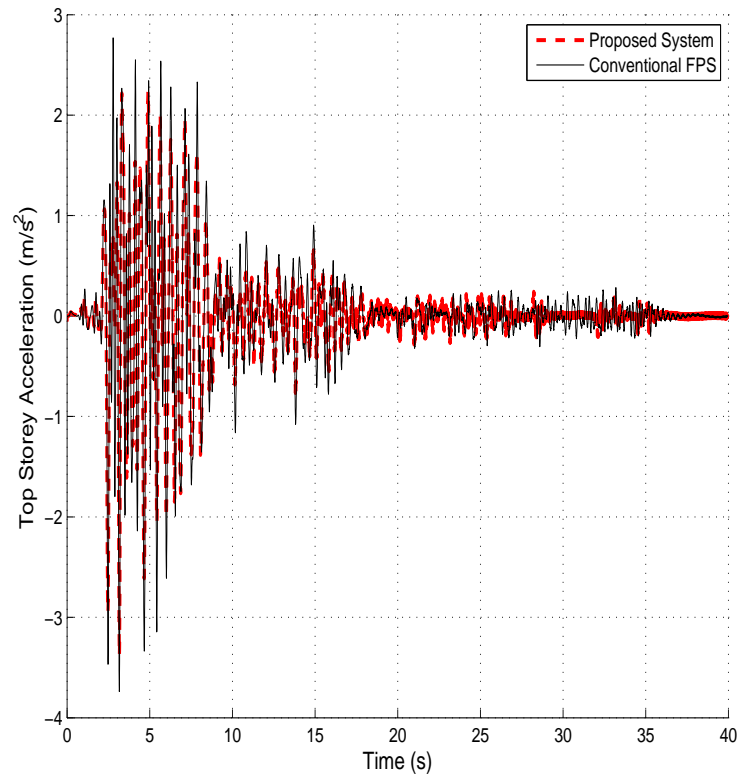


FIGURE A.59: Top storey acceleration (3-storey building) under far-field Loma Prieta earthquake

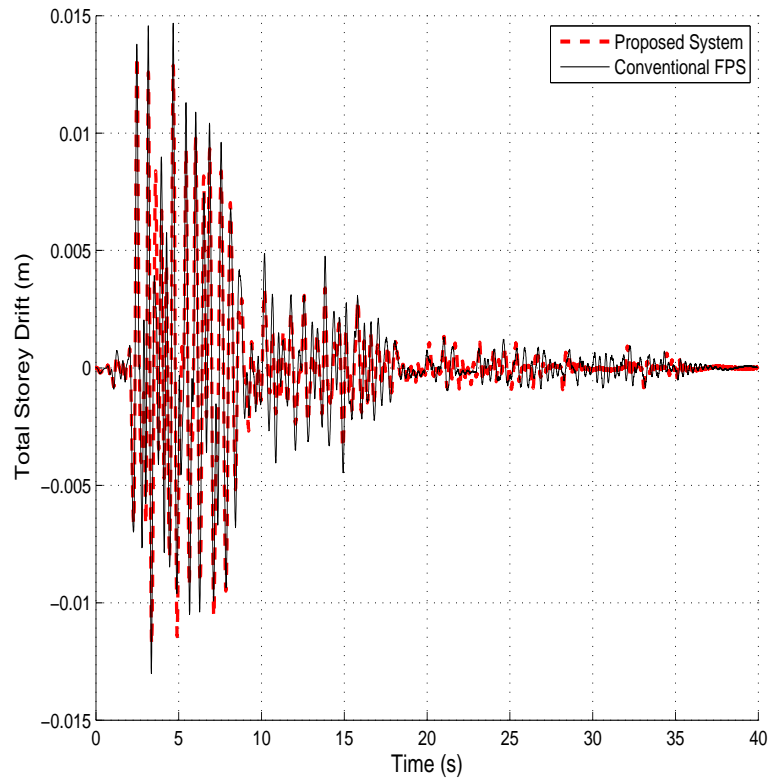


FIGURE A.60: Total Storey Drift (3-storey building) under far-field Loma Prieta earthquake

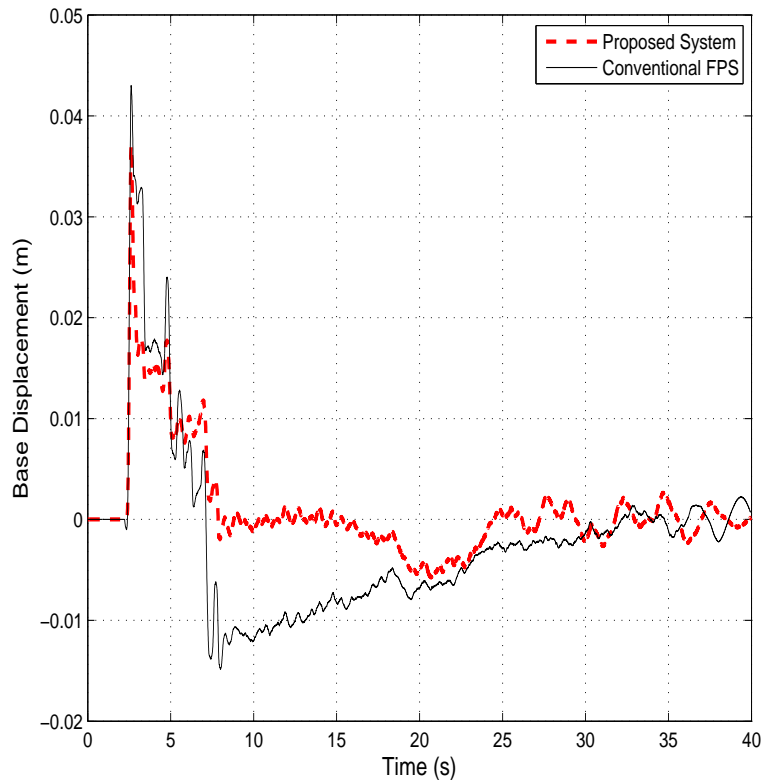


FIGURE A.61: Isolator Displacement (3-storey building) under far-field Loma Prieta earthquake

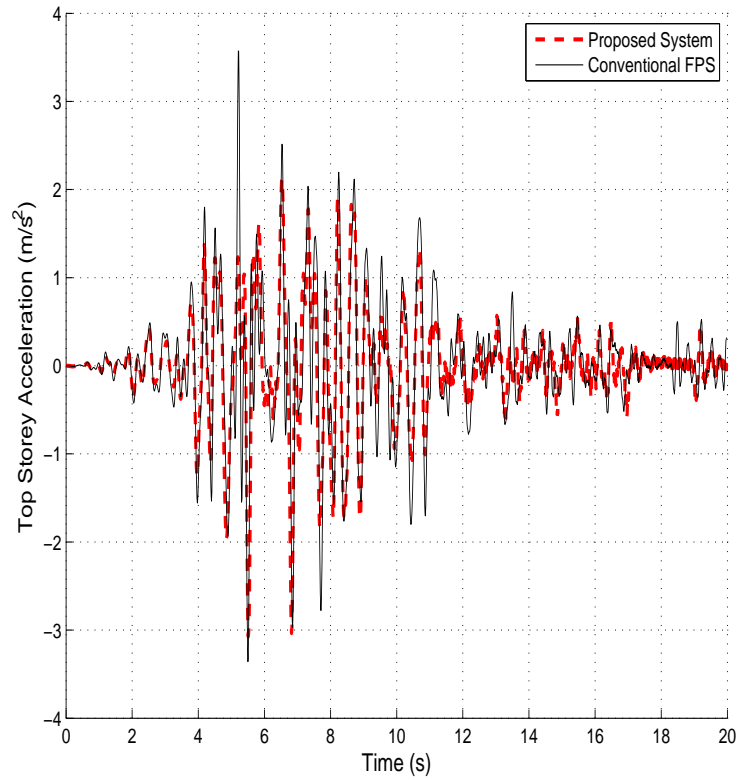


FIGURE A.62: Top storey acceleration (3-storey building) under far-field Northridge-01 earthquake

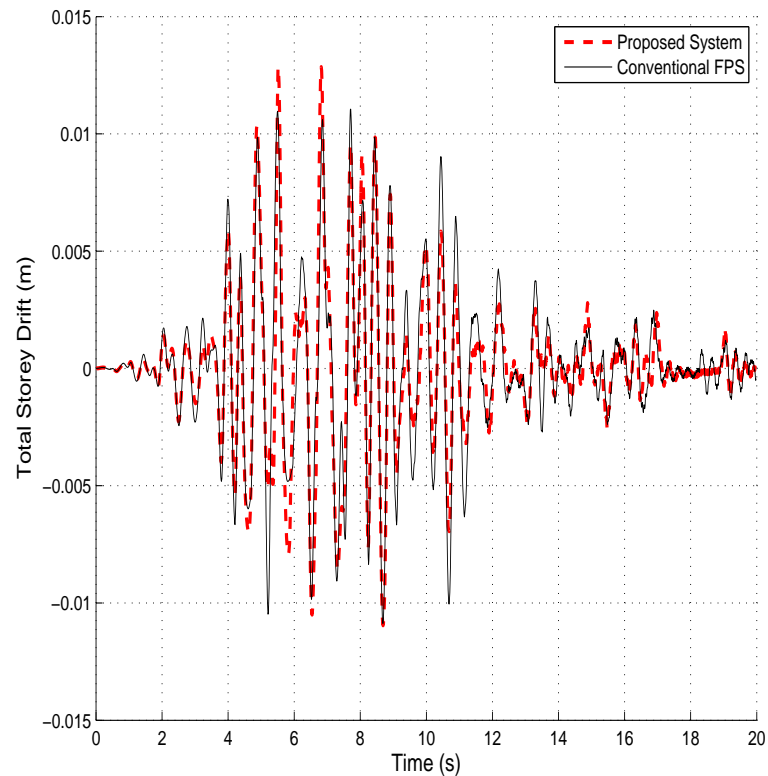


FIGURE A.63: Total Storey Drift (3-storey building) under far-field Northridge-01 earthquake

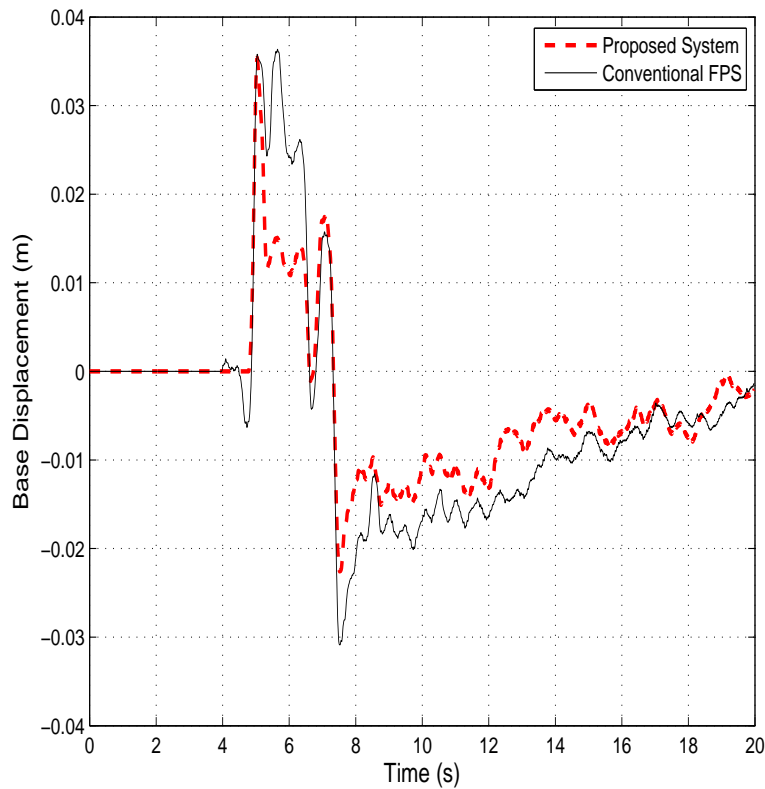


FIGURE A.64: Isolator Displacement (3-storey building) under far-field Northridge-01 earthquake

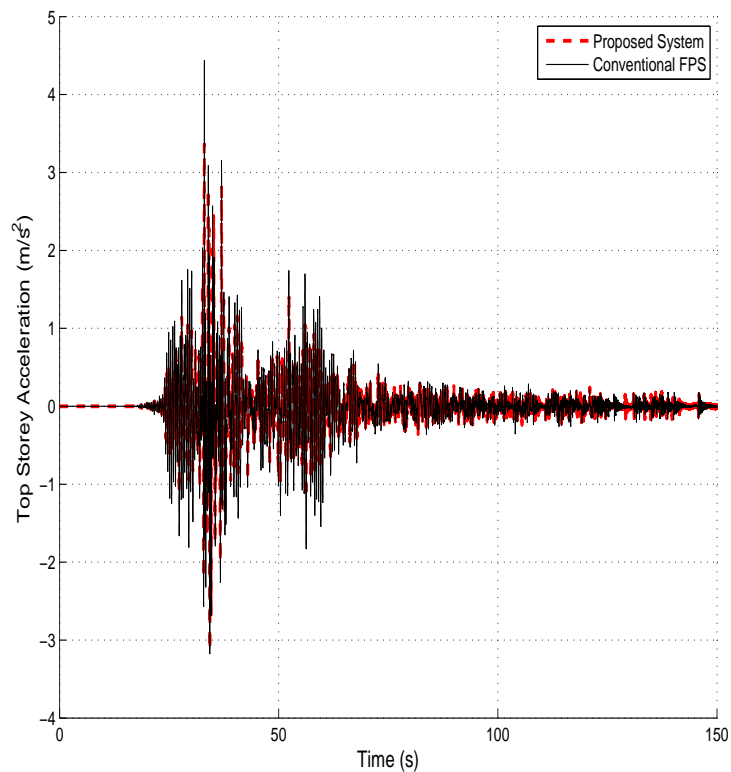


FIGURE A.65: Top storey acceleration (3-storey building) under near-fault Chi-Chi earthquake

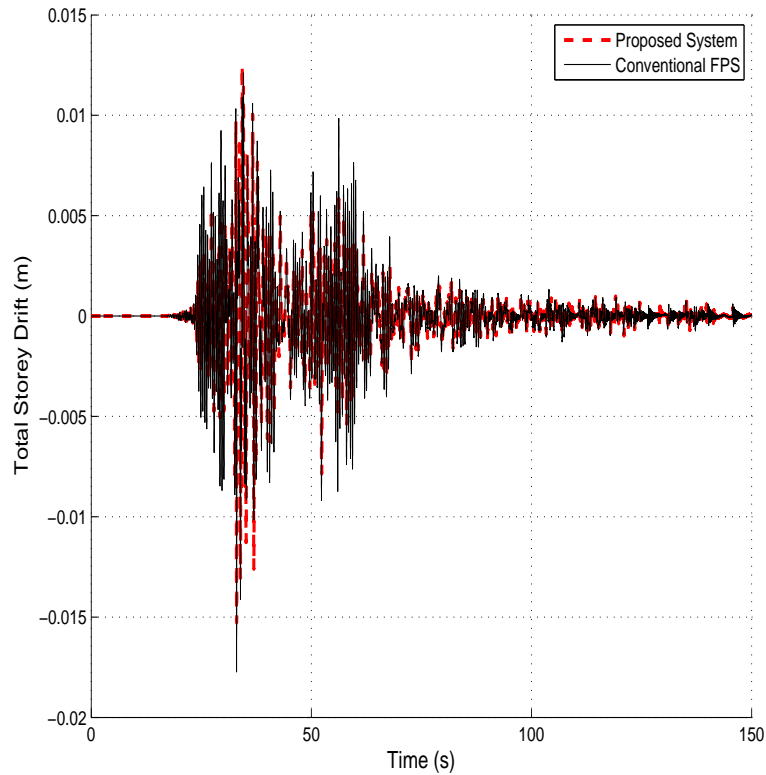


FIGURE A.66: Total Storey Drift (3-storey building) under near-fault Chi-Chi earthquake

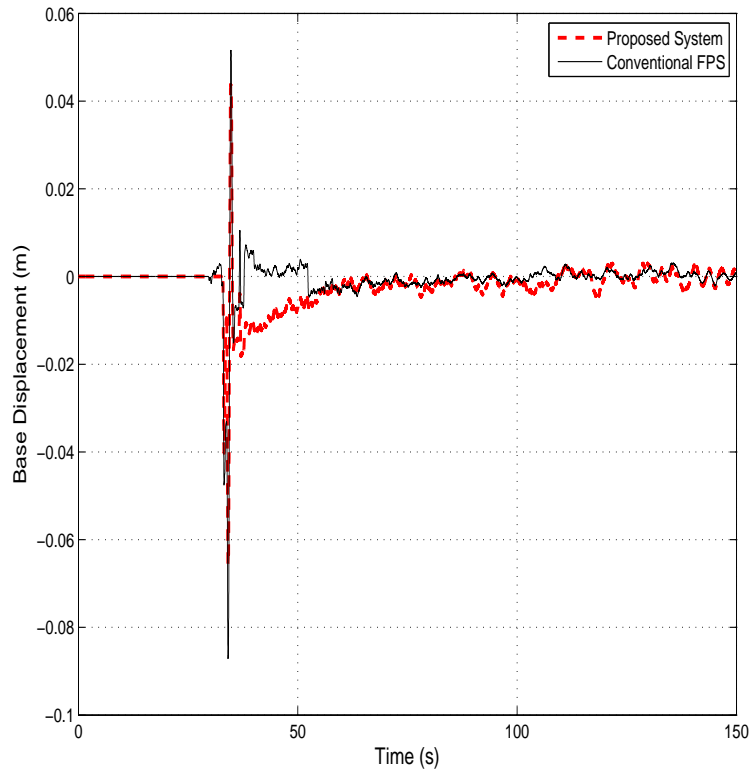


FIGURE A.67: Isolator Displacement (3-storey building) under near-fault Chi-Chi earthquake

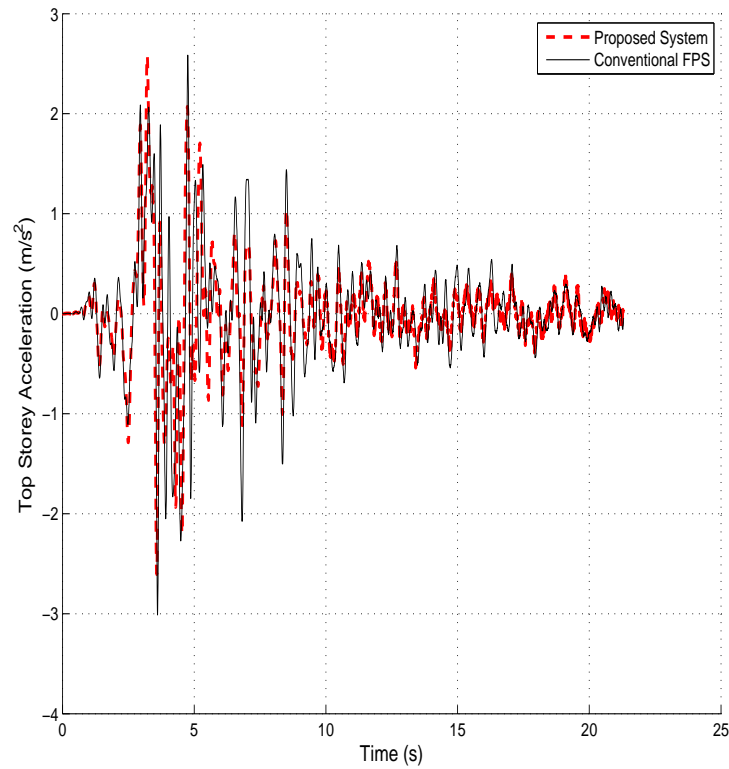


FIGURE A.68: Top storey acceleration (3-storey building) under near-fault Erzican earthquake

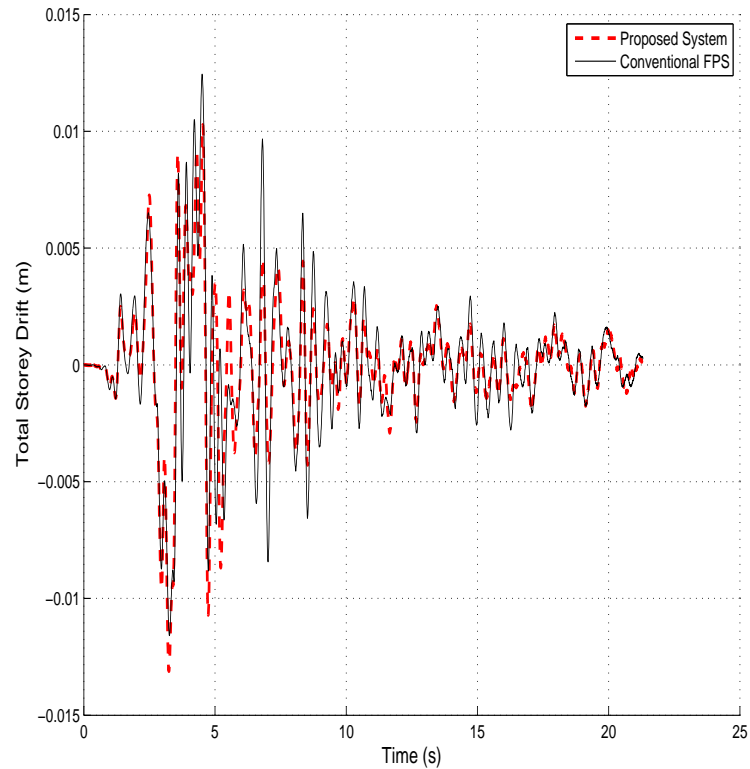


FIGURE A.69: Total Storey Drift (3-storey building) under near-fault Erzican earthquake

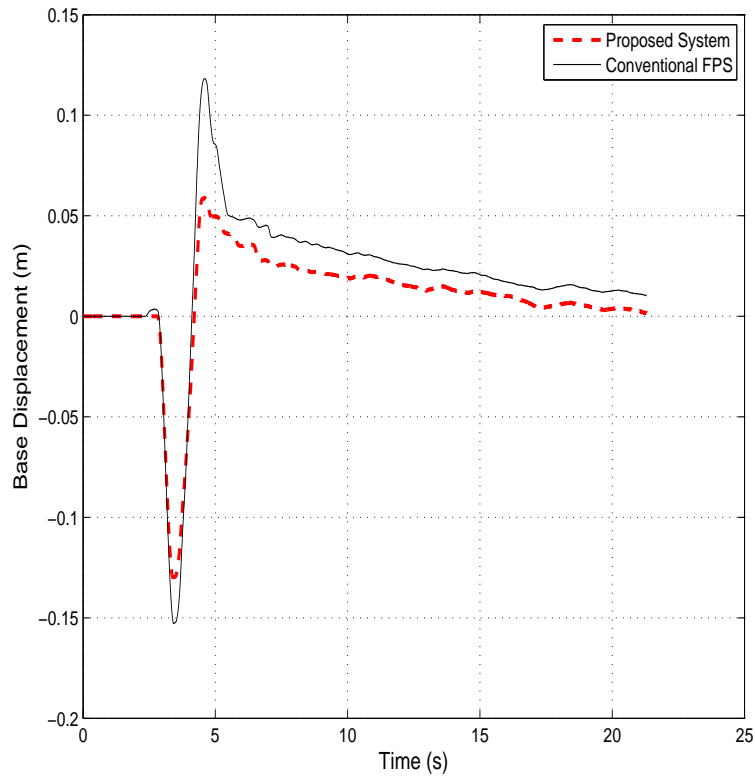


FIGURE A.70: Isolator Displacement (3-storey building) under near-fault Erzican earthquake

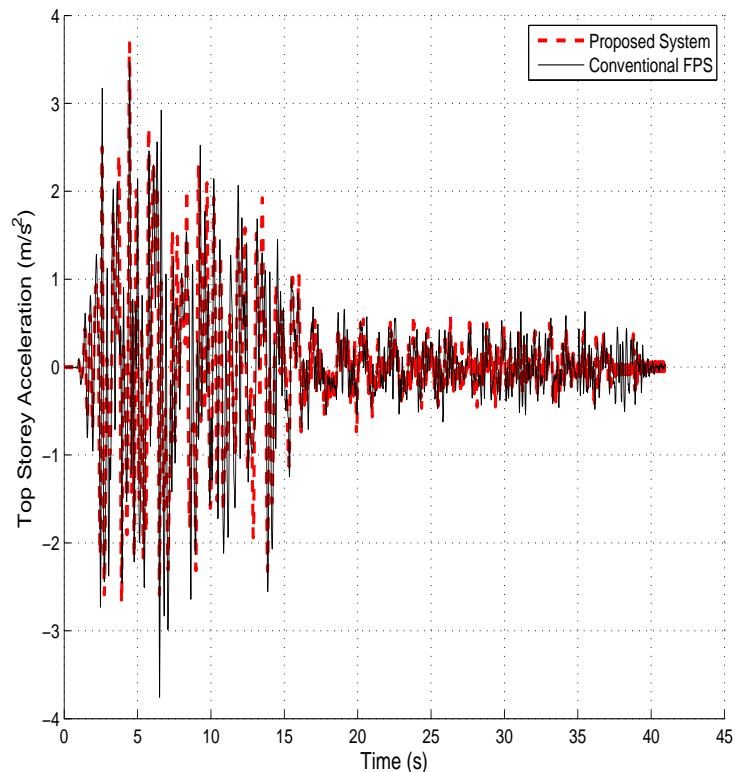


FIGURE A.71: Top storey acceleration (3-storey building) under near-fault Kobe earthquake

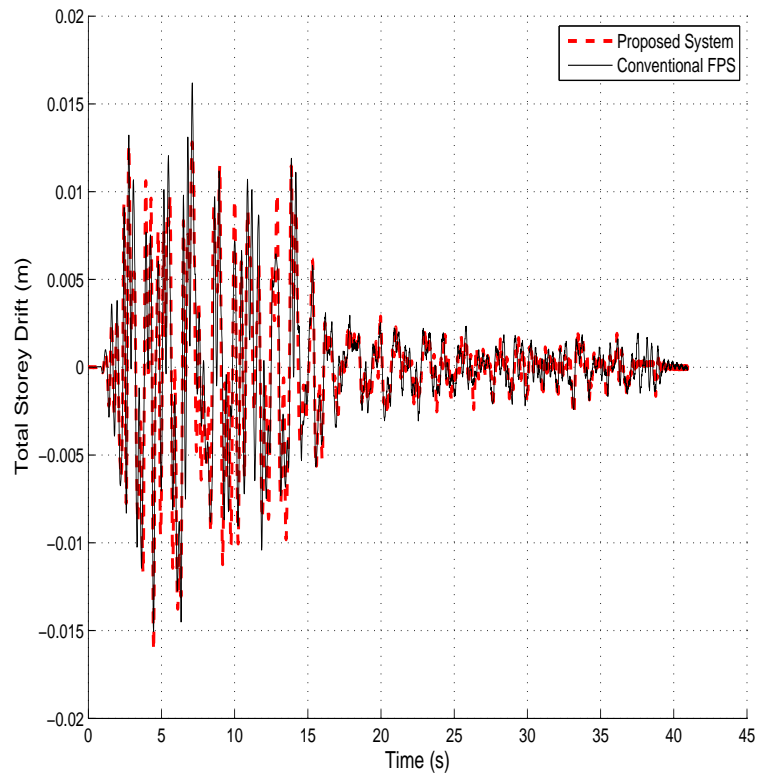


FIGURE A.72: Total Storey Drift (3-storey building) under near-fault Kobe earthquake

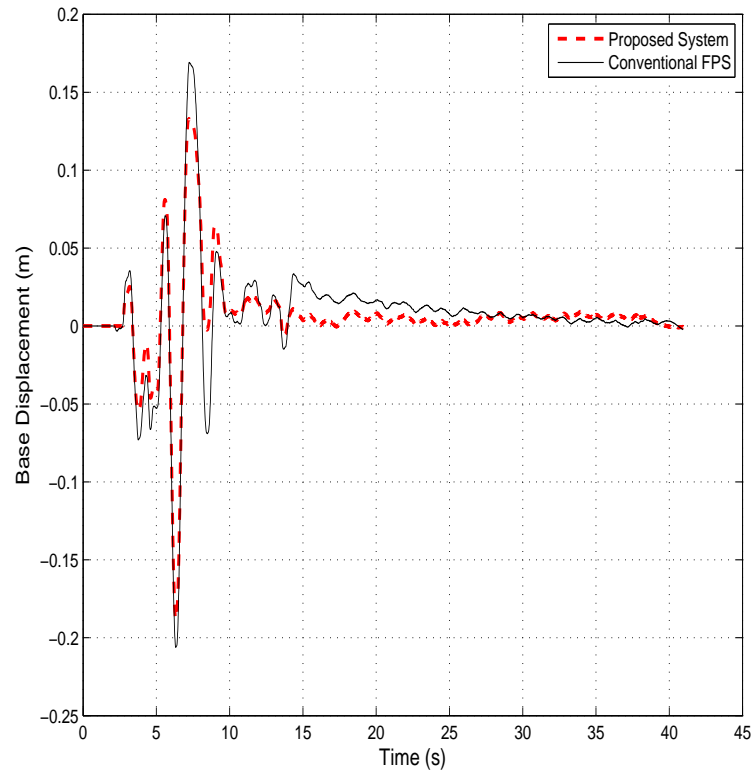


FIGURE A.73: Isolator Displacement (3-storey building) under near-fault Kobe earthquake

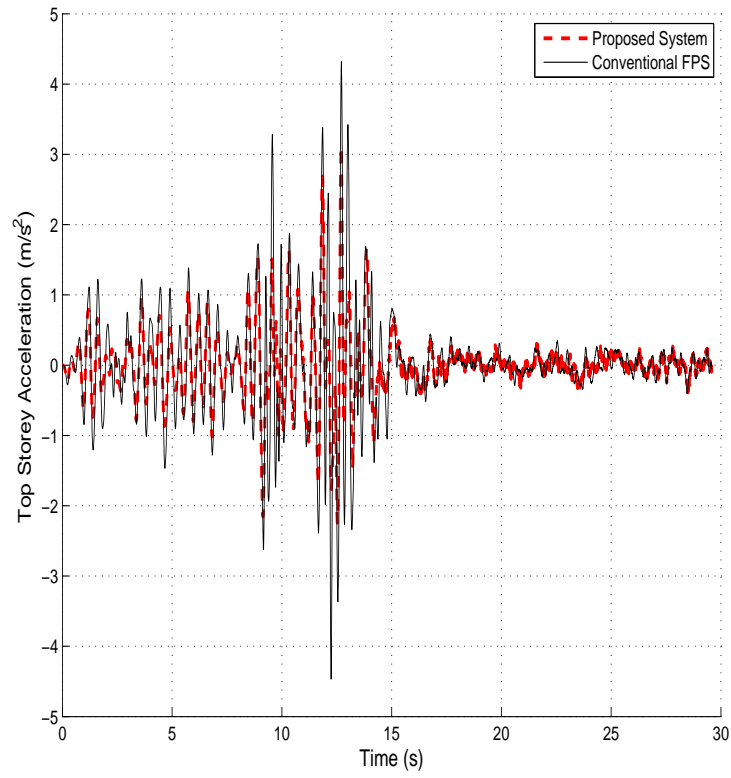


FIGURE A.74: Top storey acceleration (3-storey building) under near-fault Loma Prieta earthquake

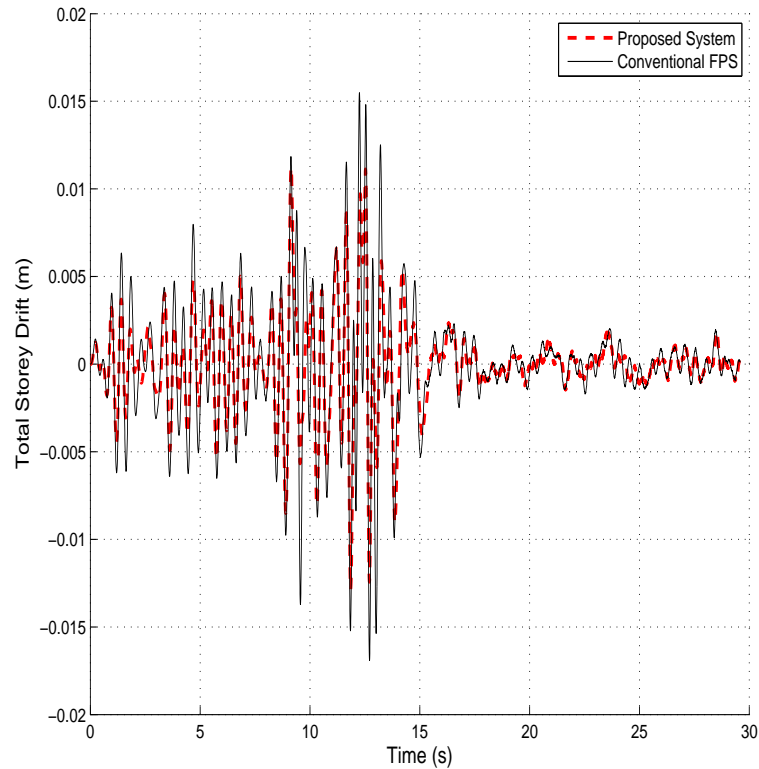


FIGURE A.75: Total Storey Drift (3-storey building) under near-fault Loma Prieta earthquake

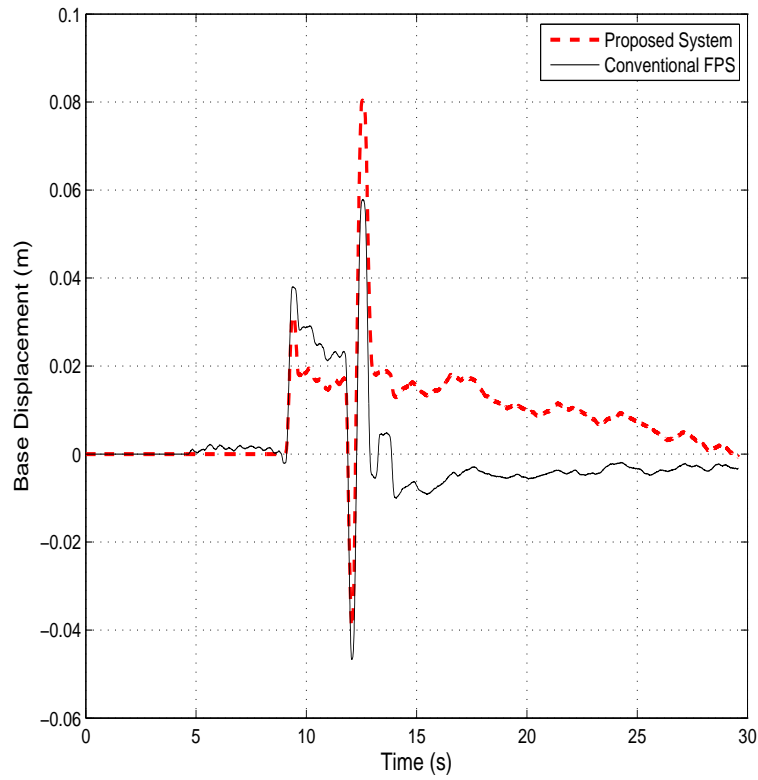


FIGURE A.76: Isolator Displacement (3-storey building) under near-fault Loma Prieta earthquake

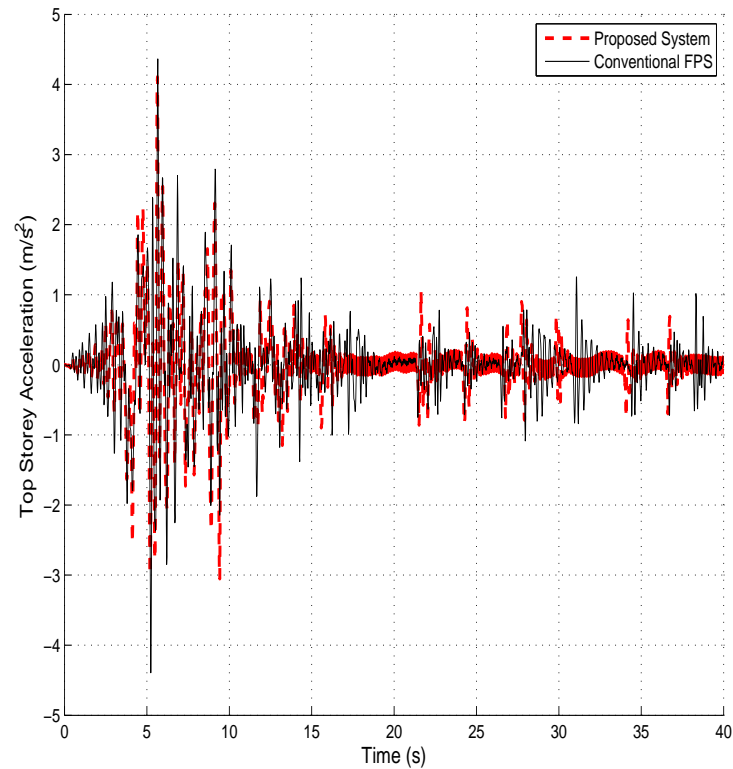


FIGURE A.77: Top storey acceleration (3-storey building) under near-fault Northridge-01 earthquake

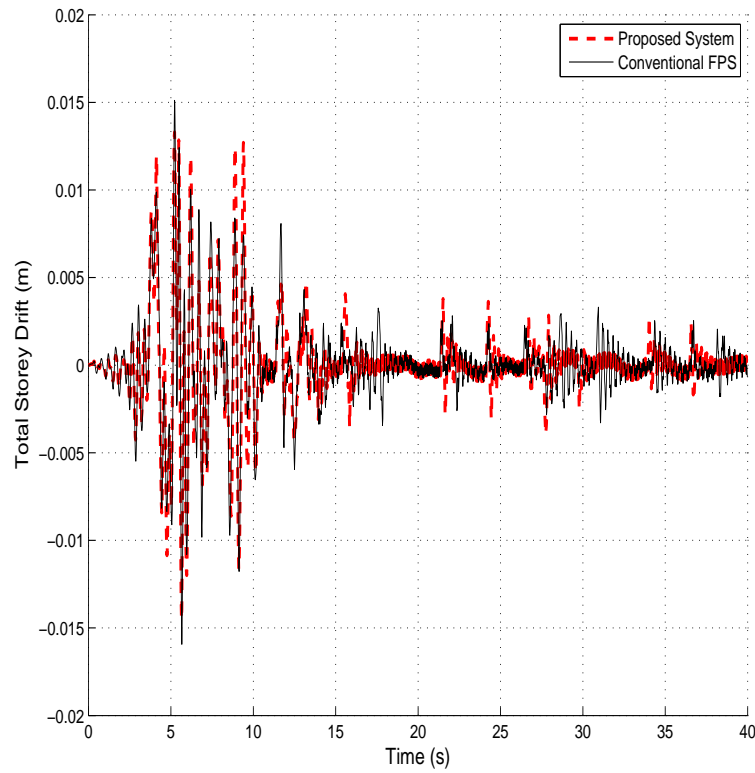


FIGURE A.78: Total Storey Drift (3-storey building) under near-fault Northridge-01 earthquake

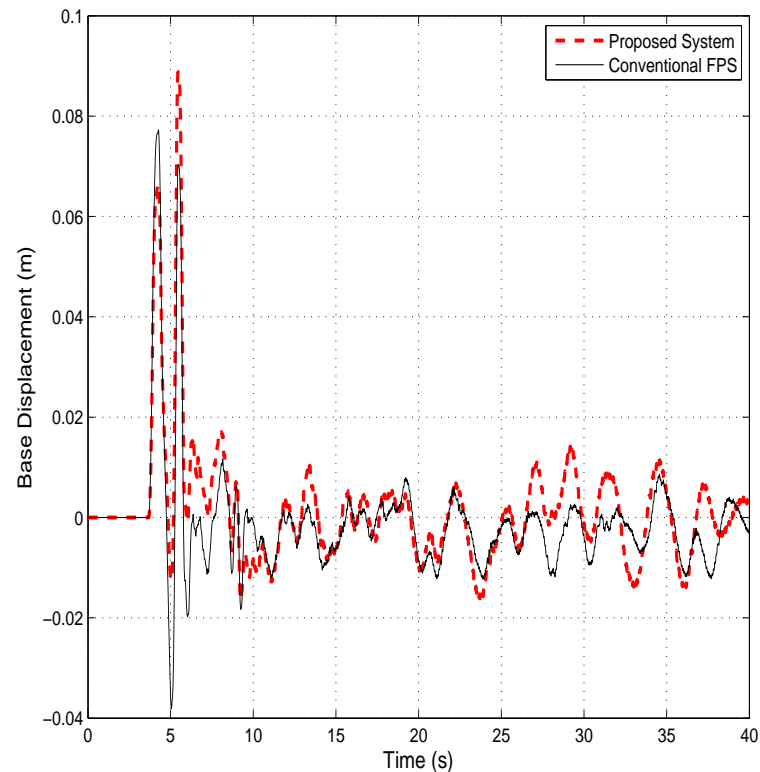


FIGURE A.79: Isolator Displacement (3-storey building) under near-fault Northridge-01 earthquake

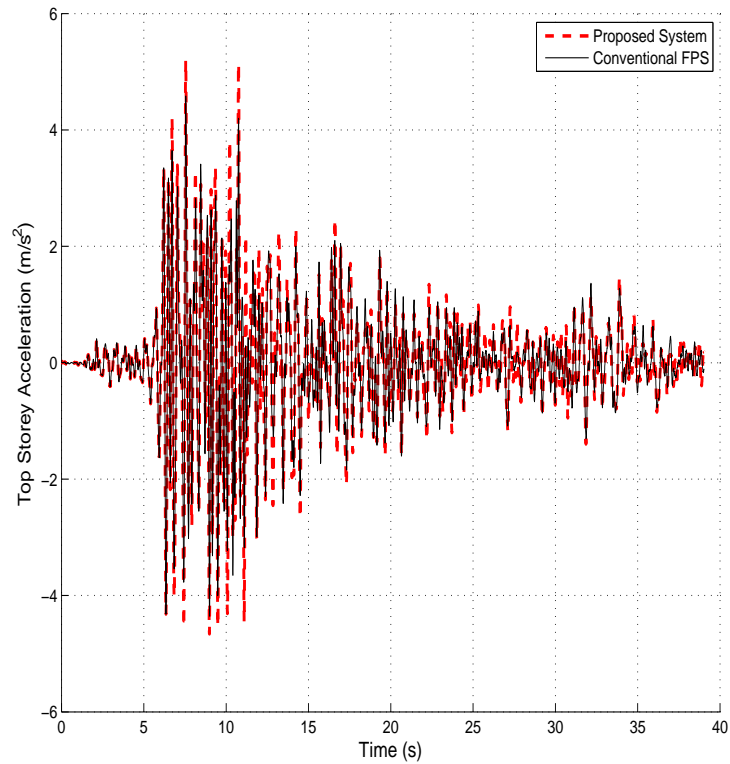


FIGURE A.80: Top storey acceleration (5-storey building) under far-field Imperial Valley earthquake

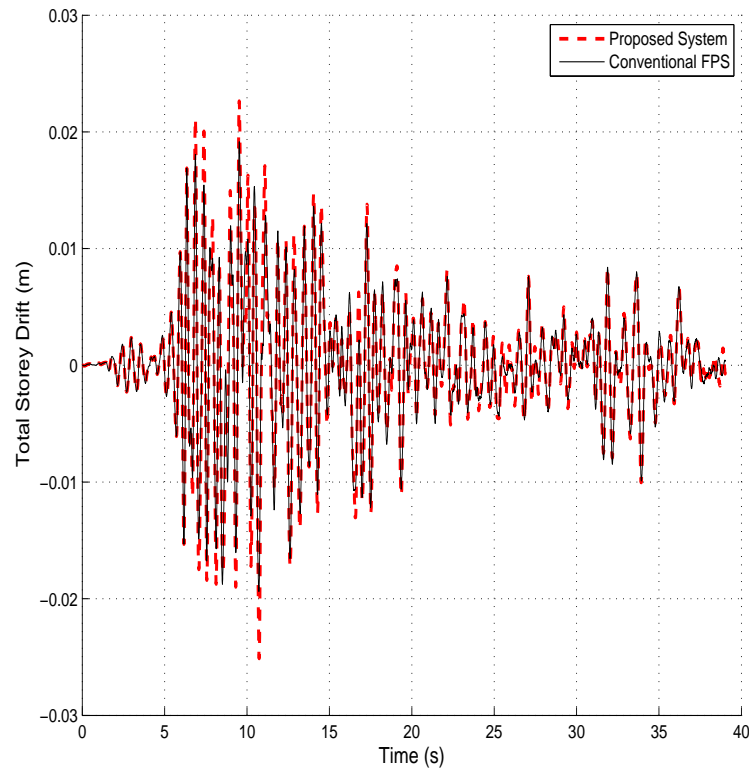


FIGURE A.81: Total Storey Drift (5-storey building) under far-field Imperial Valley earthquake

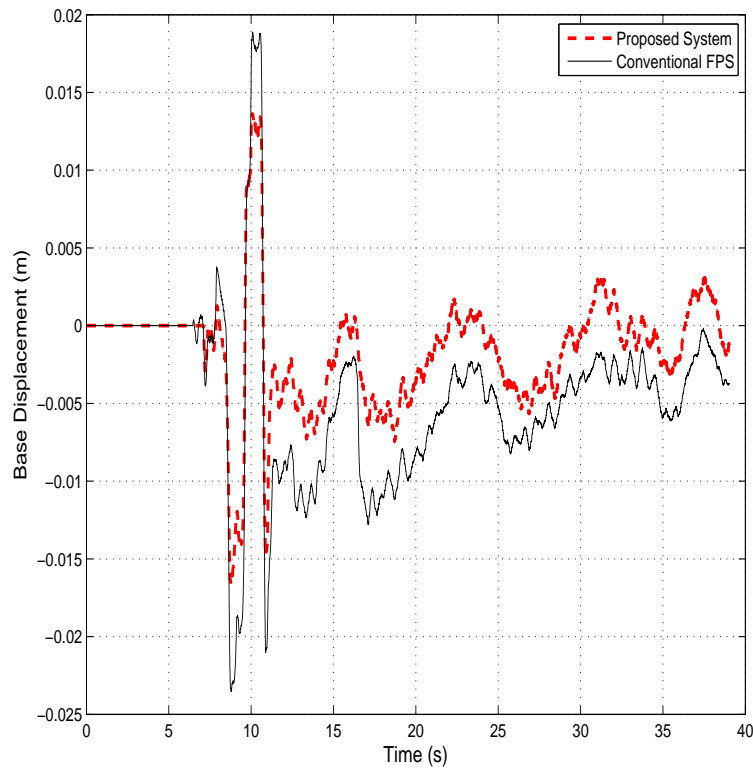


FIGURE A.82: Isolator Displacement (5-storey building) under far-field Imperial Valley earthquake

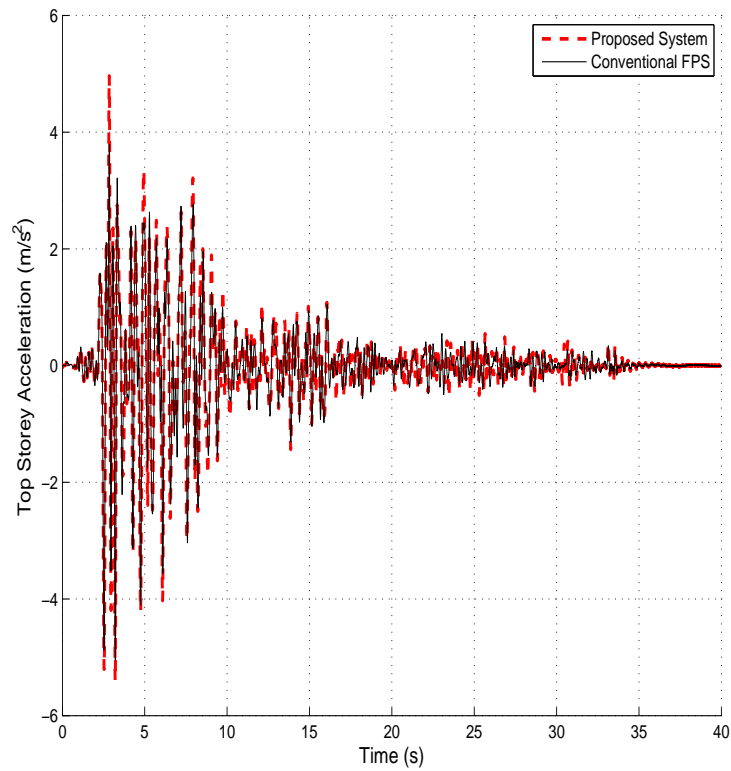


FIGURE A.83: Top storey acceleration (5-storey building) under far-field Loma Prieta earthquake

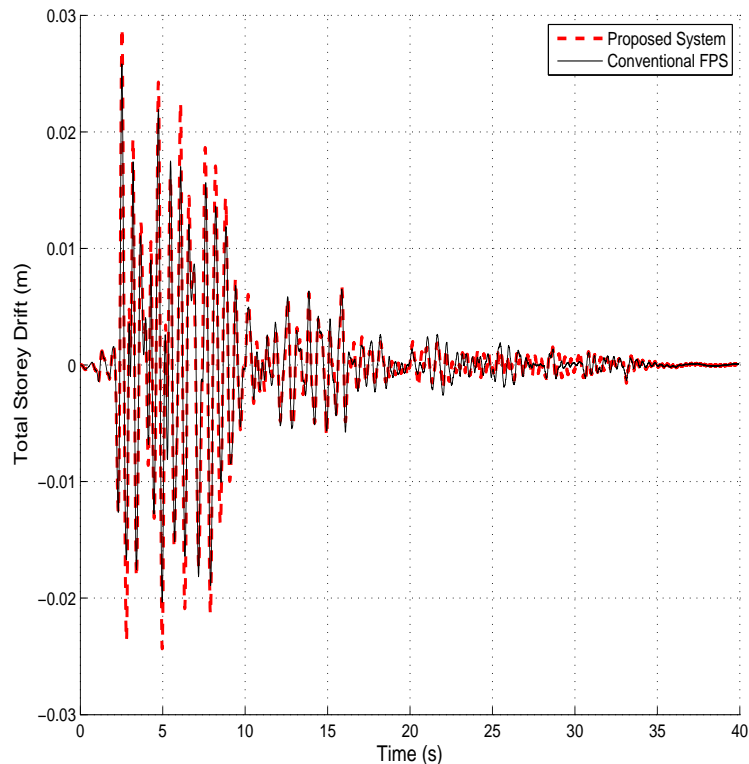


FIGURE A.84: Total Storey Drift (5-storey building) under far-field Loma Prieta earthquake

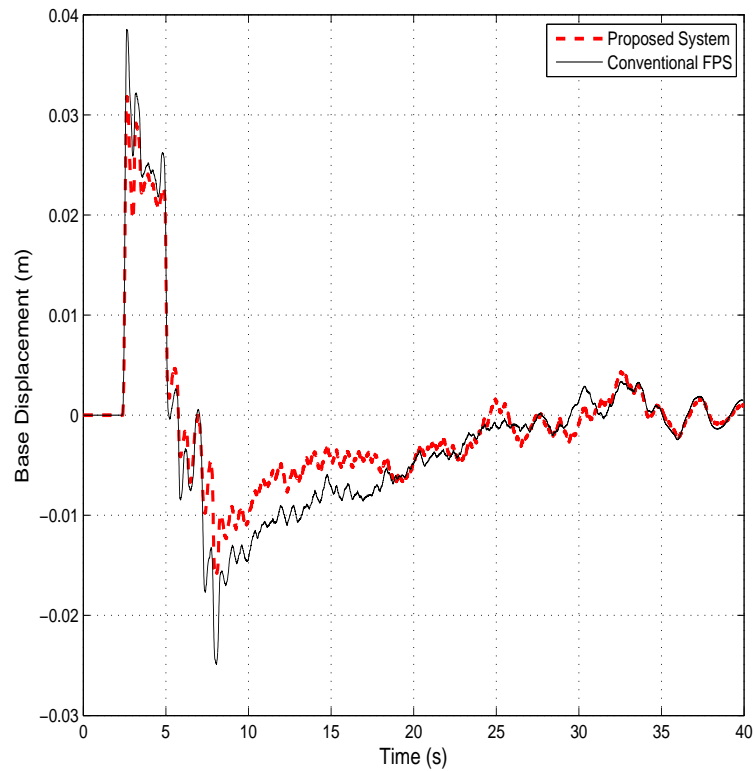


FIGURE A.85: Isolator Displacement (5-storey building) under far-field Loma Prieta earthquake

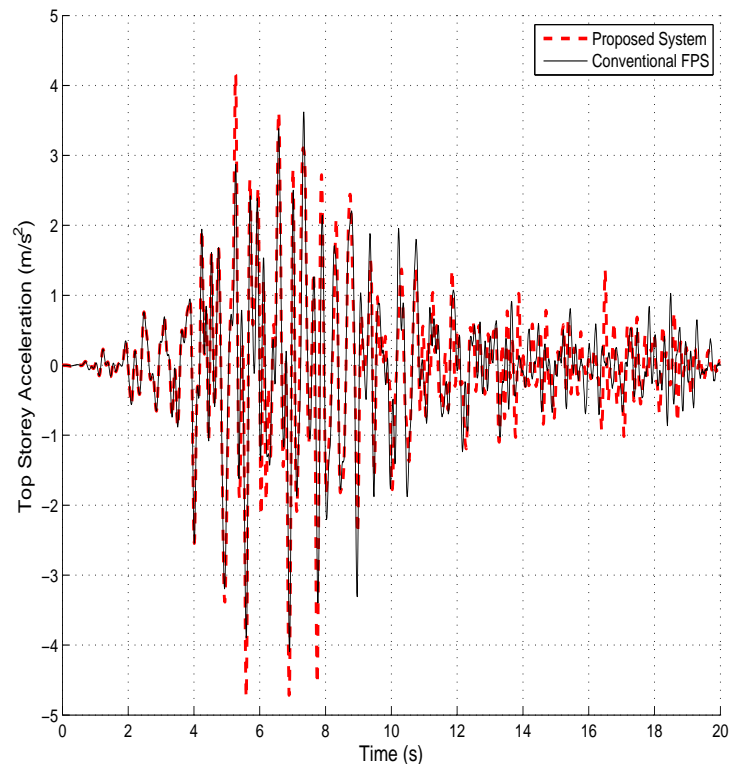


FIGURE A.86: Top storey acceleration (5-storey building) under far-field Northridge-01 earthquake

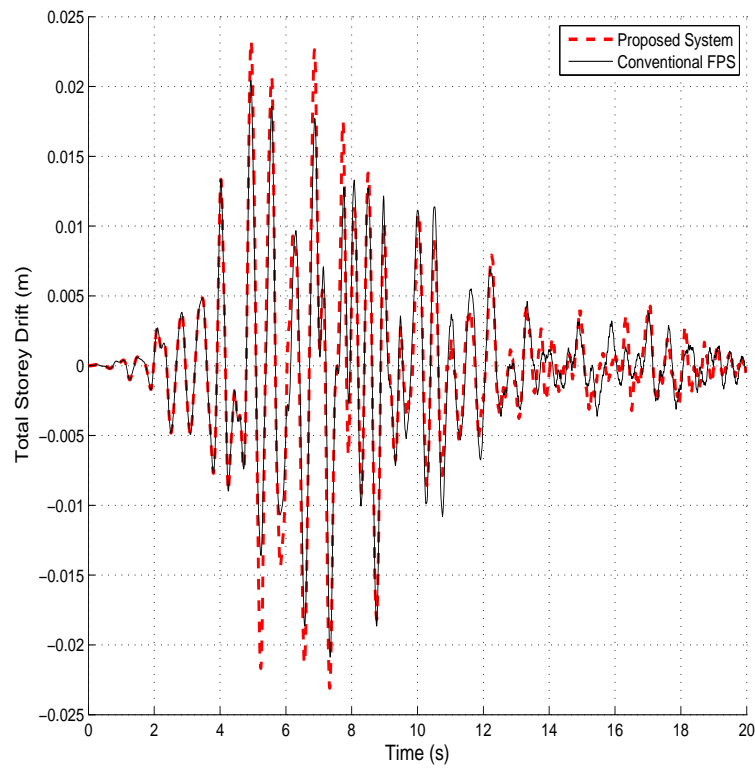


FIGURE A.87: Total Storey Drift (5-storey building) under far-field Northridge-01 earthquake

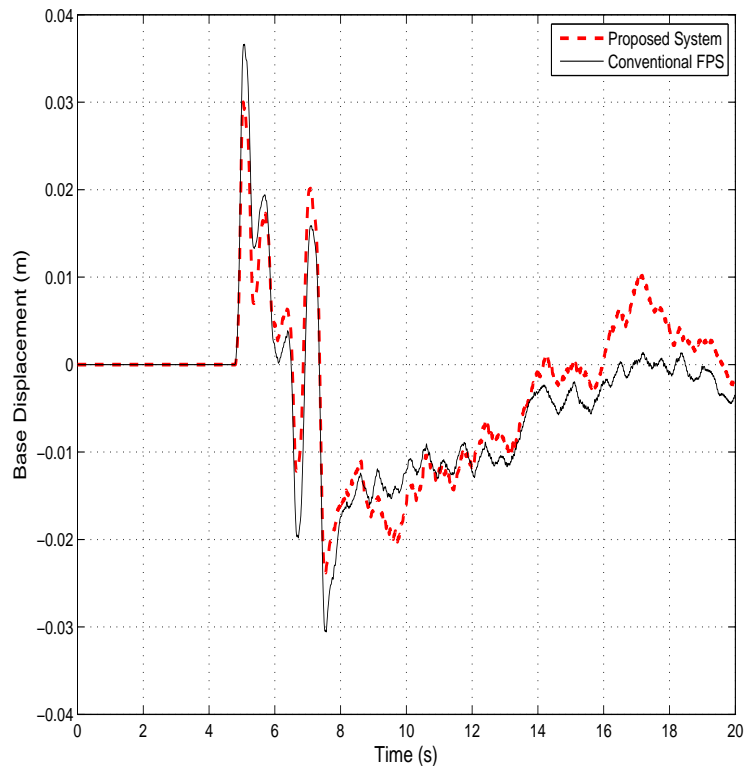


FIGURE A.88: Isolator Displacement (5-storey building) under far-field Northridge-01 earthquake

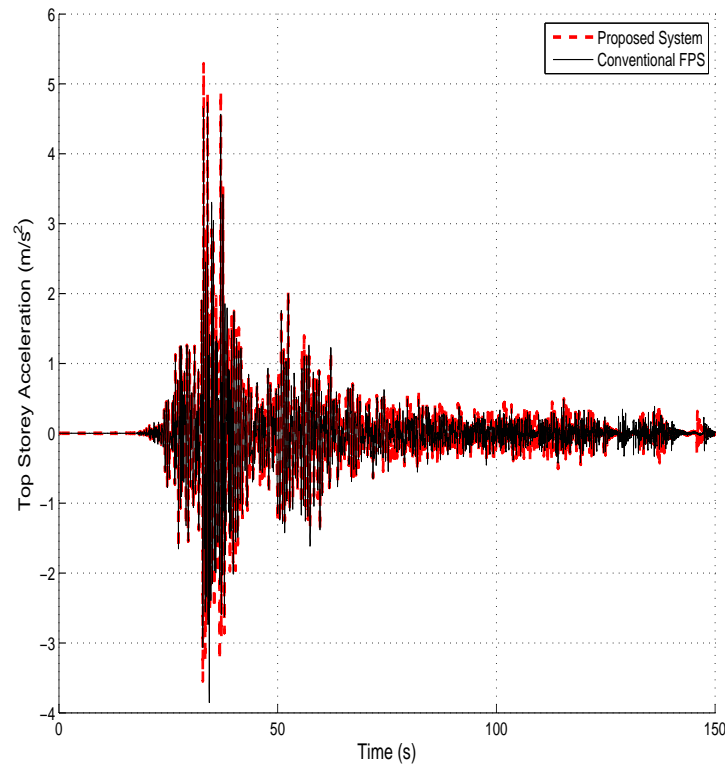


FIGURE A.89: Top storey acceleration (5-storey building) under near-fault Chi-Chi earthquake

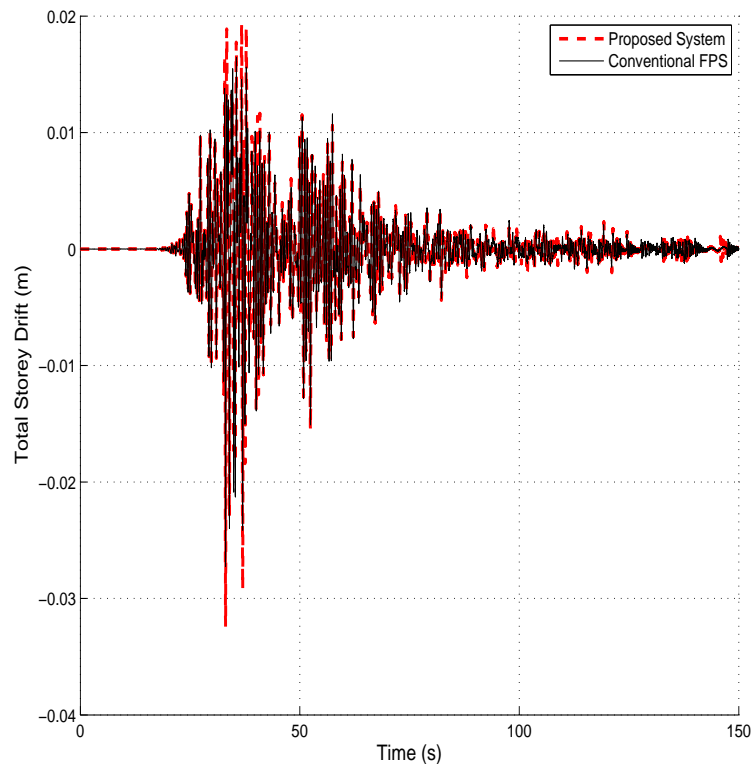


FIGURE A.90: Total Storey Drift (5-storey building) under near-fault Chi-Chi earthquake

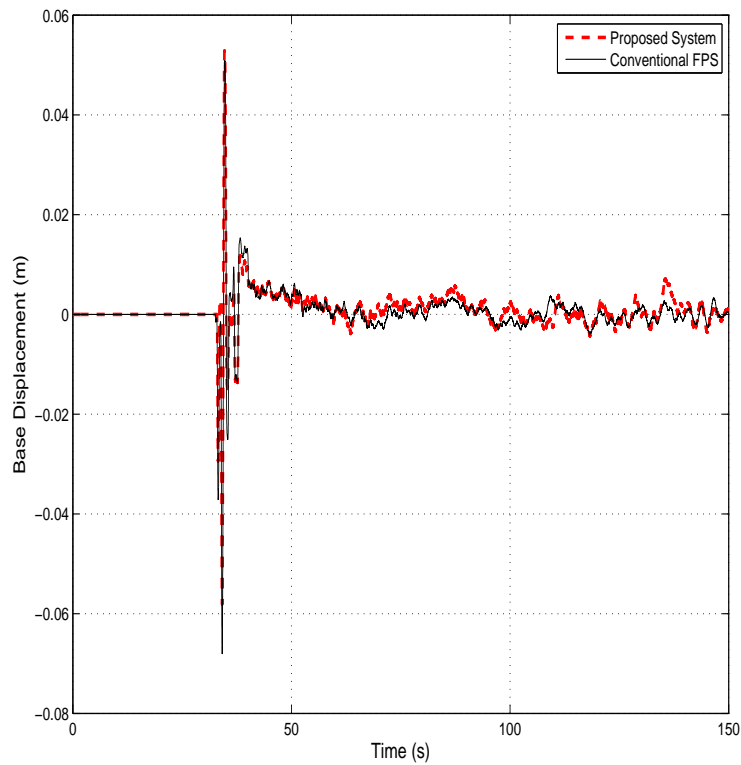


FIGURE A.91: Isolator Displacement (5-storey building) under near-fault Chi-Chi earthquake

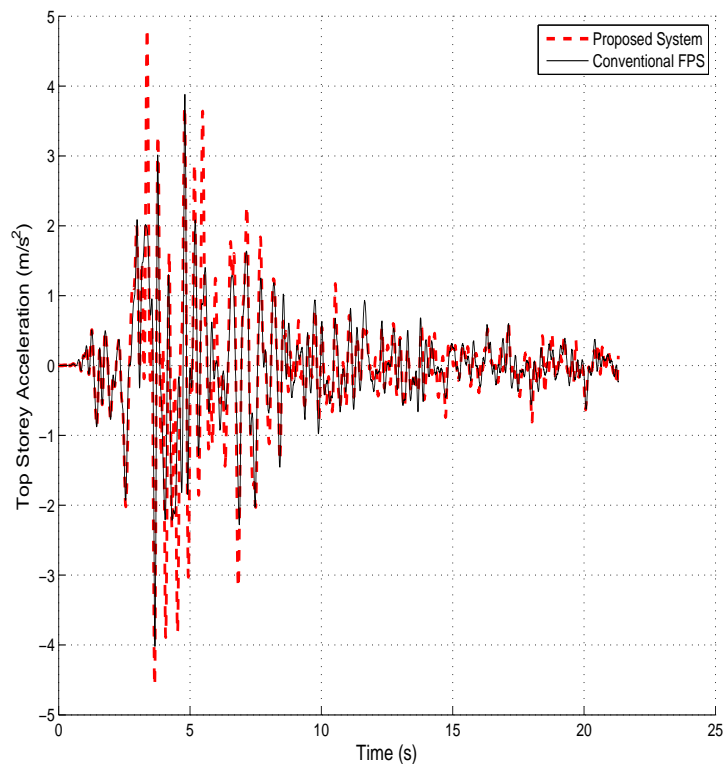


FIGURE A.92: Top storey acceleration (5-storey building) under near-fault Erzican earthquake

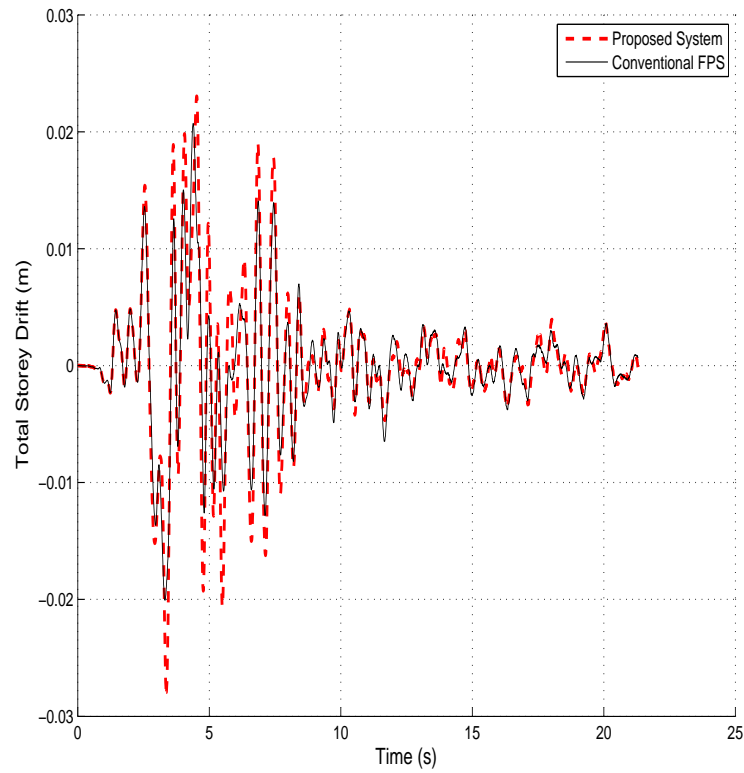


FIGURE A.93: Total Storey Drift (5-storey building) under near-fault Erzican earthquake

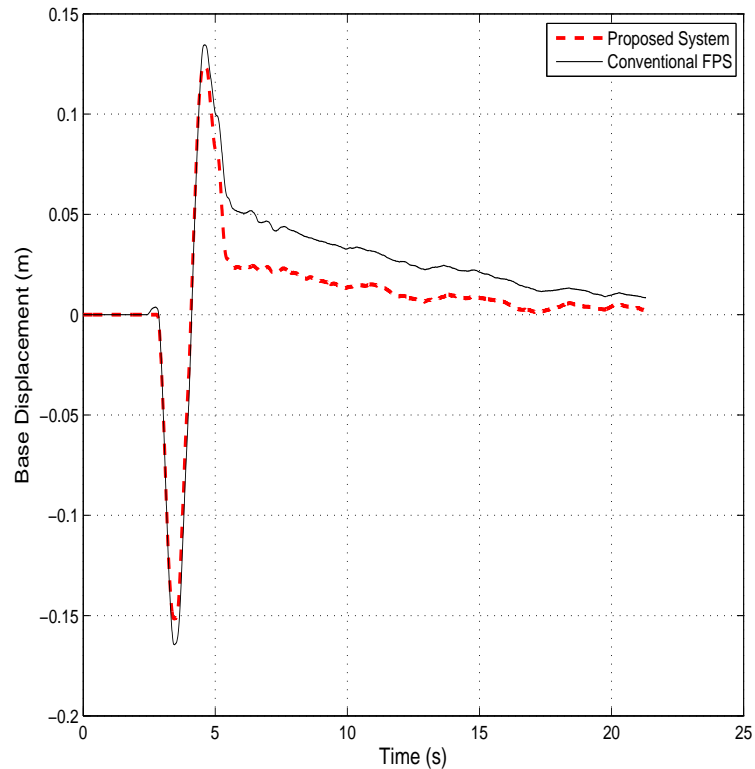


FIGURE A.94: Isolator Displacement (5-storey building) under near-fault Erzican earthquake

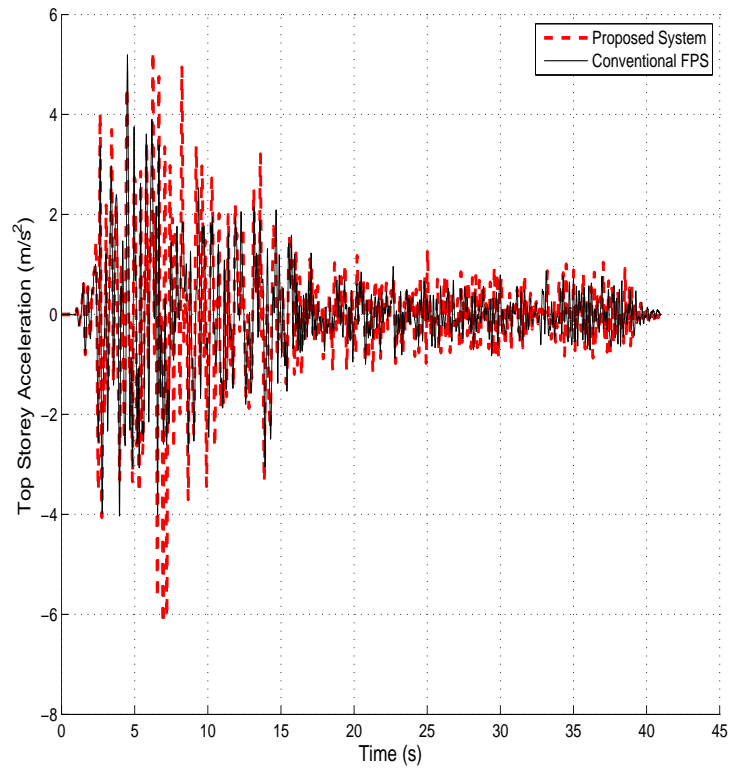


FIGURE A.95: Top storey acceleration (5-storey building) under near-fault Kobe earthquake

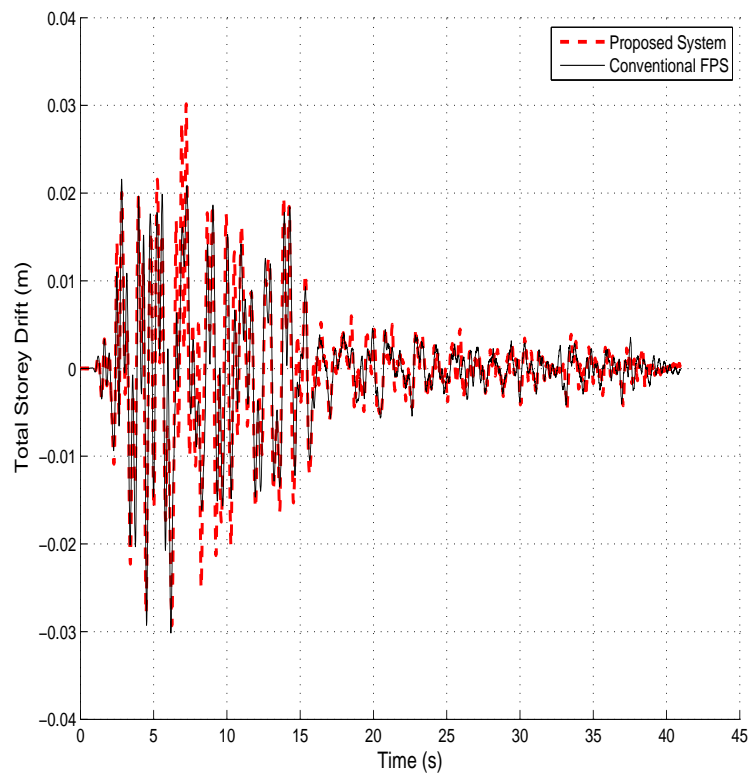


FIGURE A.96: Total Storey Drift (5-storey building) under near-fault Kobe earthquake

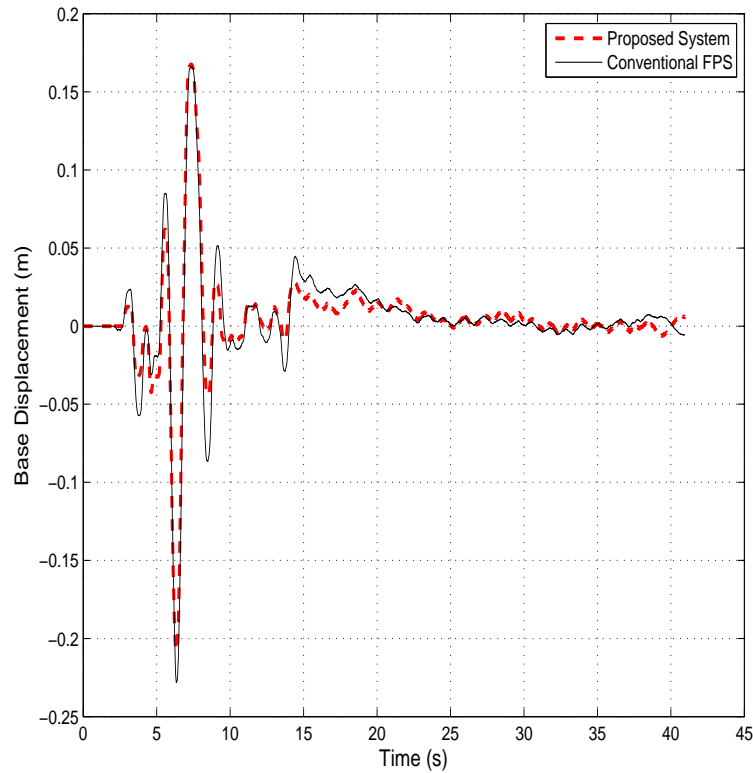


FIGURE A.97: Isolator Displacement (5-storey building) under near-fault Kobe earthquake

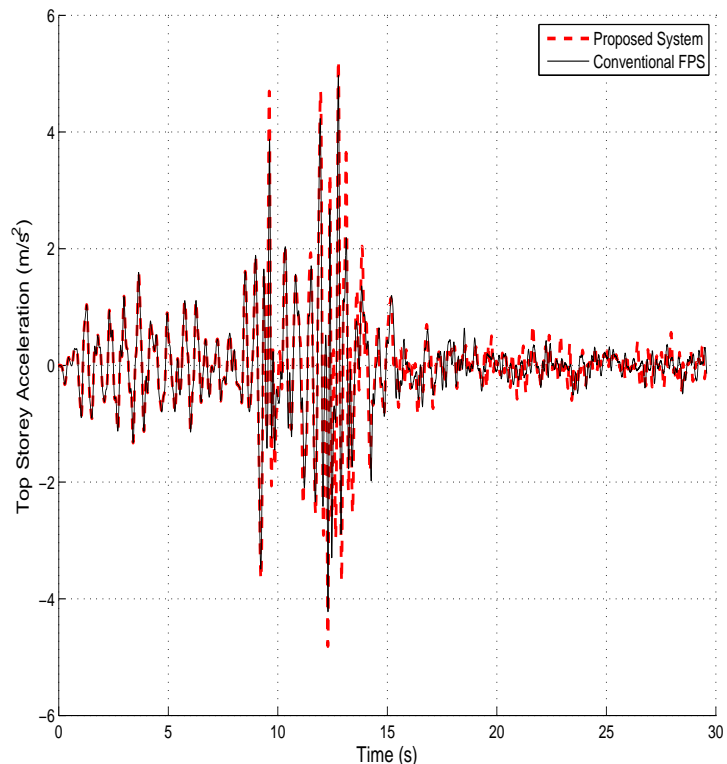


FIGURE A.98: Top storey acceleration (5-storey building) under near-fault Loma Prieta earthquake

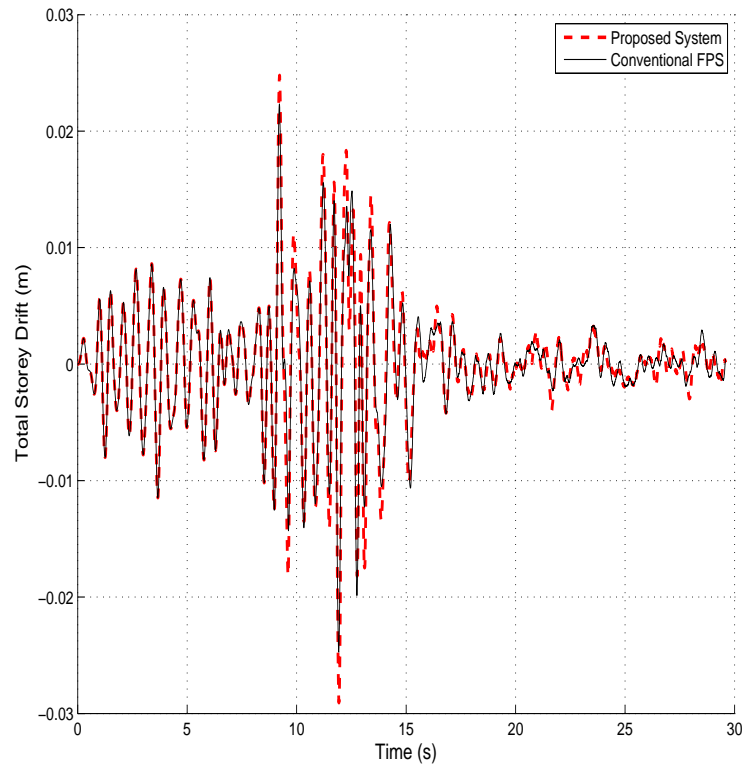


FIGURE A.99: Total Storey Drift (5-storey building) under near-fault Loma Prieta earthquake

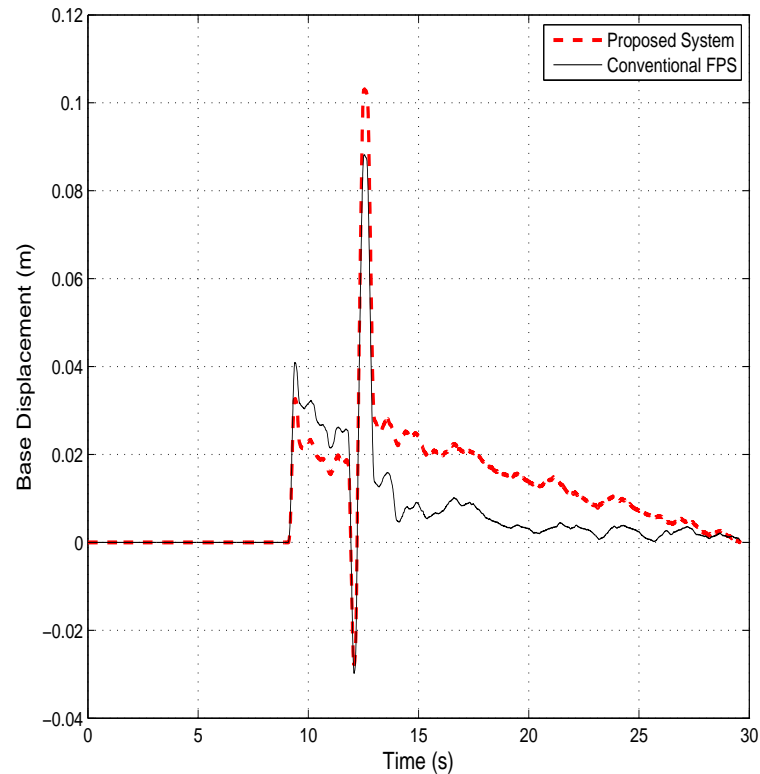


FIGURE A.100: Isolator Displacement (5-storey building) under near-fault Loma Prieta earthquake

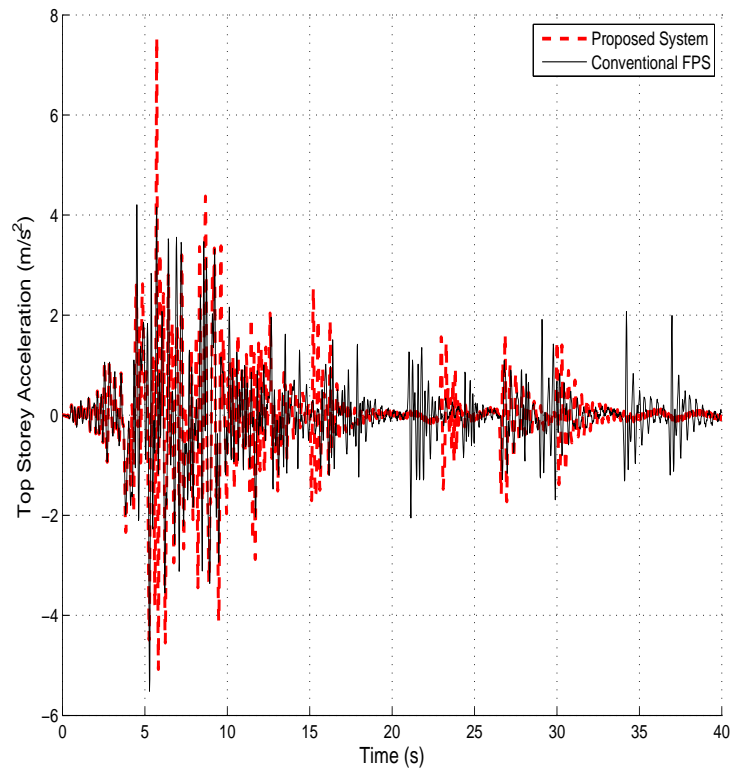


FIGURE A.101: Top storey acceleration (5-storey building) under near-fault Northridge-01 earthquake

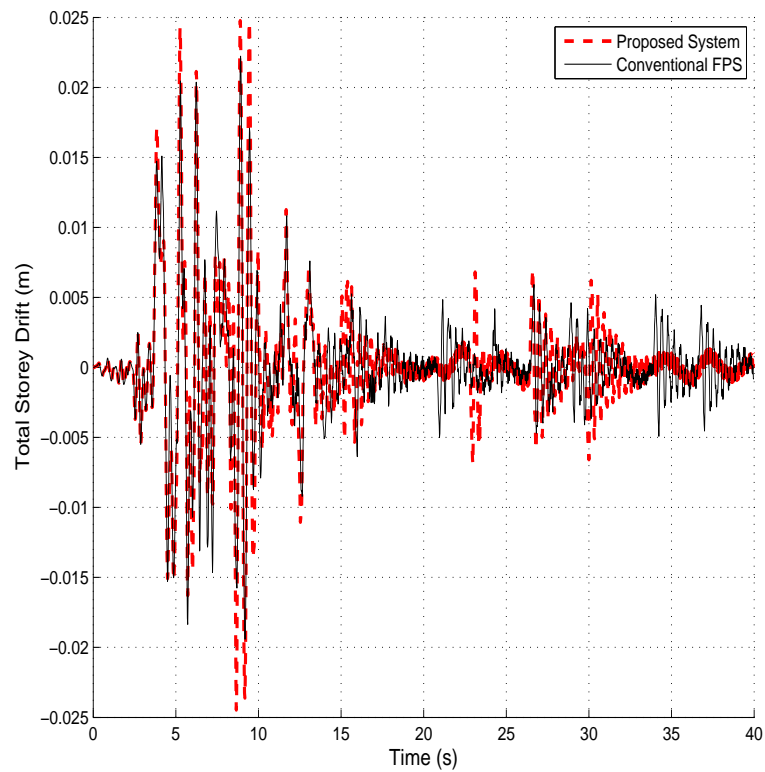


FIGURE A.102: Total Storey Drift (5-storey building) under near-fault Northridge-01 earthquake

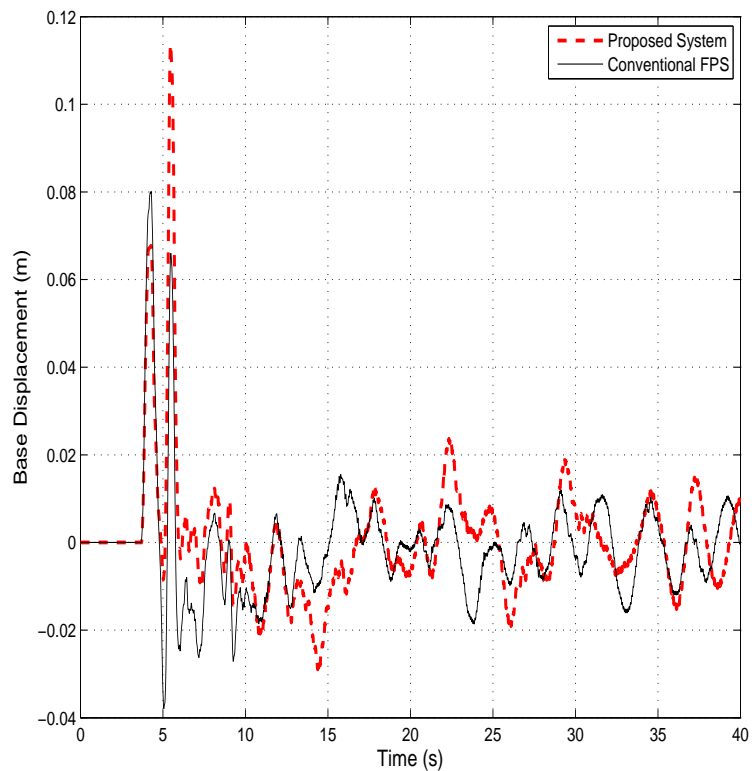


FIGURE A.103: Isolator Displacement (5-storey building) under near-fault Northridge-01 earthquake

A.4 Force-Deformation diagrams of the Isolator

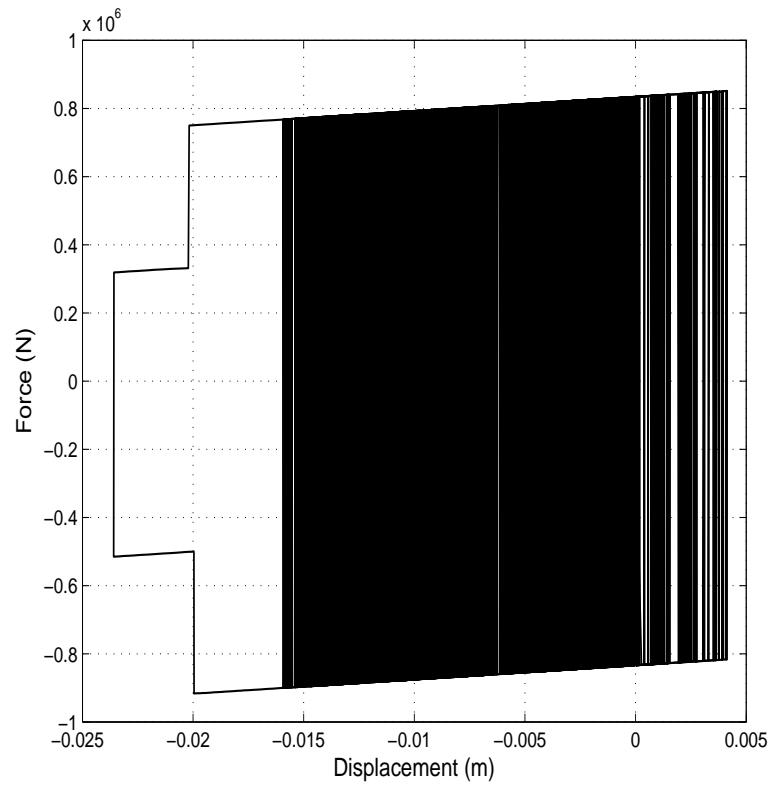


FIGURE A.104: Force-Deformation diagram (3-storey building) under far-field Imperial Valley earthquake

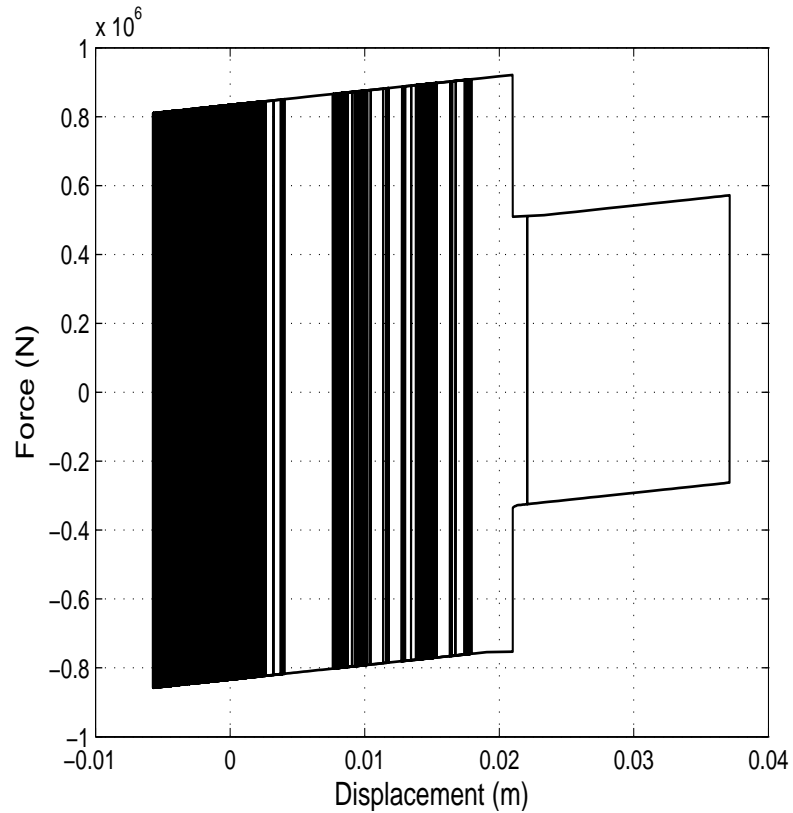


FIGURE A.105: Force-Deformation diagram (3-storey building) under far-field Loma Prieta earthquake

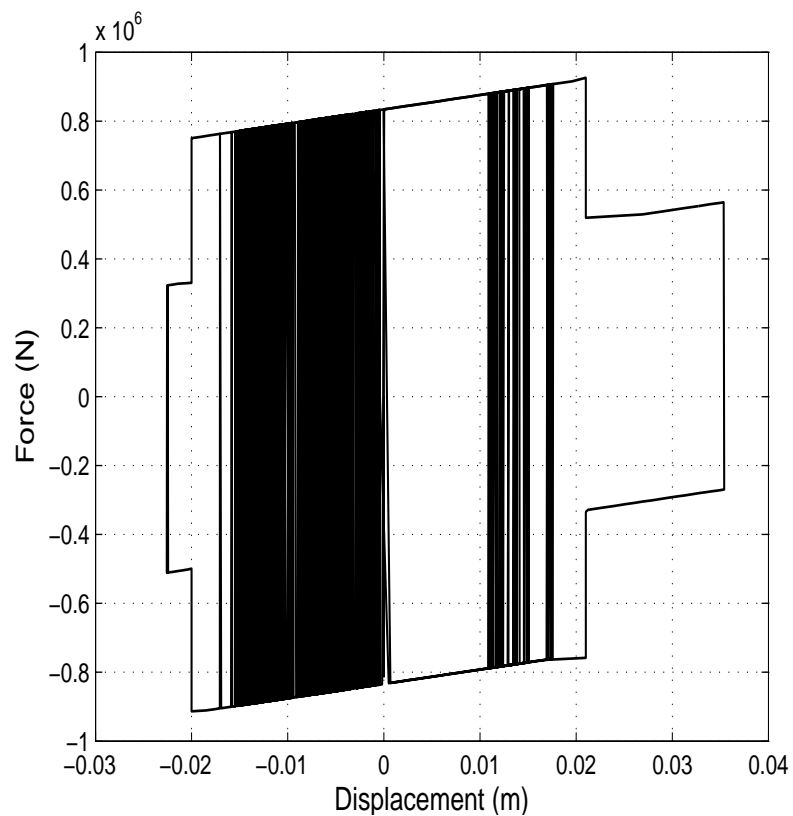


FIGURE A.106: Force-Deformation diagram (3-storey building) under far-field Northridge-01 earthquake

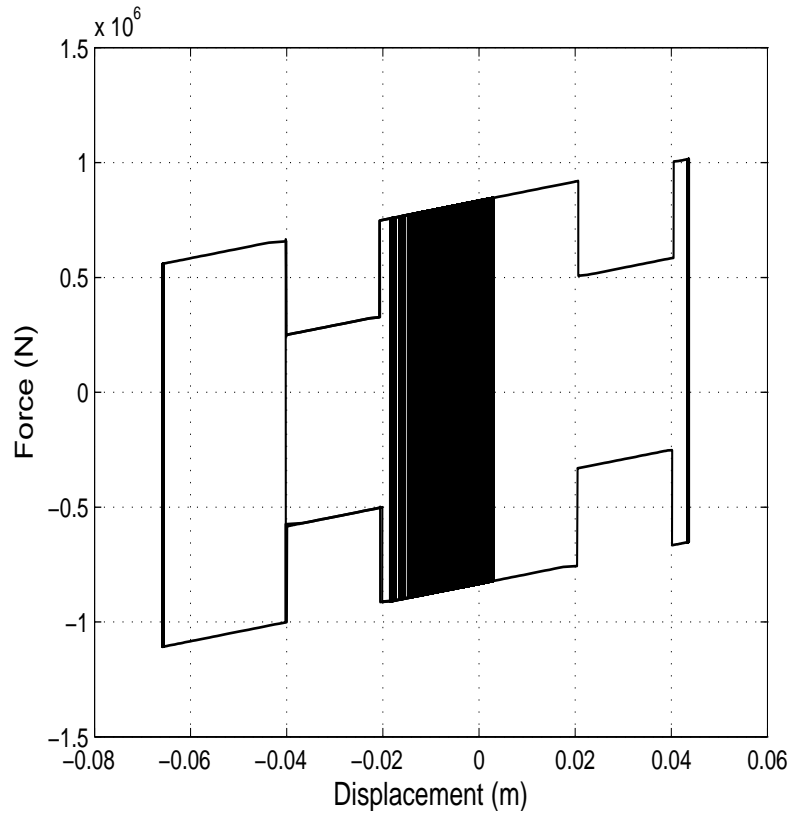


FIGURE A.107: Force-Deformation diagram (3-storey building) under near-fault Chi-Chi earthquake

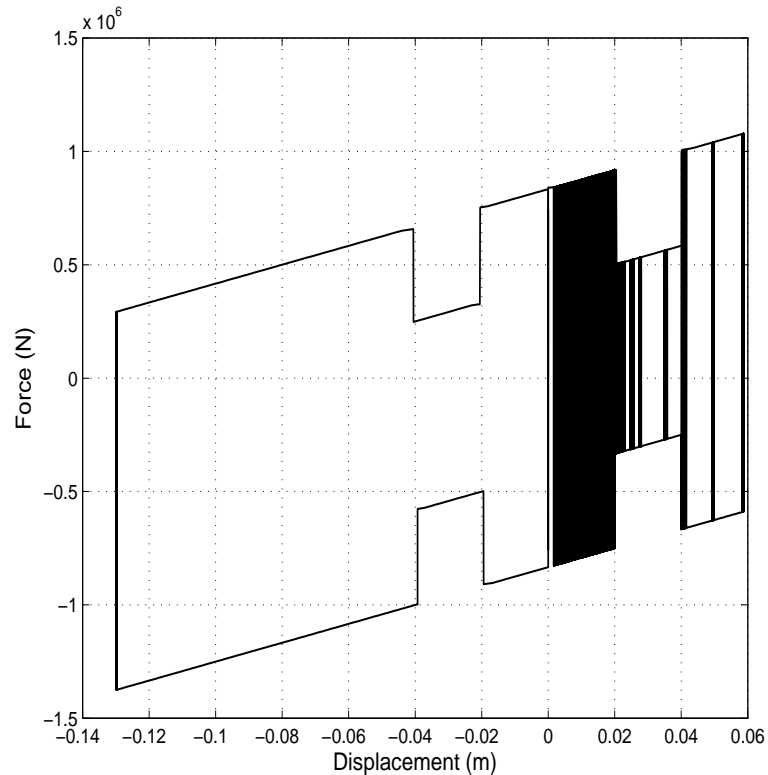


FIGURE A.108: Force-Deformation diagram (3-storey building) under near-fault Erzincan earthquake

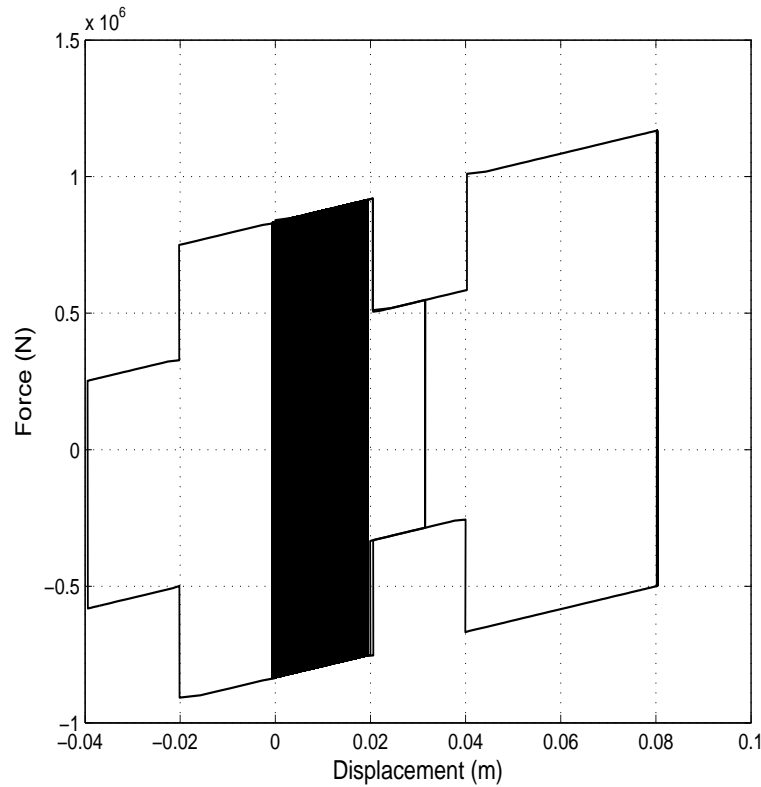


FIGURE A.109: Force-Deformation diagram (3-storey building) under near-fault Loma Prieta earthquake

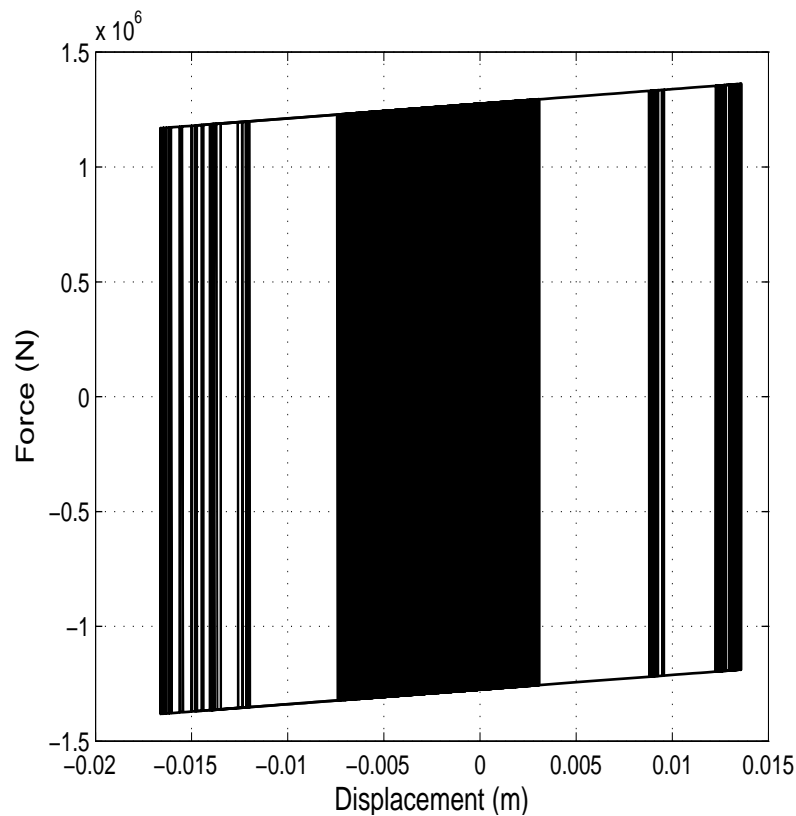


FIGURE A.110: Force-Deformation diagram (5-storey building) under far-field Imperial Valley earthquake

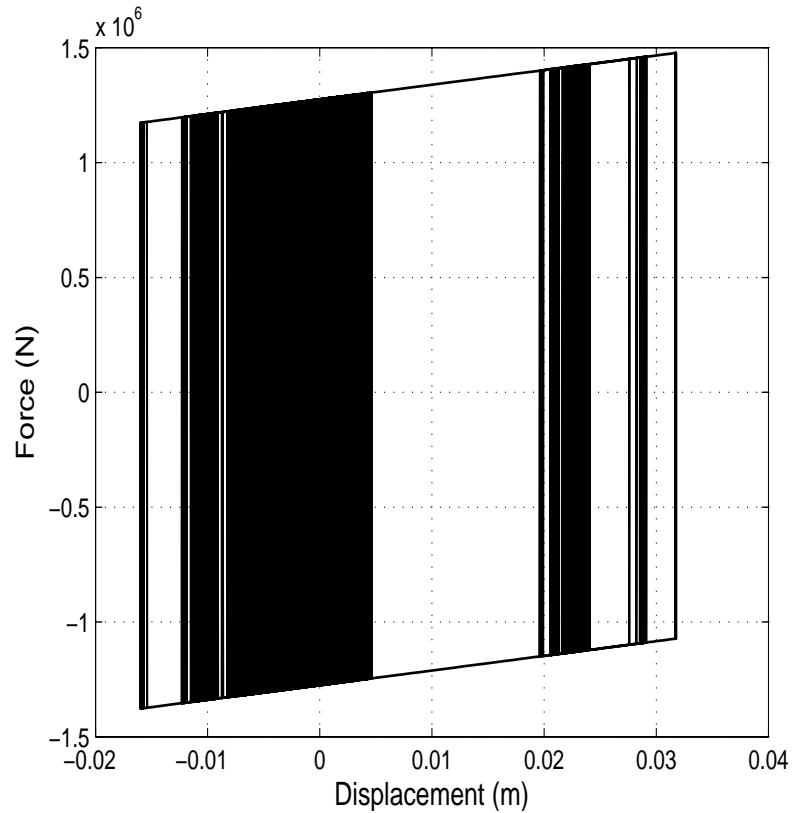


FIGURE A.111: Force-Deformation diagram (5-storey building) under far-field Loma Prieta earthquake

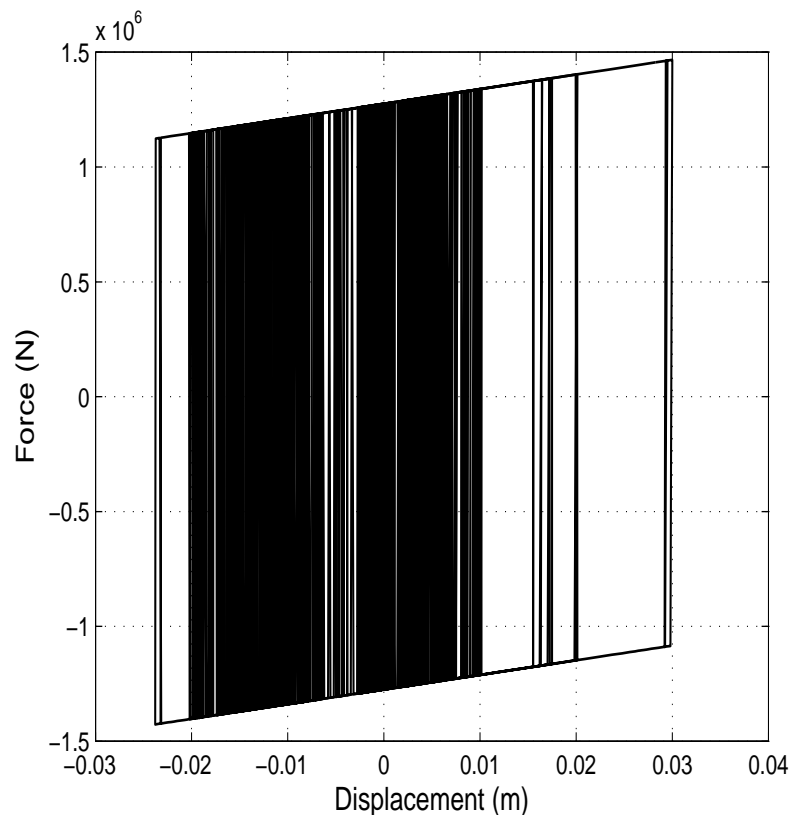


FIGURE A.112: Force-Deformation diagram (5-storey building) under far-field Northridge-01 earthquake

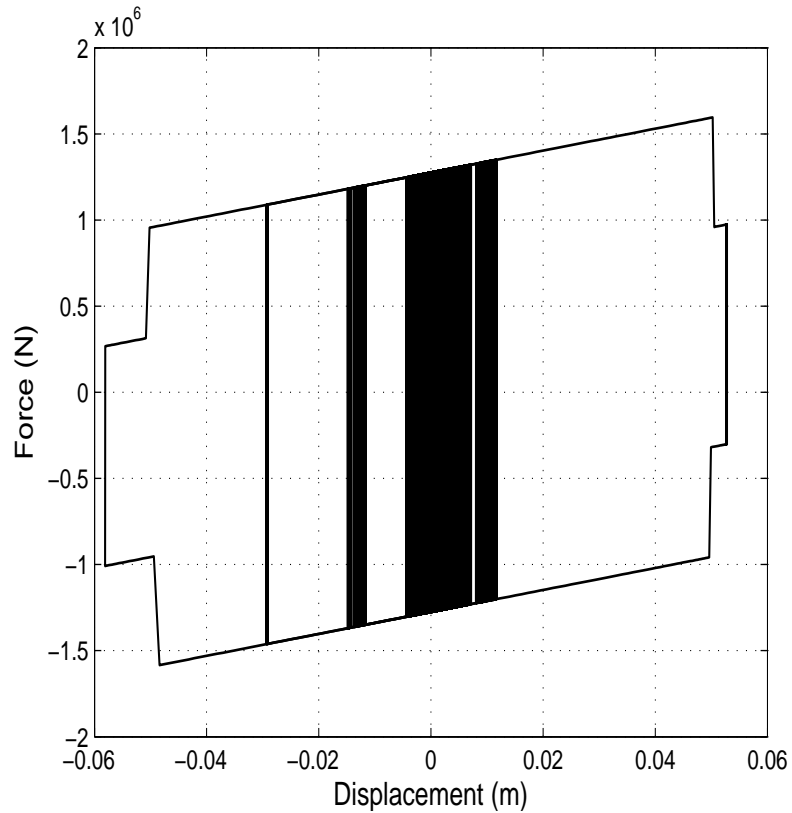


FIGURE A.113: Force-Deformation diagram (5-storey building) under near-fault Chi-Chi earthquake

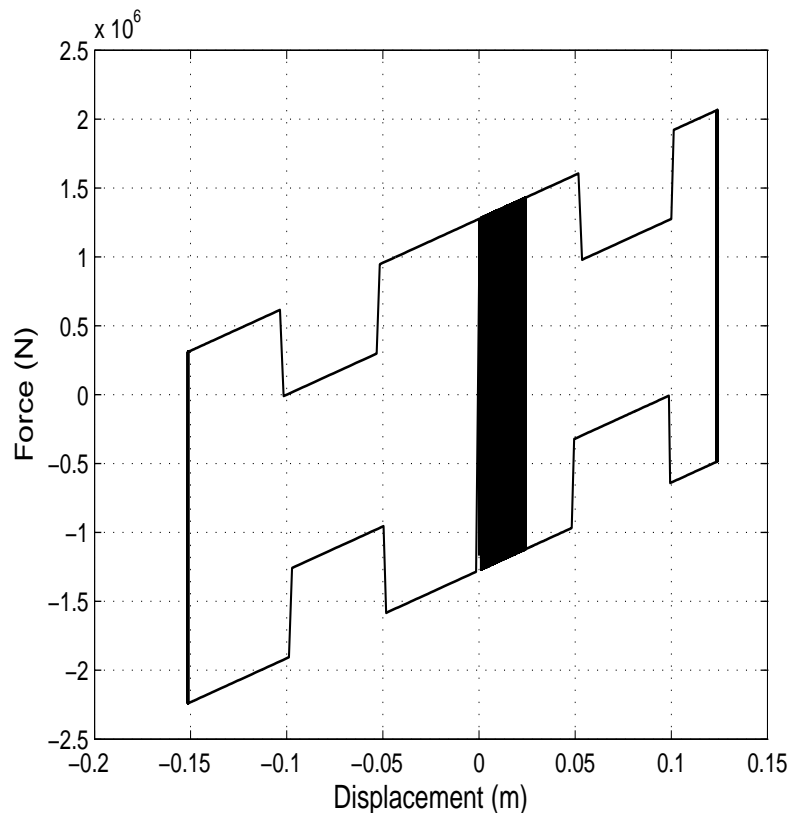


FIGURE A.114: Force-Deformation diagram (5-storey building) under near-fault Erzincan earthquake

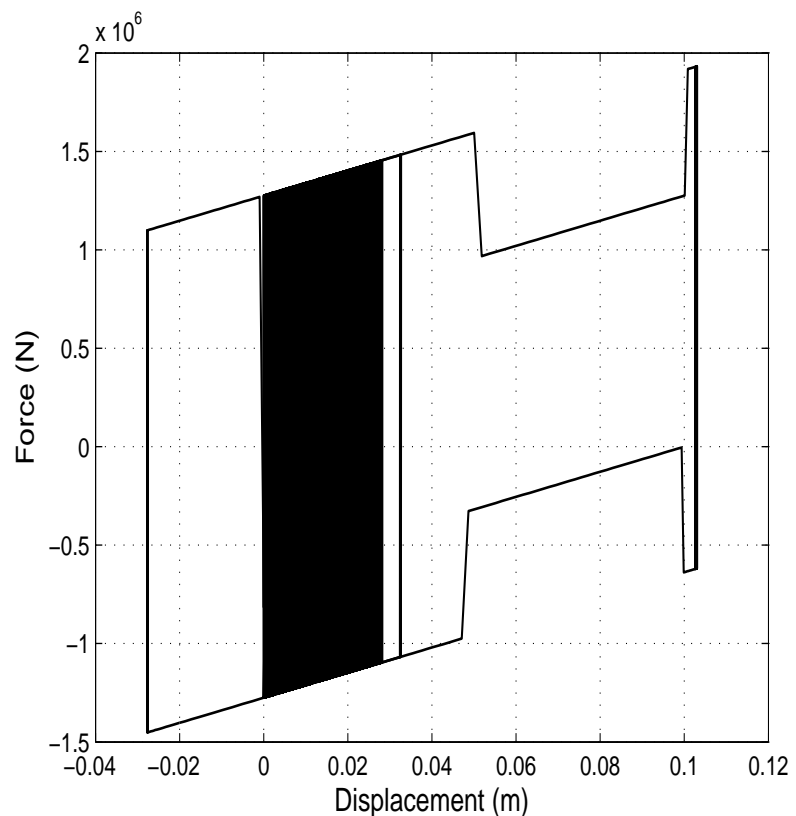


FIGURE A.115: Force-Deformation diagram (5-storey building) under near-fault Loma Prieta earthquake

Bibliography

- Al-Hussaini, T., Zayas, V., and Constantinou, M. (1994). Seismic isolation of multi-storey frame structures using spherical sliding isolation system. Technical Report NCEER-94-0007, Department of Civil Engineering, State University of New York, Buffalo, New York.
- Alavi, B. and Krawinkler, H. (2000). Consideration of near-fault ground motion effects in seismic design. In *Proceedings of the 12th World Conference on Earthquake Engineering*.
- Alhan, C. and Srmeli, M. (2011). Shear building representations of seismically isolated buildings. *Bulletin of Earthquake Engineering*, 9(5):1643–1671.
- Baker, J. W. (2007). Quantitative classification of near-fault ground motions using wavelet analysis. *Bulletin of the Seismological Society of America*, 97(5):1486–1501.
- Barghian, M. and Shahabi, A. B. (2007). A new approach to pendulum base isolation. *Structural Control and Health Monitoring*, 14(2):177–185.
- Beutler, H., Beutler, P., and Grill, U. (2011). MAURER MSM©Spherical and cylindrical bearing. Technical report, Maurer Söhne GmbH.
- Butterworth, J. W. (2001). Seismic response of a non-concentric rolling isolator system. *Advances in Structural Engineering*, 9(1):39–54.
- Calio, I., Marletta, M., and Vinciprova, F. (2003). Seismic response of multi-storey buildings base-isolated by friction devices with restoring properties. *Computers & Structures*, 81(28-29):2589–2599.
- Castellani, A. (1966). Modal analysis of shear type buildings response to earthquakes. *Meccanica*, 1(3-4):69–76.

- Constantinou, M. C. (2004). Friction pendulum double concave bearing. Technical report, State University of New York, Buffalo, New York.
- Constantinou, M. C., Whittaker, A. S., Kalpakidis, Y., Fenz, D. M., and Warn, G. P. (2007). Friction coefficients for stainless steel/PTFE (teflon) bearings. MCEER Highway Project 65A0174, Department of Civil Engineering, State University of New York, Buffalo, New York.
- Craig, R. R. (1981). *Structural Dynamics*. John Wiley & Sons, New York.
- Dolce, M., Cardone, D., and Croatto, F. (2005). Frictional behavior of steel-PTFE interfaces for seismic isolation. *Bulletin of Earthquake Engineering*, 3(1):75–99.
- Elert, G. (1998). The physics hypertextbook.
- Fakhouri, M. Y. and Igarashi, A. (2012). Dynamic response control of multi-story structures by isolators with multiple plane sliding surfaces: A parametric study. *Engineering Structures*, 34:81–94.
- Fan, F.-G., Ahmadi, G., and Tadjbakhsh, I. G. (1990). Multi-story base-isolated buildings under a harmonic ground motion part ii: Sensitivity analysis. *Nuclear Engineering and Design*, 123(1):17 – 26.
- Fenz, D. M. and Constantinou, M. C. (2006). Behaviour of the double concave friction pendulum bearing. *Earthquake Engineering & Structural Dynamics*, 35(11):1403–1424.
- Hall, J. F., Heaton, T. H., Halling, M. W., and Wald, D. J. (1995). Near-source ground motion and its effects on flexible buildings. *Earthquake spectra*, 11(4):569605.
- Hewett, D. R. (2010). A fast, non-linear, finite element solver for earthquake response of buildings. Master thesis, University of Canterbury, Christchurch, New Zealand.
- Jangid, R. (2005a). Computational numerical models for seismic response of structures isolated by sliding systems. *Structural Control and Health Monitoring*, 12(1):117–137.
- Jangid, R. (2005b). Optimum friction pendulum system for near-fault motions. *Engineering Structures*, 27(3):349–359.
- Jangid, R. (2007). Optimum leadrubber isolation bearings for near-fault motions. *Engineering Structures*, 29(10):2503 – 2513.

- Jangid, R. S. and Londhe, Y. B. (1998). Effectiveness of elliptical rolling rods for base isolation. *Journal of Structural Engineering*, 124(4):469472.
- Kani, N. (2008). Current state of seismic-isolation design. In *The 14th World Conference on Earthquake Engineering*, Bejing, China.
- Kelly, J. M. (1986). Aseismic base isolation: review and bibliography. *Soil Dynamics and Earthquake Engineering*, 5(4):202216.
- Kelly, J. M. (1999). The role of damping in seismic isolation. *Earthquake Engineering & Structural Dynamics*, 28(1):3–20.
- Kulkarni, J. A. and Jangid, R. S. (2002). Rigid body response of base-isolated structures. *Journal of structural control*, 9(3):171188.
- Lu, L.-Y., Shih, M.-H., and Wu, C.-Y. (2004). Near-fault seismic isolation using sliding bearings with variable curvatures. In *Proceedings of the 13th World Conference on Earthquake Engineering*.
- Lu, L.-Y., Wang, J., and Hsu, C.-C. (2006). Sliding isolation using variable frequency bearings for near-fault ground motions. In *4th International Conference on Earthquake Engineering, Taipei, Taiwan*.
- Lu, L. Y. and Yang, Y. B. (1997). Dynamic response of equipment in structures with sliding support. *Earthquake Engineering & Structural Dynamics*, 26(1):61–77.
- Luco, J. E. (2008). A note on classical damping matrices. *Earthquake Engineering & Structural Dynamics*, 37(4):615–626.
- Malekzadeh, M. and Taghikhany, T. (2010). Adaptive behavior of double concave friction pendulum bearing and its advantages over friction pendulum systems. *Transaction A: Civil Engineering Vol*, 17:8188.
- MATLAB (2010). *version 8.0.0 (R2012b)*. The MathWorks Inc., Natick, Massachusetts.
- Mazza, F. and Vulcano, A. (2008). Effects of horizontal and vertical near-fault ground motions on the nonlinear dynamic response of rc buildings with different base-isolation systems. In *Proceedings of the 14th World Conference on Earthquake Engineering*, Bejing, China.

- Mazza, F. and Vulcano, A. (2009). Nonlinear response of RC framed buildings with isolation and supplemental damping at the base subjected to near-fault earthquakes. *Journal of Earthquake Engineering*, 13(5):690–715.
- Mazza, F. and Vulcano, A. (2012). Effects of near-fault ground motions on the nonlinear dynamic response of base-isolated r.c. framed buildings. *Earthquake Engineering & Structural Dynamics*, 41(2):211–232.
- Mendoza, M. J. and Auvinet, G. (1988). The mexico earthquake of september 19, 1985behavior of building foundations in mexico city. *Earthquake Spectra*, 4(4):835–853.
- Mokha, A., Constantinou, M., Reinhorn, A., and Zayas, V. (1991). Experimental study of frictionpendulum isolation system. *Journal of Structural Engineering*, 117(4):1201–1217.
- Morgan, T. A. and Mahin, S. A. (2008). The optimization of multi-stage friction pendulum isolators for loss mitigation considering a range of seismic hazard. In *Proceedings of the 14th World Conference on Earthquake Engineering*.
- Moroni, M. O., Sarrazin, M., and Boroschek, R. (1998). Experiments on a base-isolated building in santiago, chile. *Engineering Structures*, 20(8):720725.
- Mostaghel, N. and Khodaverdian, M. (1987). Dynamics of resilient-friction base isolator (r-fbi). *Earthquake Engineering & Structural Dynamics*, 15(3):379–390.
- Murnal, P. and Sinha, R. (2004). Behavior of torsionally coupled structures with variable frequency pendulum isolator. *Journal of Structural Engineering*, 130(7):10411054.
- Myslimaj, B., Gamble, S., Chin-Quee, D., Davies, A., and Breukelman, B. (2003). Base isolation technologies for seismic protection of museum artifacts. In *The 2003 IAMFA Annual Conference*, San Francisco, California. International Association of Museum Facilities Administrators (IAMFA).
- Nadein, V. A., Drozdov, Y. N., Puchkov, V. N., and Puchkov, M. V. (2007). Characteristics of pendulum sliding bearings used as seismic isolators. *Russian Engineering Research*, 27(2):85–92.

- Naeim, F. and Kelly, J. M. (1999a). Chapter 1: Development of seismic isolation worldwide. In *Design of Seismic Isolated Structures: From Theory to Practice*. John Wiley, New York.
- Naeim, F. and Kelly, J. M. (1999b). Chapter 3: Isolation system components. In *Design of Seismic Isolated Structures: From Theory to Practice*. John Wiley, New York.
- Nakata, H. (2009). Japan leads the way with quake-resistant technology.
- Panchal, V. R. and Jangid, R. S. (2008). Variable friction pendulum system for near-fault ground motions. *Structural Control and Health Monitoring*, 15(4):568–584.
- Panchal, V. R., Jangid, R. S., Soni, D. P., and Mistry, B. B. (2010). Response of the double variable frequency pendulum isolator under triaxial ground excitations. *Journal of Earthquake Engineering*, 14(4):527–558.
- PEER (2010). Technical report for the PEER ground motion database web application. Technical report, Pacific Earthquake Engineering Research Center, California.
- Pranesh, M. and Sinha, R. (2000). Vfpi: an isolation device for aseismic design. *Earthquake Engineering & Structural Dynamics*, 29(5):603–627.
- Providakis, C. (2009). Effect of supplemental damping on LRB and FPS seismic isolators under near-fault ground motions. *Soil Dynamics and Earthquake Engineering*, 29(1):80–90.
- Puthanpurayil, A. M., Dhakal, R. P., and Carr, A. J. (2000). Modelling of in-structure damping: A review of the state-of-the-art. In *9th Pacific conference on earthquake engineering (PCEE)*, Auckland, New Zealand. New Zealand Society for Earthquake Engineering (NZSEE).
- Sharbatdar, M., Vaez, S. H., Amiri, G. G., and Naderpour, H. (2011). Seismic response of base-isolated structures with LRB and FPS under near fault ground motions. *Procedia Engineering*, 14:3245–3251.
- Sharma, A. and Jangid, R. S. (2012). Performance of variable curvature sliding isolators in base-isolated benchmark building. *The Structural Design of Tall and Special Buildings*, 21(5):354–373.

- Shen, J., Tsai, M., Chang, K., and Lee, G. (2004). Performance of a seismically isolated bridge under near-fault earthquake ground motions. *Journal of Structural Engineering*, 130(6):861–868.
- Soni, D. P., Mistry, B. B., Jangid, R. S., and Panchal, V. R. (2011). Seismic response of the double variable frequency pendulum isolator. *Structural Control and Health Monitoring*, 18(4):450–470.
- Soni, D. P., Mistry, B. B., and Panchal, V. R. (2010). Behaviour of asymmetric building with double variable frequency pendulum isolator. *Structural Engineering and Mechanics*, 34(1):61–84.
- Su, L., Ahmadi, G., and Tadjbakhsh, I. G. (1989). Comparative study of base isolation systems. *Journal of engineering mechanics*, 115(9):19761992.
- Taylor, J. C. and Stanton, J. F. (2010). Friction coefficients for stainless steel/PTFE (teflon) bearings. WisDOT Project WHRP 10-01, Department of Civil Engineering, University of Washington.
- Tsai, C., Chiang, T.-C., and Chen, B.-J. (2003). Finite element formulations and theoretical study for variable curvature friction pendulum system. *Engineering Structures*, 25(14):1719–1730.
- Wang, Y.-P. (2002). Fundamentals of seismic base isolation. Technical report, National Center for Research on Earthquake Engineering (NCREE), Taiwan.
- Wilson, E. L. (2004). *Static and Dynamic Analysis of Structures*. Computers and Structures, Inc., Berkeley, CA, 4 edition.
- Yang, Y.-B., Lee, T.-Y., and Tsai, I.-C. (1990). Response of multi-degree-of-freedom structures with sliding supports. *Earthquake Engineering & Structural Dynamics*, 19(5):739–752.
- Zakoda, E. (2011). Quake-resistant buildings a must-have after march 11.
- Zayas, V. A. and Low, S. S. (2000). Seismic isolation for strong near-field earthquake motions. In *The 12th World Conference on Earthquake Engineering*, Auckland, New Zealand. International Association for Earthquake Engineering (IAEE).